AD

USAAVLABS TECHNICAL REPORT 71-14

SMALL AXIAL TURBINE STAGE COOLING INVESTIGATION

By

A. Stappenbeck
S. Moskowitz

April 1971

EUSTIS DIRECTORATE
U. S. ARMY AIR MOBILITY RESEARCH AND DEVELOPMENT LABORATORY
FORT EUSTIS, VIRGINIA

CONTRACT DAAJ02-69-C-0064
CURTISS-WRIGHT CORPORATION
WOOD-RIDGE, NEW JERSEY

DISCLAIMERS

The findings in this report are not to be construed as an official Department of the Army position unless so designated by other authorized documents.

When Government drawings, specifications, or other data are used for any purpose other than in connection with a definitely related Government procurement operation, the United States Government thereby incurs no responsibility nor any obligation whatsoever; and the fact that the Government may have formulated, furnished, or in any way supplied the said drawings, specifications, or other data is not to be regarded by implication or otherwise as in any manner licensing the holder or any other person or corporation, or conveying any rights or permission, to manufacture, use, or sell any patented invention that may in any way be related thereto.

DISPOSITION INSTRUCTIONS

Destroy this report when no longer needed. Do not return it to the originator.

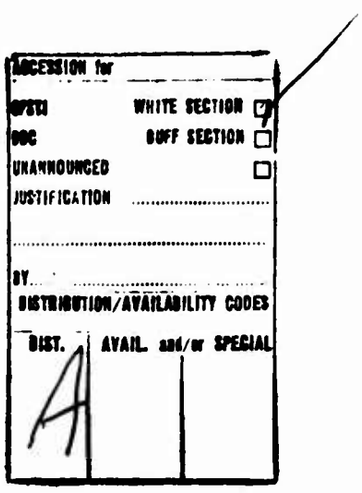

UNCLASSIFIED

Security Classification

DOCUMENT CONTROL DATA - R & D

(Security classification of title, body of abstract and indexing annotation must be entered when the overall report is classified)

1. ORIGINATING ACTIVITY (Corporate author)	2a. REPORT SECURITY CLASSIFICATION
CURTISS-WRIGHT CORPORATION ONE PASSAIC STREET WOOD-RIDGE, NEW JERSEY	UNCLASSIFIED 2b. GROUP

3. REPORT TITLE

SMALL AXIAL TURBINE STAGE COOLING INVESTIGATION

4. DESCRIPTIVE NOTES (Type of report and inclusive dates)

Final Report

5. AUTHOR(S) (First name, middle initial, last name)

A. Stappenbeck
S. Moskowitz

6. REPORT DATE	7a. TOTAL NO. OF PAGES	7b. NO. OF REFS
April 1971	198	23

8a. CONTRACT OR GRANT NO.	9a. ORIGINATOR'S REPORT NUMBER(S)
DAAJ02-69-C-0064 b. PROJECT NO. c. Task 1G162204A01409 d.	USAAVLABS Technical Report 71-14 9b. OTHER REPORT NO(S) (Any other numbers that may be assigned this report) CW-WR-69-077.F

10. DISTRIBUTION STATEMENT

Approved for public release; distribution unlimited.

11. SUPPLEMENTARY NOTES	12. SPONSORING MILITARY ACTIVITY
Details of illustrations in this document may be better studied on microfiche	Eustis Directorate U.S. Army Air Mobility R&D Laboratory Fort Eustis, Virginia

13. ABSTRACT

This report describes an investigation of advanced cooling concepts for the gas producer axial flow turbine of a small gas turbine engine. These concepts were directed toward minimizing the engine performance penalties, especially at part power, associated with conventional air cooling of the turbine. The initial phase consisted of a conceptual analysis of five stator and five rotor cooling concepts. The coolants for closed systems included liquid metal, high pressure gas, two phase H_2O, heat pipe (two-phase liquid metal), and superheated steam. Modulated compressor air for transpiration cooling was also studied. To return the heat to the cycle, heat exchangers used in conjunction with the closed coolant systems utilized compressor exit air of fuels.

Heat transfer analyses and preliminary designs were conducted on two selected turbine cooling concepts. The concepts selected as the most feasible included the closed systems using liquid metal or high pressure air for the stator and liquid metal or superheated steam for the rotor. Compressor discharge air was used as the heat sink for these systems. The effects of these systems on engine performance were also evaluated.

In the final phase, a limited fabrication and test evaluation was conducted on the liquid-metal-cooled vane concept. A two-dimensional turbine cascade rig incorporating liquid-metal-cooled vanes was tested for 5:40 hours over a range of coolant flow rates and at average gas temperatures up to 2500°F. The vanes were in excellent condition after this test. Excellent agreement between measured and predicted vane metal temperatures were obtained.

DD FORM 1 NOV 68 1473 REPLACES DD FORM 1473, 1 JAN 64, WHICH IS OBSOLETE FOR ARMY USE.

UNCLASSIFIED

Security Classification

UNCLASSIFIED
Security Classification

14. KEY WORDS	LINK A		LINK B		LINK C	
	ROLE	WT	ROLE	WT	ROLE	WT
Fluid-Cooled Turbine						
Component Technology						
Liquid Metal Cooling						
Small Gas Turbine Engine						

UNCLASSIFIED
Security Classification

DEPARTMENT OF THE ARMY
U. S. ARMY AIR MOBILITY RESEARCH & DEVELOPMENT LABORATORY
EUSTIS DIRECTORATE
FORT EUSTIS, VIRGINIA 23604

This report was prepared by the Curtiss-Wright Corporation under the terms of Contract DAAJ02-69-C-0064. The work was performed under the technical management of CPT F. S. Sherwin, Propulsion Division, Eustis Directorate, U. S. Army Air Mobility Research and Development Laboratory.

Appropriate personnel of the Eustis Directorate have reviewed this report and concur with the conclusions and recommendations contained herein with the following exceptions: at present, the modest improvement in overall engine performance offered by the advanced cooling concepts studied (when compared to conventional air cooling) does not justify further programs to apply these concepts to small Army gas turbines; the special cooling fluids, heat exchangers, and airfoils required by these concepts would adversely affect the repairability, reliability, fabricability, and vulnerability of the small axial turbine stage.

The findings described herein will be taken into consideration in the planning of future axial turbine programs.

Task 1G162204A01409
Contract DAAJ02-69-C-0064
USAAVLABS Technical Report 71-14
April 1971

SMALL AXIAL TURBINE STAGE COOLING INVESTIGATION

Final Report

by

A. Stappenbeck
S. Moskowitz

Prepared by

CURTISS-WRIGHT CORPORATION
WOOD-RIDGE, NEW JERSEY

for

EUSTIS DIRECTORATE
U.S. ARMY AIR MOBILITY RESEARCH AND DEVELOPMENT LABORATORY
FORT EUSTIS, VIRGINIA

SUMMARY

The program reported herein included the design and analysis of advanced cooling concepts for small gas turbine blades and vanes, selection of the most promising system, and a limited fabrication and test evaluation of the selected vane cooling system to demonstrate feasibility.

The study was conducted to define cooling concepts which would minimize the engine performance penalties, especially at part power, associated with conventional air cooling of the vane and blades. The initial design phase consisted of a conceptual analysis of five stator and five rotor cooling concepts. The stator concepts included the following coolant and heat sink combinations: (1) liquid metal/compressor discharge air, (2) high-pressure gas/compressor discharge air, (3) H_2O vaporizing/fuel, (4) liquid metal vaporizing (heat pipe)/compressor discharge air, and (5) modulated transpiration air cooling. The rotor concepts included the following coolant and heat sink combinations: (1) liquid metal/compressor discharge air, (2) high-pressure gas/compressor discharge air, (3) superheated steam/compressor discharge air, (4) high-pressure air/methane fuel, and (5) modulated transpiration cooling.

Two stator coolant concepts (liquid metal and high-pressure air) and two rotor concepts (liquid metal and superheated steam) were selected as the most feasible for further design evaluations. Subsequently, heat transfer analysis and preliminary engine designs were performed for these selected cooling concepts and the effects of these systems on engine performance were determined. The liquid-metal-cooled stator and rotor concepts were finally selected as the most promising internal cooling concept for advanced development.

As the final phase of this program, a limited fabrication and test evaluation was conducted on the liquid-metal-cooled vane and compressor discharge air exchanger concept. The test vanes were electrical discharge machined to meet the coolant passage requirements. The vane exchanger used 3/8" OD finned tubes with stainless clad copper core fins. The liquid-metal-cooled vanes were tested for 5:40 hours in a two-dimensional cascade at average gas temperatures up to 2500°F. The vanes were in excellent condition after this testing. The measured vane metal temperatures were in excellent agreement with the predicted values at the same test conditions. This confirms the heat transfer analysis methods and indicates that this concept is capable of providing acceptable thermal and structural characteristics, as shown in the design phase, for an advanced engine component.

FOREWORD

The work reported herein was performed by Curtiss-Wright Corporation under United States Army Contract DAAJ02-69-C-0064 to advance and demonstrate high-temperature turbine technology for small gas turbine engines. The contract was administered by the Propulsion Division of the Eustis Directorate, U.S. Army Air Mobility Research and Development Laboratory, Fort Eustis, Virginia. The program effort was directed at investigating methods of cooling the gas producer turbine stage of a small high-temperature engine by methods other than, or with a minimum amount of, compressor bleed air. The program tasks consisted of the design and analytical evaluation of rotor and stator cooling systems and the fabrication and test of a selected vane cooling system.

Mr. A. Stappenbeck and Mr. S. Moskowitz, Manager, Turbine Technology were the principal investigators. Other principal contributing engineers included Messrs. T. Dalton, H. Watts, and A. Sievers.

The study of the heat pipe concept for application to the stator vane was performed by Mr. Calvin Silverstein, an engineering consultant under a Curtiss-Wright purchase order. The test covering the heat pipe concept was extracted from Mr. Silverstein's analysis, and his efforts are gratefully acknowledged.

The guidance of Mr. H. Morrow, Mr. E. Johnson and Lt. F. Sherwin of the Eustis Directorate, U.S. Army Air Mobility Research and Development Laboratory, is also gratefully acknowledged.

TABLE OF CONTENTS

TABLE OF CONTENTS - Continued

LIST OF ILLUSTRATIONS

LIST OF ILLUSTRATIONS - Continued

LIST OF ILLUSTRATIONS - Continued

LIST OF TABLES

LIST OF TABLES - Continued

LIST OF SYMBOLS

A	area, ft^2
b	fin thickness, ft
C_p	specific heat, Btu/lb °R
D	diameter, ft
G	mass flux, lb/ft^2 sec
g	gravitational acceleration, ft/sec^2
h	heat transfer coefficient, Btu/ft^2 hr °R
J	mechanical equivalent of heat, ft-lb/Btu
k	thermal conductivity, Btu/ft hr °R
L	heat exchanger length, ft
P	flow channel perimeter, ft
Pr	Prandtl number
Q	heat flow, Btu/hr
R	recovery factor
r	radius, ft
Re	Reynolds number
r_h	hydraulic radius, ft
S	blade height, ft
T	temperature, °R
Δ T	temperature difference, °R
v	air specific volume, ft^3/lb
V	velocity, ft/sec
W	mass flow, lb/sec
X	distance, ft
τ	fin length, ft
η	effectiveness
θ	angle measured from stagnation point, deg
μ	viscosity, lb/ft hr
ρ	density, lb/ft^3
μ	combined heat transfer coefficient, $Btu/hr\ ft^2$ °R
β	coefficient of thermal expansion
ω	angular acceleration, ft/sec sec
σ	core minimum free flow area/duct area
ΔPs	core static pressure drop, lb/ft^2

Subscripts

a	adiabatic
b	bare surface
f	finned surface or condition at average of total and free stream temperature
0	stagnation or total conditions
S	surface condition
W	wall condition
θ	cylindrical surface location
-1	upstream location
+1	downstream location
∞	freestream conditions
1	inlet
2	outlet
m	core

1.0 INTRODUCTION

The future development of small, lightweight gas turbine engines depends on the advancement of high-temperature component technology. Shaft horsepower and engine specific fuel consumption are directly related to turbine inlet temperature. Gas turbine engine designs currently operate at turbine inlet temperatures at which the mechanical properties of the most advanced turbine materials limit the engine operating life. Therefore, as turbine inlet temperatures have been raised, highly stressed components such as stator vanes and rotor blades require cooling to obtain reasonable service life. Direct cooling with compressor air is a practical and convenient technique but results in engine performance penalties as a result of cycle and component efficiency effects. In the case of the cycle effect, the air bleed from the compressor bypasses the combustor and therefore does not contribute to the hot working fluid entering the turbine and in fact dilutes the gas temperature where it effuses or is discharged into the main stream. In the case of component effects, the efficiency of blades incorporating air cooling is generally lower than that of solid noncooled blades for several reasons, which include coolant mixing losses and airfoil contour compromises for structural and thermal considerations. These add to the losses in small, low-aspect turbines produced by high Mach number and end wall and secondary flow effects.

Reduction in some of these penalties can be achieved by using an indirect cooling system with a heat transfer fluid or coolant that removes heat from the vanes and blades and regeneratively rejects this heat to compressor discharge air, to the fuel, or to other heat sinks. The indirect cooling concept heat flow path is shown schematically in Figure 1.

The objective of this program was to investigate these indirect cooling concepts and the modulated transpiration cooling concepts to determine effects on engine performance, size, and weight. The airfoil thermal characteristics were to be defined in relation to engine operating conditions and life requirements. Materials selection and methods of fabrication were to be considered for the concepts. Finally, these design analyses were to result in the selection of the most feasible vane and blade cooling concept and testing of the selected vane concept to validate its thermal and mechanical design.

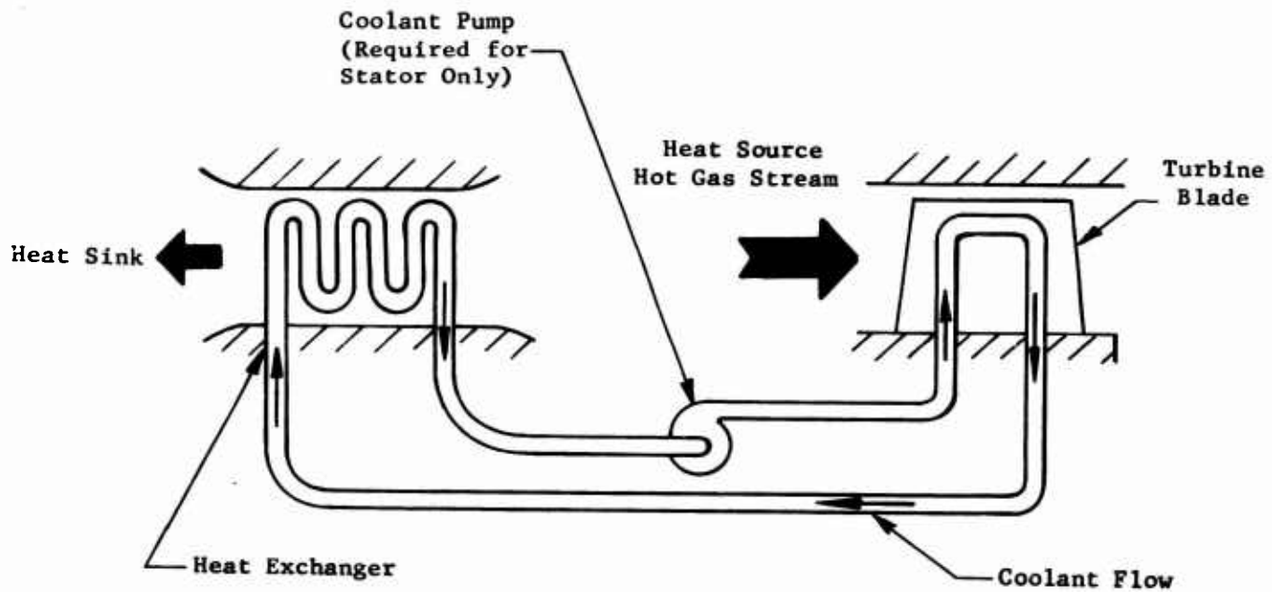

Figure 1. Heat Flow Diagram of an Internally Cooled Turbine.

2.0 CONCEPTUAL ANALYSIS

2.1 ENGINE DESCRIPTION AND DEFINITION OF BLADE/VANE PROFILES

The selection of an engine configuration which essentially satisfies the design parameters specified for this program was simplified by utilizing the preliminary engine design generated during a program for supersonic compressor component research under USAAVLABS Contract DA 44-177-AMC-392(T) (Reference 1). This design, presented in Figure 2, is an advanced non regenerative engine with a variable two-stage free-power turbine providing power extraction at the rear of the engine. The gas generator consists of two spools with a single-stage axial-flow high-pressure turbine driving the centrifugal compressor and a single-stage axial-flow low-pressure turbine driving the axial flow compressor. The design incorporates an annular in-line combustor. This design was used to establish the available envelope for incorporating turbine cooling systems in a typical gas turbine.

The design point performance parameters of the gas generator presented in Figure 2 which were specified for this study are as follows:

Airflow	4.0 lb/sec
Pressure Ratio	16:1
Compressor Adiabatic (Total-Total) Efficiency	80%
Combustor Efficiency	99%
Combustor Total Pressure Drop	3%
Turbine Adiabatic (Total-Total) Efficiency	83-85%
HP & LP Rotor Speed	50,700 rpm
Average Turbine Inlet Temperature	2500°F

Specific fuel consumption and horsepower at the design point was estimated to be .431 and 785, respectively.

The level of efficiency which can be achieved from a small cooled turbine is expected to be significantly lower than that of larger turbines with similar stage loading because mechanical and thermal considerations limit chord and trailing edge thickness to values which are large in comparison to annulus height and blade pitch, respectively. Table I describes the efficiency losses associated with a small size turbine, and therefore, a turbine efficiency of 83-85% was prescribed for this program. The aerodynamic profile of the stator and rotor airfoils were influenced by manufacturing, structural, and cooling considerations. The values for minimum trailing-edge thickness, leading-edge radius and trailing-edge wedge angle

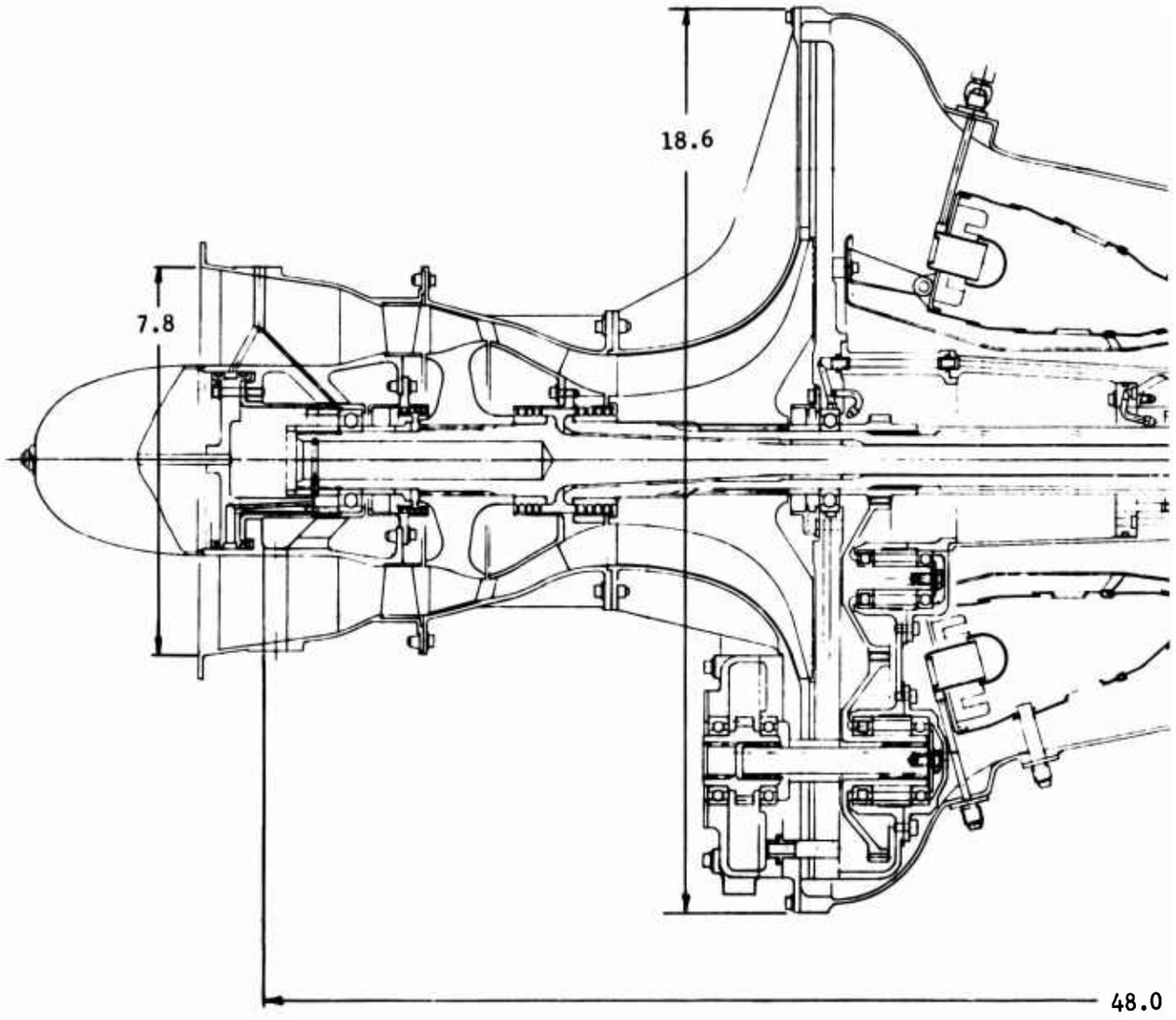

Figure 2. Typical Small Gas Turbine Engine.

1 B

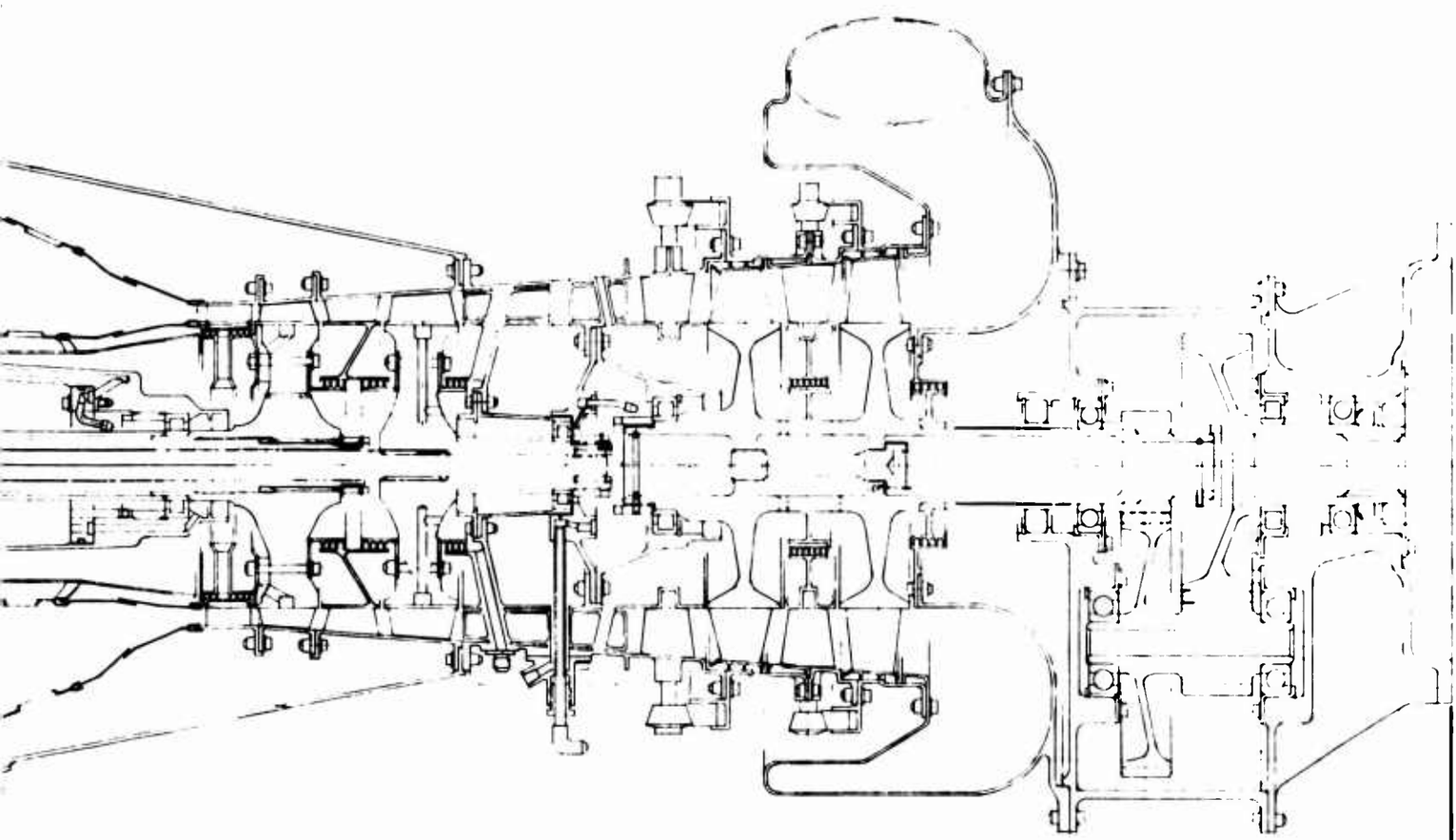

48.0

TABLE I. ADIABATIC (TOTAL-TOTAL) TURBINE EFFICIENCY		
Large Turbine Design		91%
Efficiency Decrement for:		
a) Mach Number Effects	1-2%	
b) Low-Aspect-Ratio Airfoils	3-4%	
c) Blade Changes To Incorporate Cooling	1%	
Total (Average)		6%
Small Turbine Design Efficiency (Excluding Leakage)		85%
Small Turbine Design Efficiency (Including Leakage)		84%

were selected on the basis of design experience to assure good aerodynamics and provide sufficient internal passage area to effectively cool these sections of the blade or vane. The rotor blade area taper ratio was also selected on the basis of design experience with other small cooled turbines to limit the root P/A stresses. These considerations resulted in the following constraints being placed in the airfoil geometry:

Minimum trailing-edge thickness	0.02 in.
Minimum leading-edge radius	0.04 in.
Minimum trailing-edge wedge angle	8° (stator)
Minimum trailing-edge wedge angle	4° (rotor)
Minimum rotor area (hub/tip) taper ratio	1.5
Stator vane area (hub/tip) taper ratio	1.0
Minimum chord	0.8

The HP turbine physical characteristics are as follows:

Mean diameter	6.3 in.
Number stator vanes	37
Stator vane height	0.40 in.
Number rotor blades	36
Rotor blade height at inlet	0.42 in.

Figures 3 and 4 present the airfoil contour of the high-pressure stage stator vane and rotor blade at the mean section.

The combustor is an annular vaporizing design with a temperature pattern factor $\frac{T_{max} - T_{avg}}{T_{avg} - T_{in}}$ equal to 0.20.

Based on extensive experience with annular combustors and the temperature pattern factor of 0.20, the combustor temperature profile over the turbine annulus height was estimated and is presented in Figure 5. This figure established a local peak gas temperature of 2840°F for the stator vane and a maximum gas temperature of 2618°F for the rotor blade.

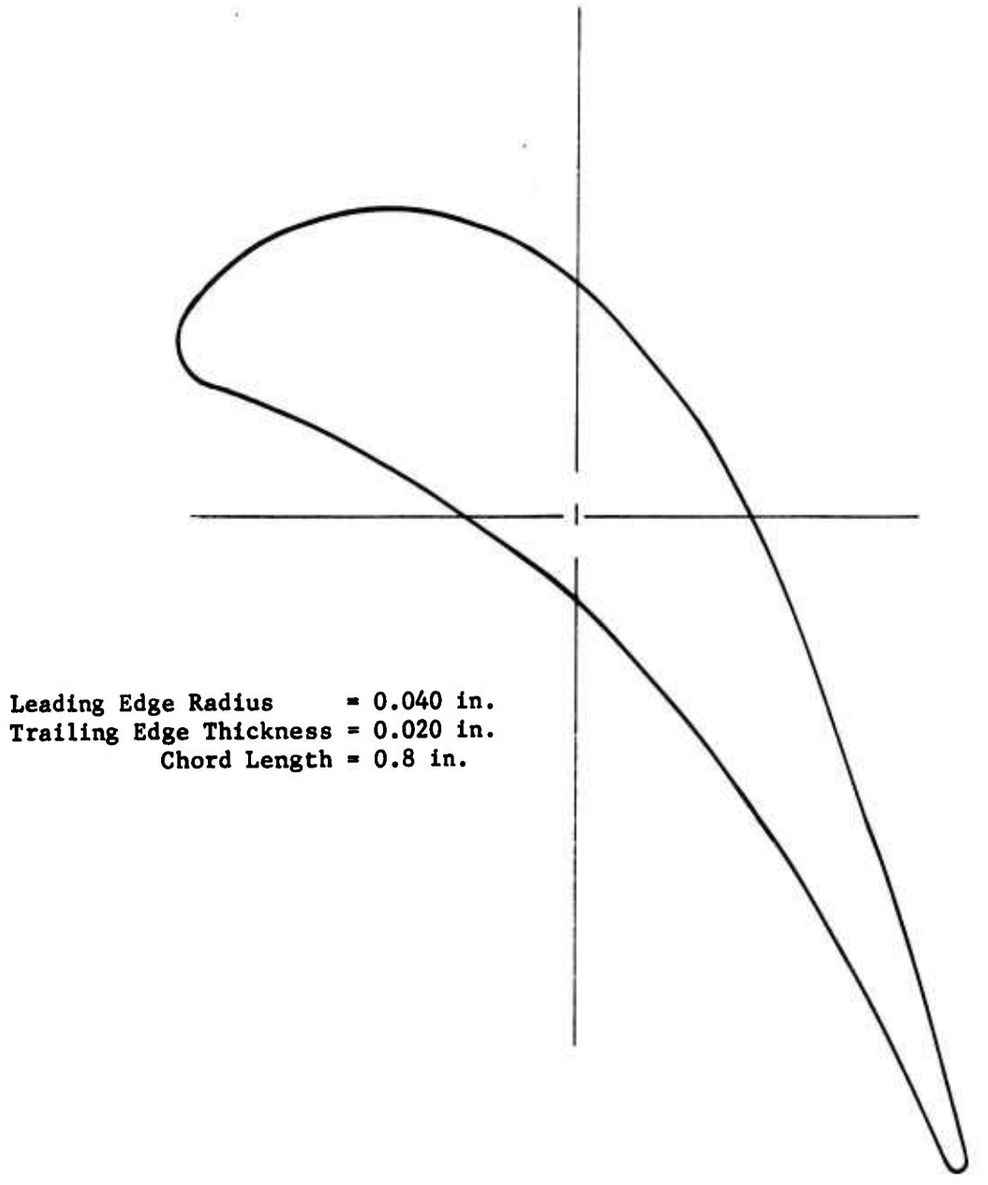

Figure 3. Typical Stator Vane Profile at Mean Section.

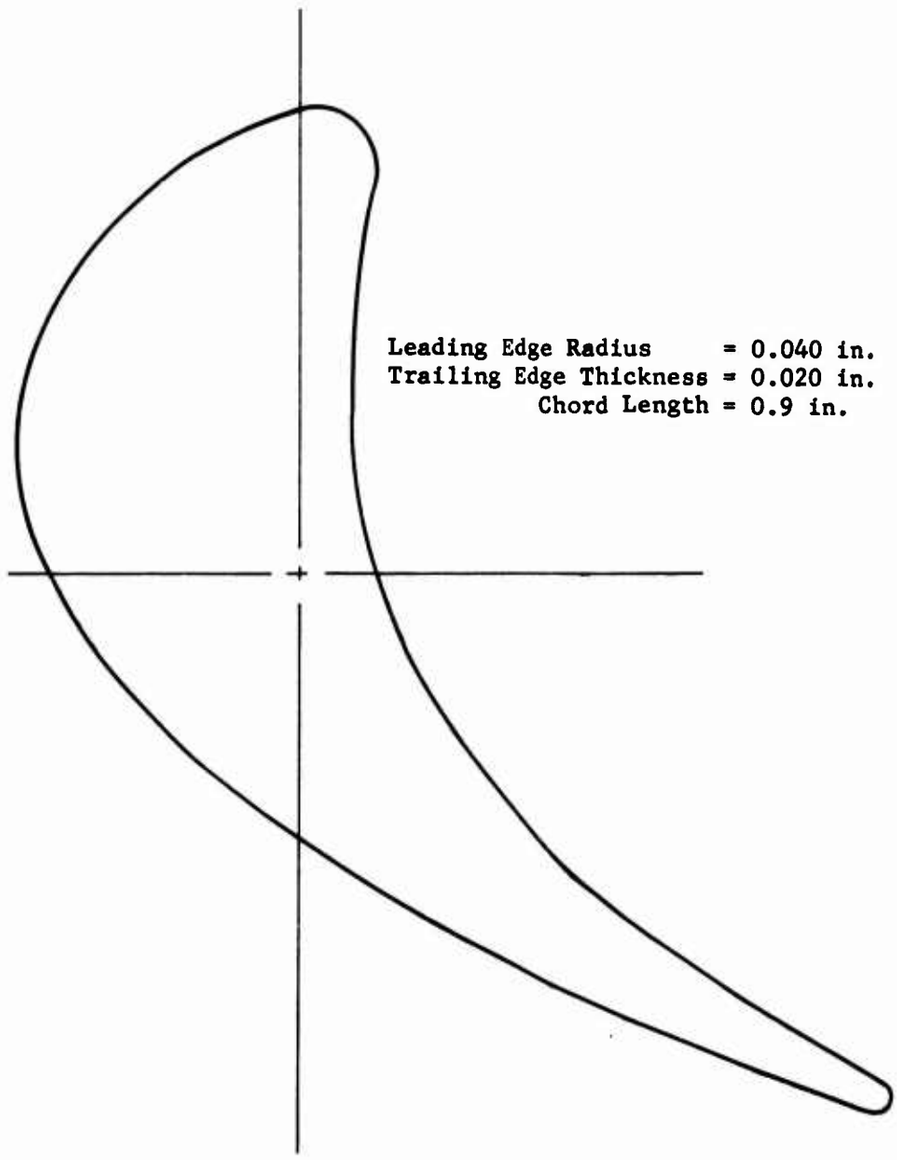

Figure 4. Typical Rotor Blade Profile at Mean Section.

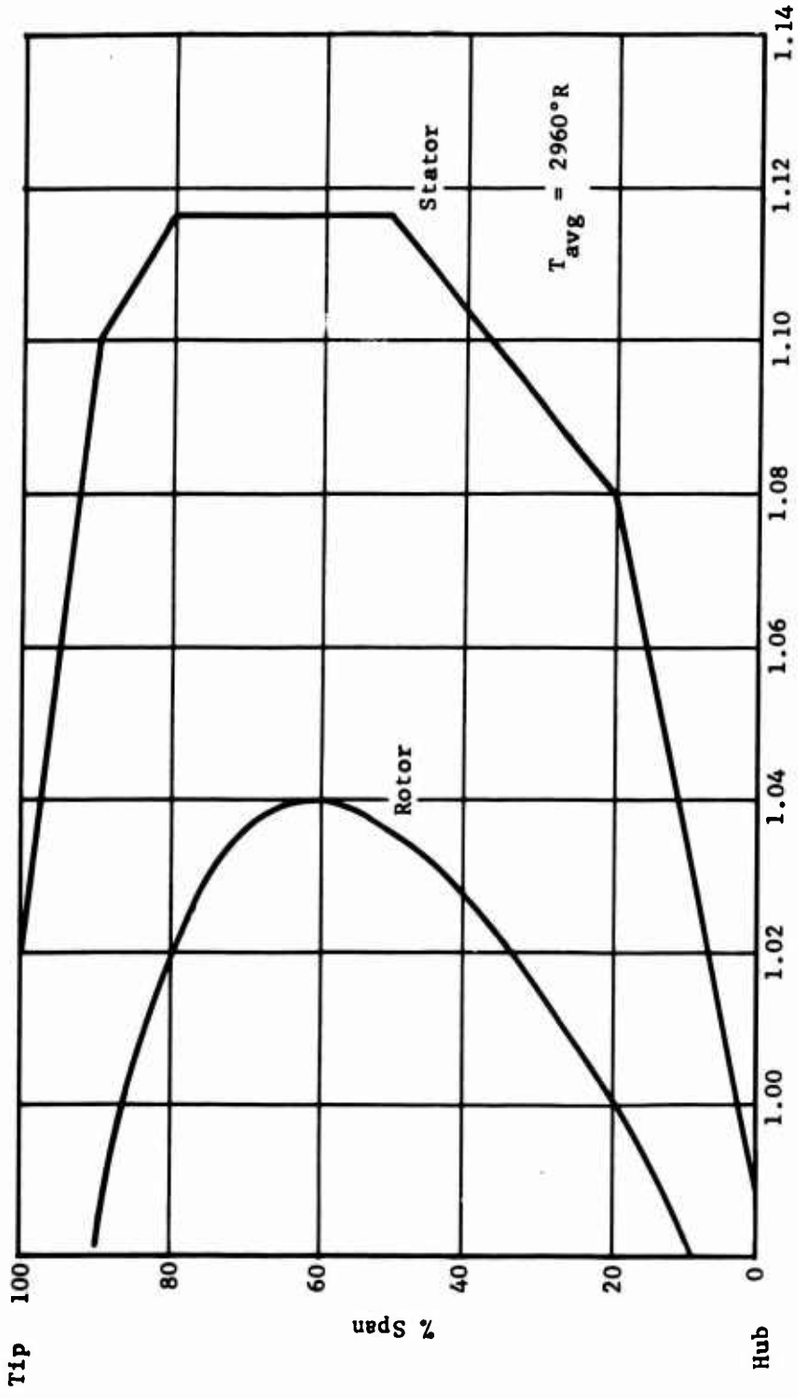

Figure 5. Estimated Combustor Outlet Temperature Profile.

2.2 INITIAL SELECTION OF COOLING METHODS

As gas turbine temperatures have increased, investigators have found it necessary to consider various methods of turbine cooling to maintain or extend the life of the critical engine components. Figure 6 is a flow chart presenting the general classifications of basic cooling methods that may be applicable to turbine blade and vane cooling. From this chart, it is apparent that there are a number of alternative concepts for turbine cooling and a logical approach may be initiated to make a preliminary selection of the cooling concepts for the stator and the rotor that are to be investigated. Two main criteria were followed in this preliminary selection process: (1) the cooling concept should appear feasible for aircraft application and (2) the cooling concept should have significant differences from others selected so that a broad base may be achieved for the evaluation. Referring to Figure 6, the external cooling includes all of the cooling methods currently in use or under development. These include convection, impingement, film and transpiration cooling, and combinations thereof, using compressor discharge air as the airfoil coolant. Of the conventional external cooling methods, transpiration cooling will require the lowest usage of cooling air (Reference 2). This concept would produce the smallest penalty on engine performance of all the external cooling modes as a result of low cooling airflow requirements and therefore was selected to serve as a baseline to evaluate the unproven concepts.

Figure 6 also shows a number of internal cooling methods that include forced or natural (thermosyphon) convection with a liquid or gas as the coolant. For the natural convection method, an open or closed coolant system may be used. The closed system may be fully or partially filled with the coolant. A special case of this system with a liquid coolant utilizes the evaporative cooling method. The heat pipe concept is one example of this case.

The following paragraphs discuss the general considerations for selection of the coolant and heat sink and subsequently review the selection of the five stator vane and five rotor blade cooling concepts.

2.2.1 General Coolant Considerations

The factors which are important include:

1. Good heat-absorbing capacity as exhibited by high values of density, specific heat, or heat of vaporization.

2. Large unit convection coefficients with reasonable velocity.

3. Appropriate melting and boiling points and vapor pressures for the operating temperature range.

4. Compatibility with component materials.

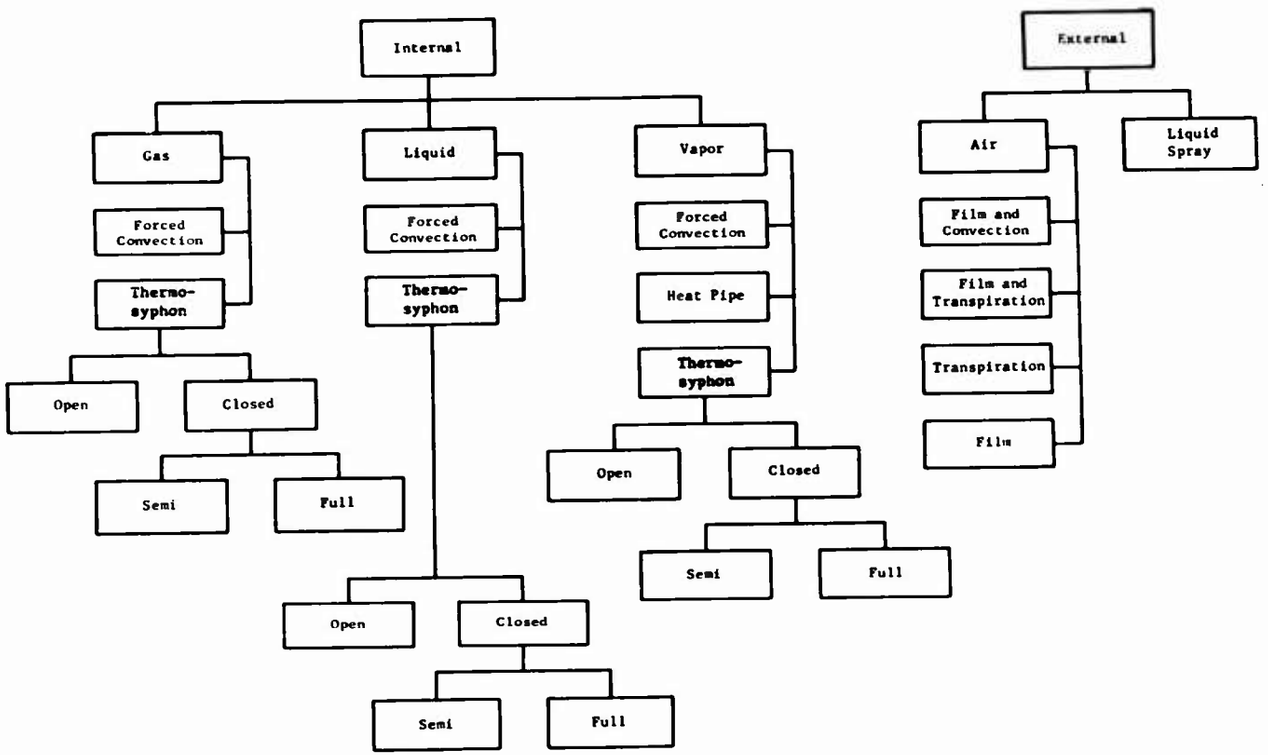

Figure 6. Turbine Cooling Methods.

The first factor is required to obtain a high heat capacity per unit volume which provides a low system volume and reduced weight. Properties of representative fluids which may be used as the coolant are presented in Table II. The second factor insures that the required quantity of heat can be absorbed by the fluid with reasonable cooling passage design and without excessive pressure drop. This is usually evident in such fluid properties as high thermal conductivity and viscosity. Appropriate melting and boiling points and low vapor pressure at high temperatures are required to eliminate problems associated with melting at startup and solidification at shutdown and excessively high system pressure requirements. Material compatibility is required for design feasibility especially where corrosive fluids are used as the coolant.

In the selection of a cooling fluid, an important consideration is its ability to remove heat from a solid surface which is proportional to its convection coefficient. This coefficient depends in turn on the fluid properties and coolant passage geometry. The convection coefficient h can be expressed as

$$h = \frac{q}{A(T_s - T_f)} \qquad (1)$$

Representative convection coefficients that can be obtained with a gas, a liquid, and a liquid metal are shown in Table III.

It is evident that higher coefficients can be attained with liquid metals and that boiling is especially effective. The significance of high coefficients is that for a given amount of heat to be absorbed, either less contact area is required or a lower temperature difference is sustained, or both. This in turn means fewer or smaller cooling passages.

An initial estimate of the turbine stage total heat load was calculated by assuming an average gas side heat transfer coefficient of 230 Btu/hr ft^2 °F (Reference 3), and using heat transfer surface area of .525 ft^2 calculated from the airfoil presented in Figure 3. An estimate of 1500°F for the bulk temperature of the airfoil was based on two factors: (1) the turbine blade material properties at temperatures above 1500°F will generally provide low stress rupture or thermal fatigue life for highly stressed blades or vanes; and (2) the leading and trailing edge sections, where the heat flux is highest, may produce large temperature gradients with local airfoil metal temperatures of 1700° to 1800°F.

Using these inputs and the equation $q = hA\,(T_f - T_s)$, the total vane heat load for the design condition of 2500°F stator inlet temperature was calculated to be 120,000 Btu/hr.

Based on this heat load and an estimated coolant temperature of 1000°F, the coolant flow rates are calculated from the equation

$$W = \frac{q}{C_p\ \Delta T} \qquad (2)$$

TABLE II. PROPERTIES OF REPRESENTATIVE HEAT TRANSFER FLUIDS

(REFERENCES 4,5)

	Average Coolant Temperature*(°F)	Specific Heat (Btu/lb °F)	Heat of Vaporization (Btu/lb)	Density ($lb\ m/ft^3$)
Gas				
Air at 2500 psia	1250	.27	-	3.89
Helium at 2500 psia	1250	1.24	-	0.53
Hydrogen at 2500 psia	1250	3.62	-	0.39
Liquid				
Sodium-Potassium	1450	.21	1400	41.8
Sodium	1450	.31	1615	39.4
Potassium	1450	.19	840	40.8
Water at 1000 psia	545	1.00	649	46.4

* Estimate of the average inlet to outlet coolant temperature in the blade or vane.

TABLE III. REPRESENTATIVE CONVECTIVE COEFFICIENTS	
	Btu/hr ft^2°F
Air, forced convection	5 - 100
Water, forced convection	50 - 2000
Water, boiling	500 - 10,000
Liquid metal, forced convection	3000 - 15,000
Liquid metal, boiling	3000 - 20,000

and are presented in Table IV. In descending order, the minimum mass flow rates are obtained with vaporizing liquids, gases (other than air), air, and liquids. However, when volumetric flow rates are considered, the vaporizing liquids are lowest while the nonvaporizing liquids follow with gases requiring the highest volumetric flow rates. Since weight of a cooling system will vary with volumetric flow rate, evaporating liquids and then nonevaporating liquids are potentially more attractive heat transfer fluids than gases, when considering system size.

Two criteria for selecting the heat transport fluid were used. In the case of forced convection, the second term of the right side of the equation describing the heat transfer coefficient in Appendix I is used in the following form:

$$(C_p \mu/k)^{.67}/\rho \tag{3}$$

A fluid with a low value for the above would be superior since this would yield a high value for the heat transfer coefficient. The above term is only dependent on physical properties of the fluid. The magnitude of the other term in the equation of Appendix I

$$.023\left(\frac{VCp}{Re^{.2}}\right) \tag{4}$$

can be influenced by modifying the mass flow rate and coolant passage geometry.

In the case of natural convection, the second term of the right side of the equation describing the heat transfer coefficient in Appendix II is used in the following form:

$$(\rho C_p)^2 (k)^2 \beta \tag{5}$$

TABLE IV. REPRESENTATIVE COOLANT FLOW RATES

	Nonvaporizing		Vaporizing	
	Mass Flow Rate (lb/hr)	Volumetric Flow Rate (ft^3/hr)	Mass Flow Rate (lb/hr)	Volumetric Flow Rate (ft^3/hr)
Gas				
Air	980	252	-	-
Helium	213	402	-	-
Hydrogen	73	187	-	-
Liquid				
Sodium-Potassium	1256	30.1	94.3	2.25
Sodium	853	21.6	81.7	2.08
Potassium	1390	34.1	157.0	3.84
Water	264	57.0	204.0	4.40

This term also contains only fluid-dependent terms. A fluid with a high value for the above would be superior since this would yield a high value for the heat transfer coefficient.

Table V lists typical values for the forced and natural convection criteria of a wide range of heat transport fluids. The values were calculated using fluid properties obtained from References 4 and 5. Table V shows that properties of natural convection gases such as hydrogen or helium are as attractive as liquid metals from a heat transfer standpoint. For forced convection, liquids are substantially better than gases. Among the liquids, low melting point and high boiling point also are important considerations in the final selection. For all coolants, considerations such as pumping requirements, thermal stability, difficulty of sealing, cost, availability, corrosiveness at operating temperatures, materials compatibility, safety, etc., would have a significant influence on the selection of the coolant.

2.2.2 General Heat Sink Considerations

The heat that has been absorbed by the heat transfer fluid from the airfoils must be rejected to a heat sink. Potential heat sinks include the compressor discharge air and the fuel. Ram air represents a nonregenerative system and therefore was not considered. Oil or hydraulic fluid was not considered appropriate since the sink capacity would be limited.

The compressor discharge air stream has significant heat sink capabilities. Based on the previously estimated first stage turbine heat load and a compressor discharge air mass flow rate of 4 lb/sec, the temperature rise of cooling air was calculated from equation (2) to be 34°F. If consideration is given to cooling a second stator row, the total temperature rise of the air would be approximately 51°F. These low values for temperature rise indicate that the heat transfer requirements could be accomplished by a relatively small heat exchanger.

Aircraft fuels also have a heat sink capacity. For an assumed 100% power fuel flow rate of 400 lb/hr which is representative of a small gas turbine and the first stage turbine heat load previously presented, the fuel temperature rise would be approximately 610°F. NASA (Reference 6) has heated ASTM Jet A fuel to 700°F above its critical pressure and measured carbon and coke deposition. At pressures above 350 psi with deoxygenated fuel, incipient deposits occur from 570°F to 705°F wall temperatures. Thus, if fuel is used to absorb the heat load, the temperature rise would be above the point of deposition in a low-pressure fuel system. However, use of JP fuel to cool a blade row, such as the high-pressure rotor, may be practical from a coking standpoint due to the lower heat transfer load.

TABLE V. - COOLANT SELECTION PARAMETERS

Gas	Natural Convection Criteria* ($x10^{-10}$)	Forced Convection Criteria**
Helium	29,800	2.75
Hydrogen	166,000	5.12
Air	2,540	0.40
Methane	24,200	1.10
Steam	20,900	0.63
Neon	1,360	0.37
Krypton	52.6	0.09
Xenon	82.1	0.12
Nitrogen	1,810	0.39
Mercury Vapor	90.5	0.0094
Argon	185	0.192

Liquid	Natural Convection	Forced Convection ($x10^{-2}$)	Melting Point (°F)	Boiling Point (°F)
NaK	3.36	6.95	10	1540
Pb - Bi	0.222	.85	257	3038
Cesium	-	2.3	83	1274
Bismuth	0.435	.68	520	2691
Sodium	37.7	4.84	208	1621
Lead	3.64	.79	622	3171
Potassium	3.83	4.75	147	1400
Mercury	23.6	.50	-40	675
Water	0.0716	8.60	32	212
Tin	15.4	1.28	450	4118
JP-4	0.004	0.20	-65	—
Lithium	24.3	78.11	354	2403

2 Phase	Latent Heat (Btu/lb)	Melting Point (°F)	Vapor Pressure At 1400°F (psi)
Water/Steam	900	32	-
Hg	125	-40	1180
Na	1810	208	4.14

* High value desired
** Low value desired

NASA studies (Reference 7 and 8) indicate the potential of methane as an alternate fuel for gas turbine engines for some aircraft applications: methane (a) offers a higher heating value, which should result in a reduced specific fuel consumption, and (b) has good availability. Therefore, alternate fuels were considered as useful in this turbine cooling study as heat sinks or as direct coolants. For example, liquid methane, when heated from -280°F to 1000°F, absorbs about 1000 Btu/lb. On this basis, the stage heat load could be absorbed by 120 lb/hr of methane. Although cryogenic fuels offer a large heat sink potential, they present problems not encountered with conventional jet fuels. These problems include the design requirements to account for the large volumetric changes and thermal expansion rates. Also, special handling and storage of the fuel would add to the normally difficult logistics problems.

2.2.3 Selection of Five Stator Cooling Concepts

The selection of five turbine stator and five rotor cooling concepts for investigation was directed at including the broadest range of system variables which would benefit engine performance and meet the 1000-hour turbine life requirements.

To obtain a wide range of system variables, the following basic, forced convection, contained coolant system concepts for the stator were initially selected for investigation:

1. Liquid-metal system
2. High-pressure gas system
3. Two-phase vaporizing system

The heat pipe concept, which represents an advanced liquid metal vaporizing system, was included as the fourth selection. Finally, the modulated transpiration air cooling system was included since it represented the method for minimum usage of cooling air among the external air cooling methods.

To select the coolant, the data presented in Tables II through V was reviewed. All the liquid metals have good heat transfer characteristics, but their high melting points or low boiling points eliminate many. Only mercury, the eutectic alloy of sodium-potassium, in addition to water, and fuel have melting points sufficiently near or below ambient to be considered. For engine start-ups in cold weather, the pumping of the coolant will not occur if the coolant is below its melting temperature. Therefore, selection of a coolant which has a low melting temperature is desired. However, the cold weather start-ups could be achieved by heating the coolant through (a) false starts or (b) electric or space heaters.

Another approach to this problem involves the use of an additive to lower the melting temperature. In the case of Nak-78, the addition of 40% by

weight of cesium will lower the melting temperature of the eutectic alloy to -65°F.

The eutectic alloy of sodium and potassium has found increased use in recent years as a coolant in heat exchangers and rocket nozzles. Its chemical and mechanical properties have been well established by government and private agencies (Reference 9). Although it is corrosive to some materials, sufficient data exists to specify its use in systems where high nickel or cobalt content alloys and the 300 series of stainless steels are used.

Mercury has been used for many years by the steam generating industry, and sufficient data exists to warrant its application to this cooling concept from heat transfer considerations. However, the corrosiveness and high toxicity make its application hazardous.

Water and fuel (JP) could be acceptable coolants, but both are temperature limited -- water by its low critical point, and fuel by its propensity for coking. In addition, if the coolant temperature is too low, high thermal wall gradients could exist in the vanes and result in premature airfoil buckling and cracking.

From these considerations, the liquid metal eutectic mixture of sodium and potassium was selected as the coolant.

In considering gases for the stator cooling application, mercury vapor appears to have a distinct heat transfer advantage, but its highly corrosive properties make it undesirable. The rare gases krypton and xenon also have a slight advantage, but limited properties data are available. Of the remaining gases, no distinct heat transfer advantages are apparent, and air, being most available, and with well defined properties, was selected as a representative gaseous coolant.

For the two-phase system, water was selected as the coolant. Other coolants considered were mercury and sodium. Mercury has a low latent heat of vaporization and a high vapor pressure, both of which are undesirable for this application. The melting point of sodium is marginal for this application and may have resulted in a redundant concept since the sodium/potassium alloy had been previously specified for the liquid system.

The selection of potassium as the heat pipe fluid is described in section 2.3.

The compressor discharge air was specified as the heat sink for the liquid metal, high-pressure air, and heat pipe concepts. The low operating temperature of the two-phase water steam system requires a low temperature heat sink, and fuel was specified which coincidentally added completeness to the study.

The five stator vane cooling concepts selected for study are summarized in Table VI, and the preliminary design arrangements are described in the following pages.

TABLE VI. STATOR VANE COOLING CONCEPTS

Basic Concept	Coolant	Method of Heat
Liquid Metal	Sodium-Potassium Alloy	Compressor Discharge Air
Gas	Air	Compressor Discharge Air
Two Phase	Water	Engine Fuel
Heat Pipe	Potassium	Compressor Discharge Air
Modulated Transpiration	Compressor Discharge Air	Not Required

Modulated Transpiration Cooled Concept

Transpiration air cooling is an external or direct cooling method which uses compressor discharge air as the coolant. For this design the vane consists of a load-carrying ribbed strut and a porous airfoil which forms the aerodynamic gas passage. The airfoil is weld-attached to the strut along the ribs. The ribs form spanwise cooling air passages with the airfoil. Each passage receives the coolant which is extracted from compressor discharge air and metered at the blade butt. The cooling air effuses through the porous airfoil into the boundary layer on the hot gas side and forms a relatively cool air film, insulating the airfoil surface from the hot gas stream.

The feasibility of this concept has been demonstrated in engines or turbine stage rotating rigs over an airflow range of 3 lbs/sec to 168 lbs/sec and at average gas temperatures up to 2750°F (References 10, 11 and 12). The vane cooling requirement is sized as a percentage of engine airflow for the 100% design point conditions. For part-power conditions where a high degree of vane cooling is not required, the cooling airflow as a percentage of engine airflow remains constant. Hence, at the part-power conditions the cooling airflow rate is in excess of the vane design requirements.

To eliminate this penalty a concept has been defined whereby the transpiration cooling airflow is modulated at reduced power engine operation.

Figure 7 presents a representative transpiration-cooled turbine design which incorporates cooling airflow modulation. The vane incorporates a partition which separates the cooling air plenum feeding the leading-edge cooling passage from the plenum feeding the other passages in the vane. Thus the leading-edge passage is supplied with cooling throughout the engine operating regime in order to prevent the inflow of gas at the stagnation region of the airfoil. The other passages are supplied with compressor discharge air metered through a ported valve ring which translates fore and aft to increase or decrease the flow area of the valve ports. At the 100% power condition, the valve would be positioned forward and throttling of the cooling air would not occur. At part-power conditions, the valve would be positioned rearward to achieve varying degrees of throttling. At low power settings where the gas temperatures are low, the valve ports would be closed to preclude cooling airflow to the stator vane plenums and the rotor blades. For the closed position of the valve, cooling air is introduced to purge the labyrinth seals.

An alternate method of throttling the cooling air to the stator vanes utilizes a poppet valve in the trunnion or stem of each stator vane. Radial or rotational motion of the valve disk would open or close ports in the wall of the vane trunnion. This would provide throttling of the cooling air to the metering orifice at the hub plenum of the vane which feeds the spanwise cooling air passages. Use of a partition in the trunnion and plenum would again assure cooling airflow to the leading edge at all power settings.

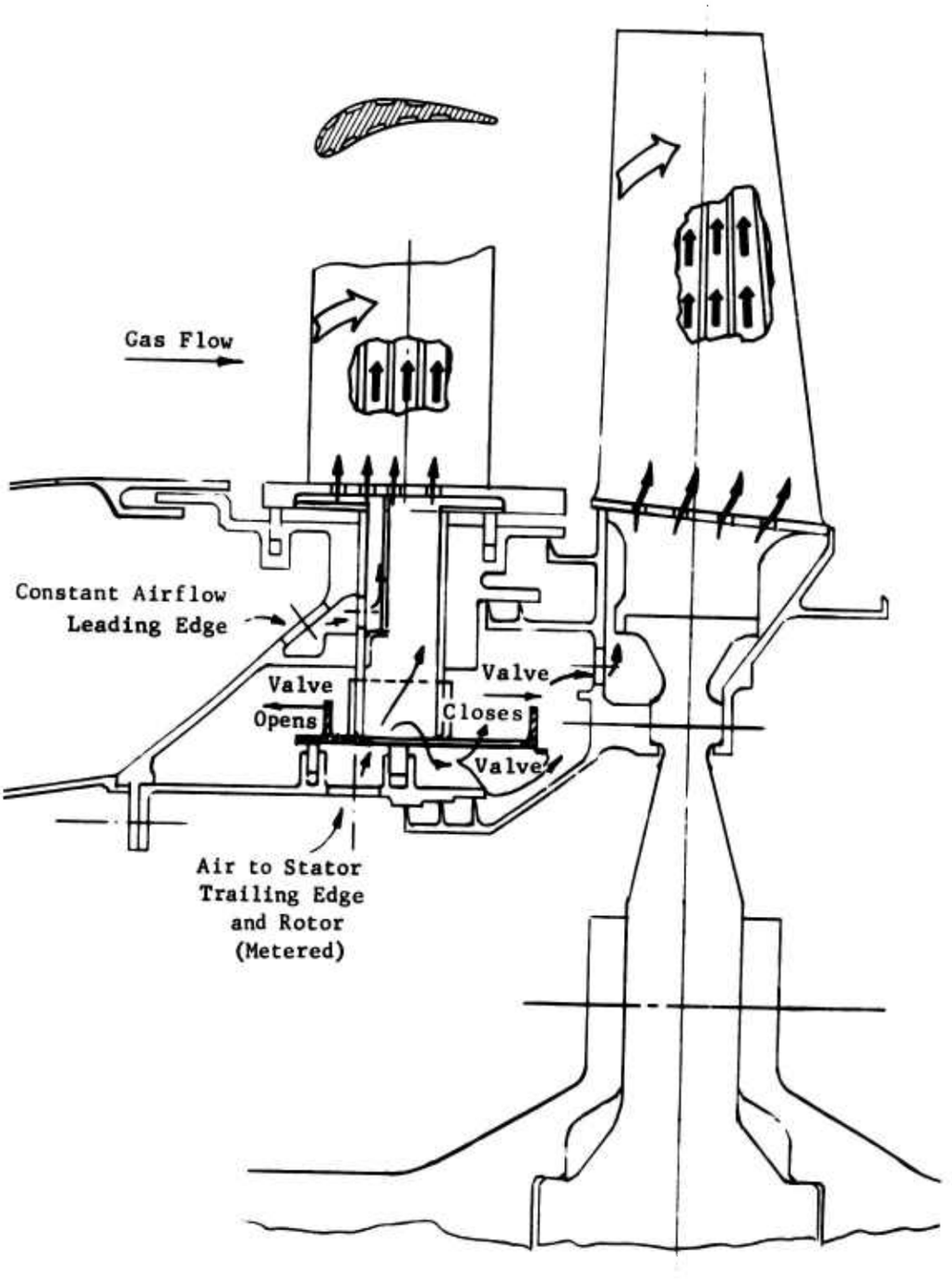

Figure 7. Stator and Rotor Transpiration Air Cooling - Modulated Flow.

Valve movement of the designs described may be accomplished by conventional actuators powered by hydraulic, pneumatic, electrical or mechanical systems.

Modulation designs similar to those described have been tested in rig or prototype engines. However, incorporation of this concept into a flight engine would require the design of an appropriate sensing and control system which would actuate the valve as changes in engine power level occurred. The control system instrumentation would establish that a power level change was in process or had been completed through measurement of significant engine parameters such as gas temperature, compressor discharge pressure, rpm, etc. For an engine with a variable-geometry free power turbine, sensing the gas generator rpm may be unsatisfactory since rpm varies over a small range and is disproportionate to the power level. Therefore, to select the appropriate parameter, a study would be required of the engine state conditions over the full range of power settings.

Although the control system design was not within the scope of this contract, the effects of the cooling air modulation concept on engine performance was calculated and the design complexity was evaluated in relation to other selected concepts.

Liquid Metal Cooling Concept

A preliminary design scheme to show a general arrangement for the liquid metal cooling concept is presented in Figure 8. Cooling the vanes is accomplished by circulating the liquid metal through a thin-wall vane with multiple coolant passages. Each vane is connected to inlet and outlet headers which in turn are connected to a finned tube annular or sectored heat exchanger in the compressor discharge flow path. Circulation of the liquid metal (NaK-78) is accomplished by a rotary induction (permanent magnet) pump driven by a hydraulic motor or the accessory drive gearbox.

The liquid metal makes two passes through the vane. For the first pass, liquid metal enters the leading-edge coolant passages at the vane tip plenum and travels spanwise to the butt plenum. For the second or return pass, liquid metal enters the mid-chord and trailing-edge coolant passages at the butt plenum and travels spanwise to the tip plenum.

The heat exchanger incorporates thin-wall finned tubes formed in a two-pass serpentine configuration to provide cross-counterflow conditions. The finned tubes are attached to inlet and outlet headers which are connected by piping to the vane assembly and pump, respectively. The finned tube rows are positioned on a triangular pitch. This design offers a compact, high-effectiveness and low-pressure-drop exchanger and is based on advanced liquid metal regenerator development described in Reference 13.

The liquid metal system characteristics include the high coolant operating temperature, and the small difference between the airfoil and the coolant temperatures. This combination will produce a uniform thermal distribution in the vane. In addition, the required coolant pressure is low. This

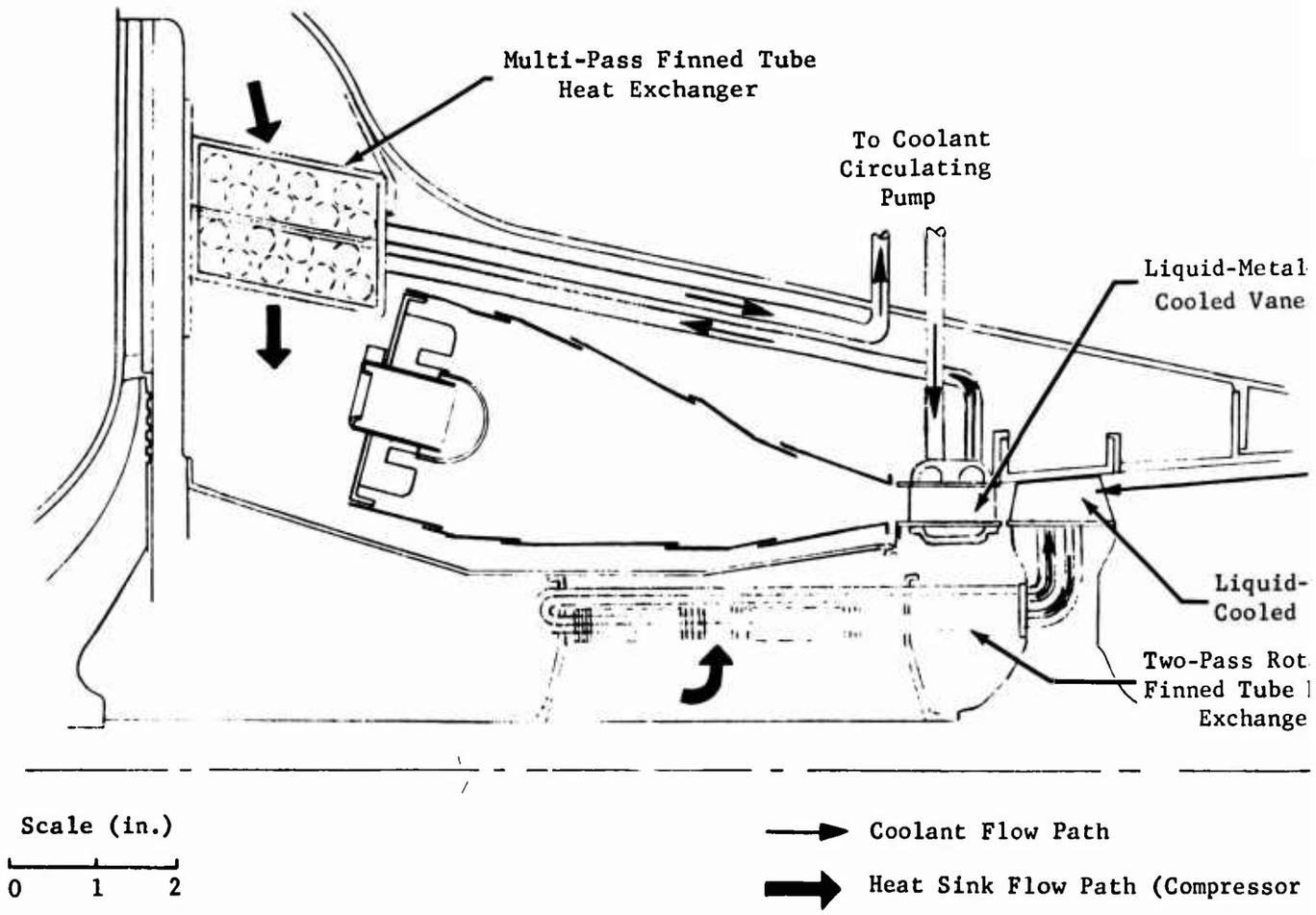

Figure 8. Liquid-Metal-Cooled Stator Vane and Rotor Blade Concepts.

1 B

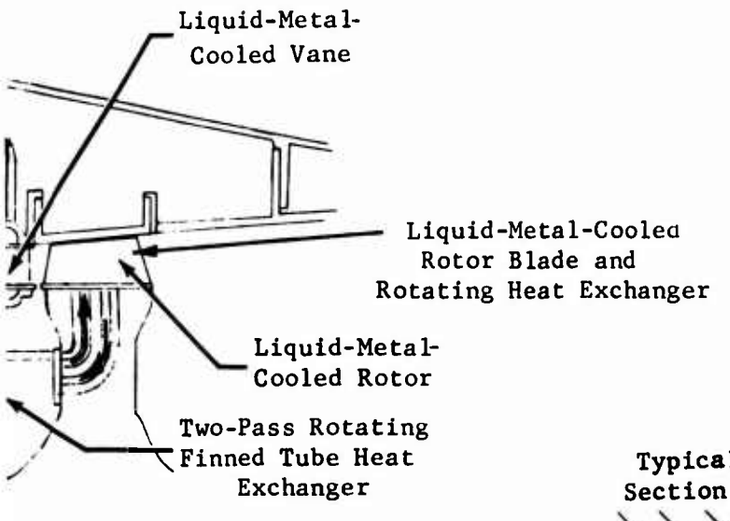

Flow Path

ık Flow Path (Compressor Air)

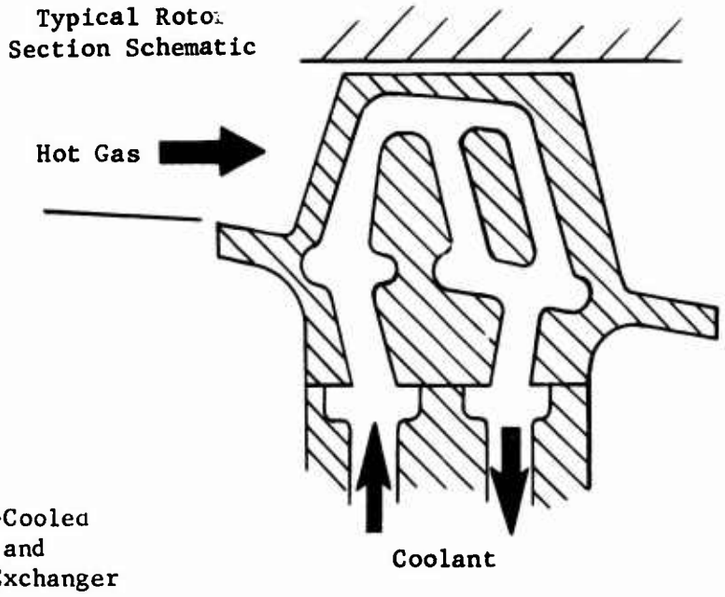

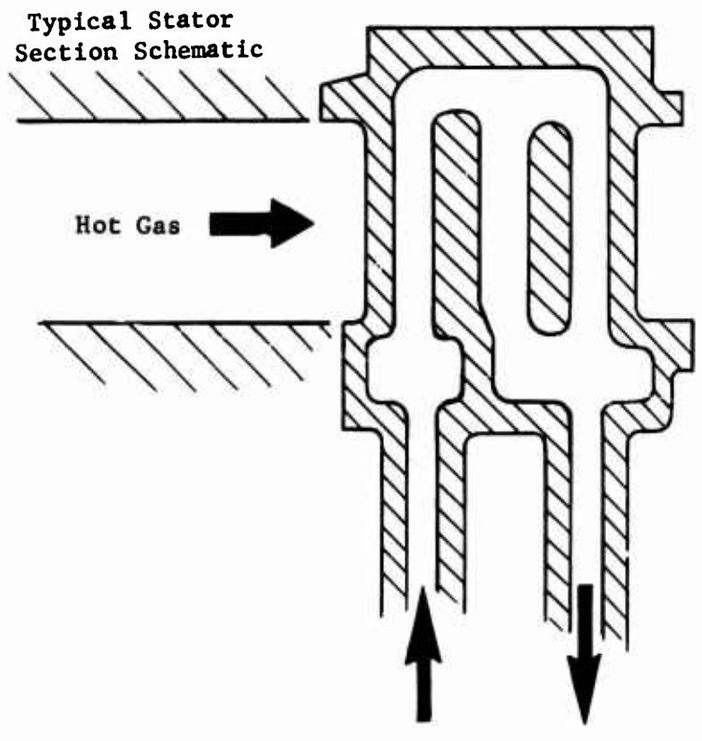

2 1a

allows flexibility in the passage sizing to provide favorable heat transfer characteristics. The system is designed for installation or removal as a completely integral and hermetically sealed unit (including stator assembly, heat exchanger, pump, expansion system and piping) to avoid handling the liquid metal or exposing it to the atmosphere.

Joining of the details and subassemblies to form the integral assembly is accomplished by welding. Selection of materials that are compatible with liquid metals is necessary, but a large group of candidate alloys is applicable.

High-Pressure Air Cooling Concept

The general arrangement of the high-pressure air-cooled vane concept is presented in Figure 9. The geometric design of this concept is similar to the liquid metal. However, more stringent design requirements are placed on the overall system. To obtain the necessary heat transfer coefficients and coolant mass flow rates, the closed system is highly pressurized. The pressure requirement must be balanced with stress analysis to obtain an acceptable vane life.

The coolant makes two passes in the vane as described for the liquid-metal concept. Circulation of the coolant is accomplished by a boost pump, located in the coolant piping between the nozzle and heat exchanger. The pump is only required to overcome the system pressure loss.

The heat exchanger is a plate and fin brazed unit located in the compressor discharge flow path.

This nozzle and exchanger component is also designed as an integral unit, and the use of furnace brazing or welding techniques could be applied for the assembly of the component.

Two-Phase Water/Steam Cooling Concept

A cooling concept using a two-phase fluid to cool the vanes consists of introducing water, under high pressure, into the vane passages. The water is vaporized by the heat load of the vanes. The steam is pumped to a finned-tube exchanger in the fuel system, where the latent heat of vaporization is removed and the water is recirculated to the vanes by a pump.

The coolant makes two passes through the vanes as described for the liquid metal concept.

Use of the engine fuel to cool the steam will at design point fuel flow increase the bulk temperature of the fuel to 304°F. Locally, on the exchanger heat transfer surface the fuel temperature may reach 500°F, which is above the coking temperatures of current jet engine fuels.

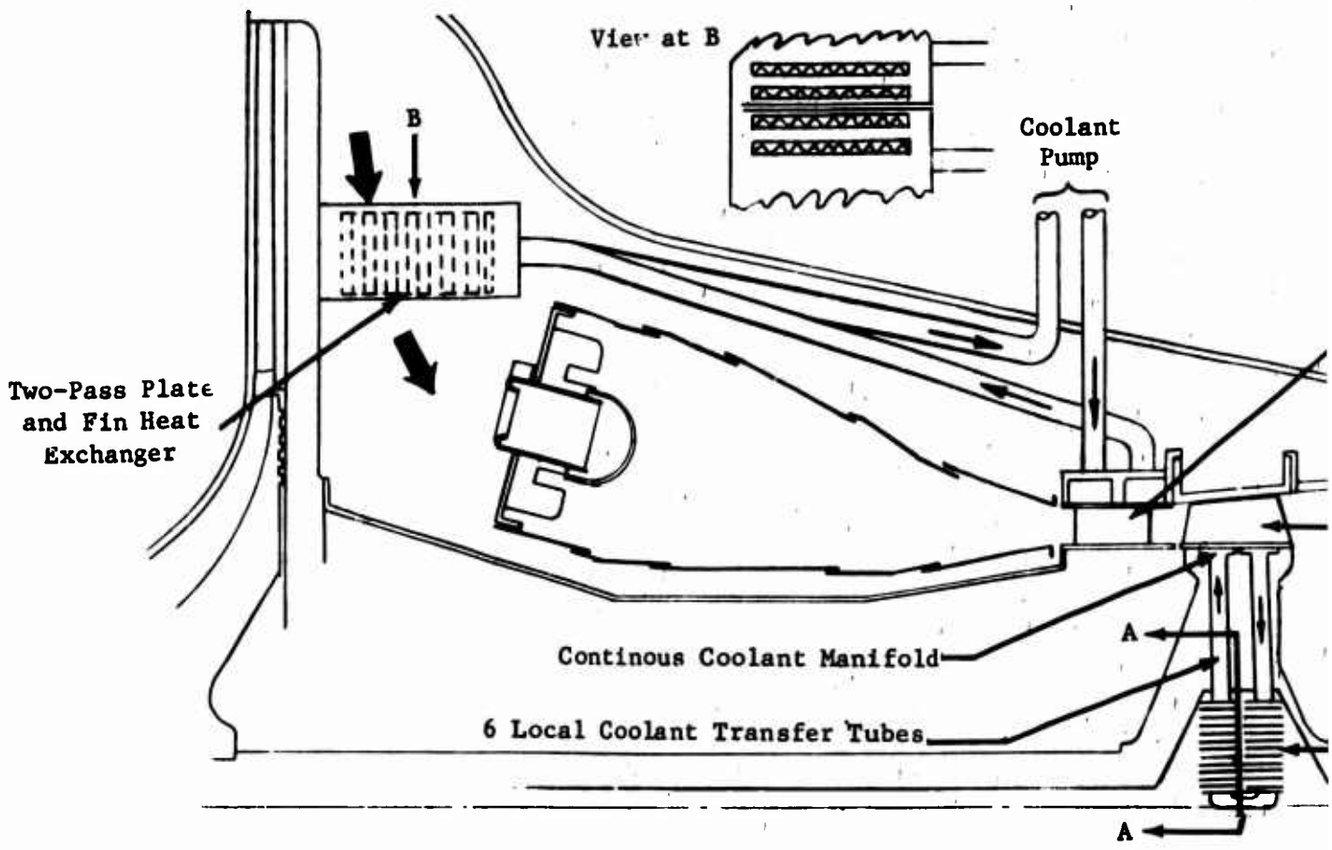

Figure 9. High-Pressure Air-Cooled Stator and Rotor Concepts.

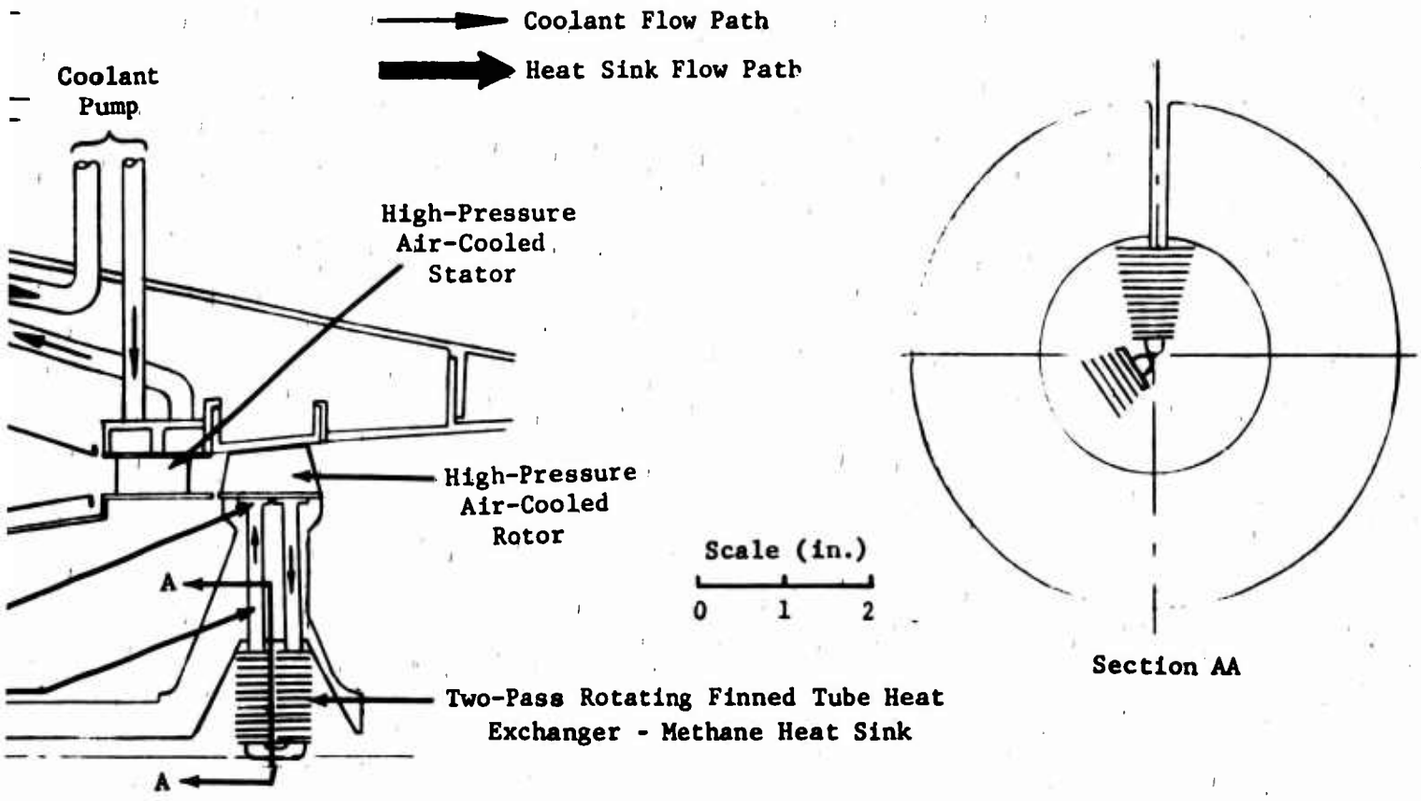
Coolant Flow Path
Heat Sink Flow Path
Coolant Pump
High-Pressure Air-Cooled Stator
High-Pressure Air-Cooled Rotor
A
A
Scale (in.)
0 1 2
Two-Pass Rotating Finned Tube Heat Exchanger - Methane Heat Sink
Section AA

Heat Pipe Cooling Concept

The heat pipe concept, shown schematically in Figure 10, consists of a hollow closed tube. The inner surface of the tube is lined with a porous mesh tube used as a capillary wick. The mesh is saturated with an appropriate liquid, whose vapor occupies the remaining internal volume. The addition of heat over the evaporator section of the heat pipe causes the evaporation of liquid from the mesh. This vapor travels along the inner diameter of the heat pipe and condenses at the region where heat is being removed. The condensate then returns to the evaporation region via the capillary mesh to complete the cycle.

The internal flow of liquid and vapor and hence the continuous transport of heat from the evaporator to the condenser section is maintained by pressure differentials across the liquid-vapor interface. These differentials result from the finite curvature which develops in the liquid-vapor interface as liquid withdraws into the pores of the capillary mesh in the evaporator and accumulates in the pores of the condenser section. When operating within design restrictions, the transfer of heat along a heat pipe is accomplished almost isothermally.

A preliminary design arrangement utilizing the heat pipe concept for cooling the turbine stator vanes is presented in Figure 11. The heat pipe design of the vane (or evaporator) section and the heat exchanger (or condenser) section is shown in Figure 12. Each vane incorporates an internal airfoil-shaped capillary mesh liner which is connected through a mesh transition section to a 10-inch-long capillary mesh tube in the condenser section. Each condenser tube is encased in a finned tube and compressor discharge air flows over the finned tube prior to entering the combustor. This tube makes an angle of 8 degrees with the engine axis. This angle is selected to minimize the effective height of the heat pipe in order to maintain a low head which must be overcome by capillary forces.

The wick inside the finned tube is 0.003 inch thick and has a maximum effective pore diameter of 20 microns and a porosity of 30%. The wick is made of a 300 series stainless steel.

A 0.009-inch-thick liquid metal flow annulus between the wick and the finned tube extending the length of the condenser section is provided as an additional coolant flow return path to minimize coolant pressure loss. This annulus height is maintained by locally dimpling the wick.

The wick inside the hollow stator vane is identical in material thickness, pore size and porosity to the wick in the condenser section. However, the liquid metal flow annulus provided between the wick and the vane wall is reduced to 0.004 inch thick as a result of the reduced wick length in the evaporator section.

Since the wick cannot physically fit sufficiently into the trailing edge region (extending about 3/16 inch), it is necessary to increase the vane's

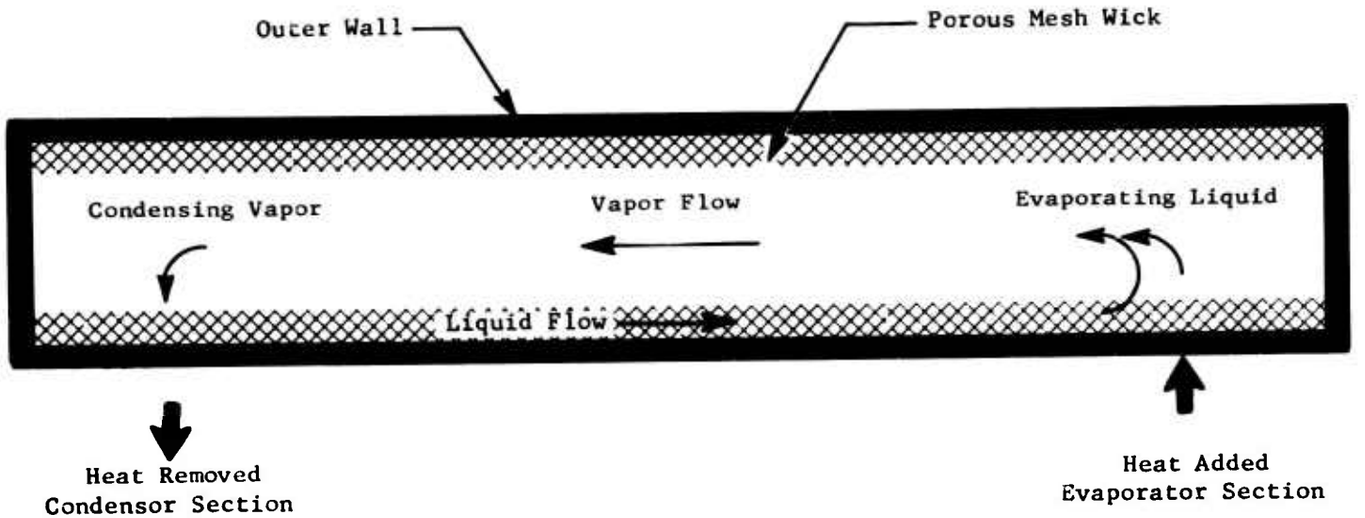

Figure 10. Heat Pipe Concept Schematic.

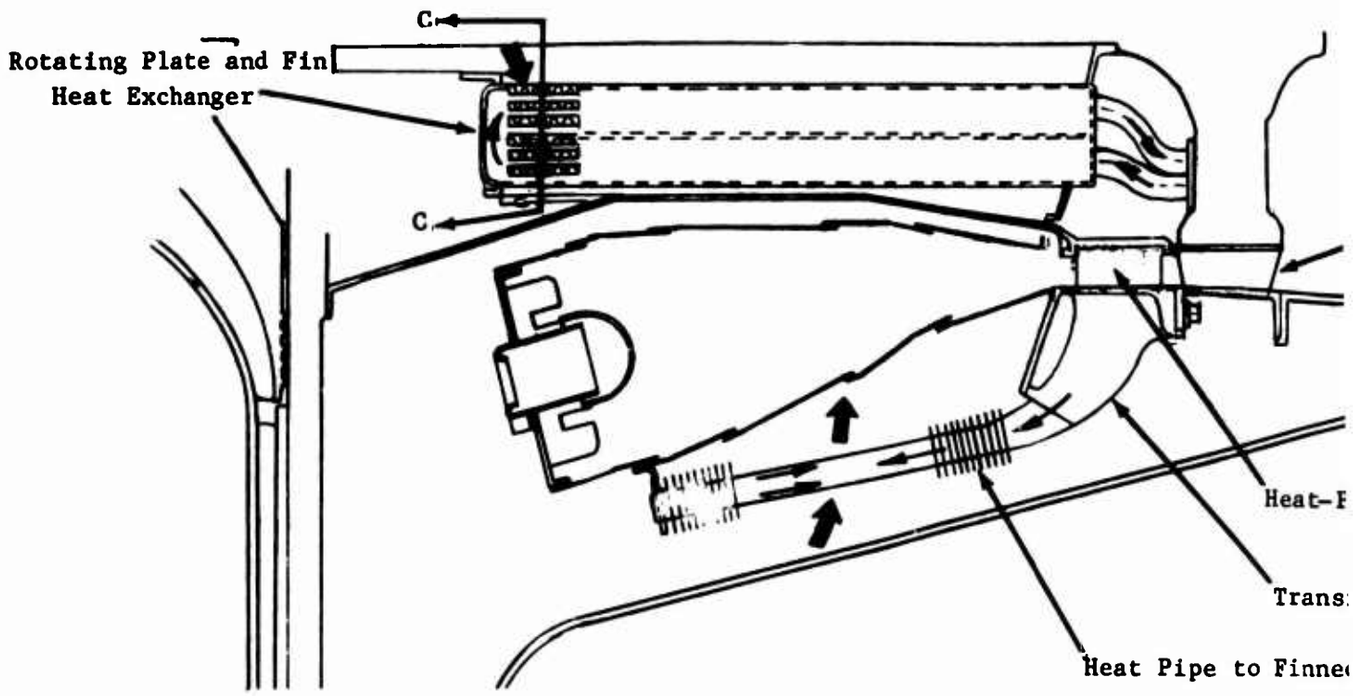

Figure 11. Heat-Pipe-Cooled Stator and High-Presure Air-Cooled Rotor.

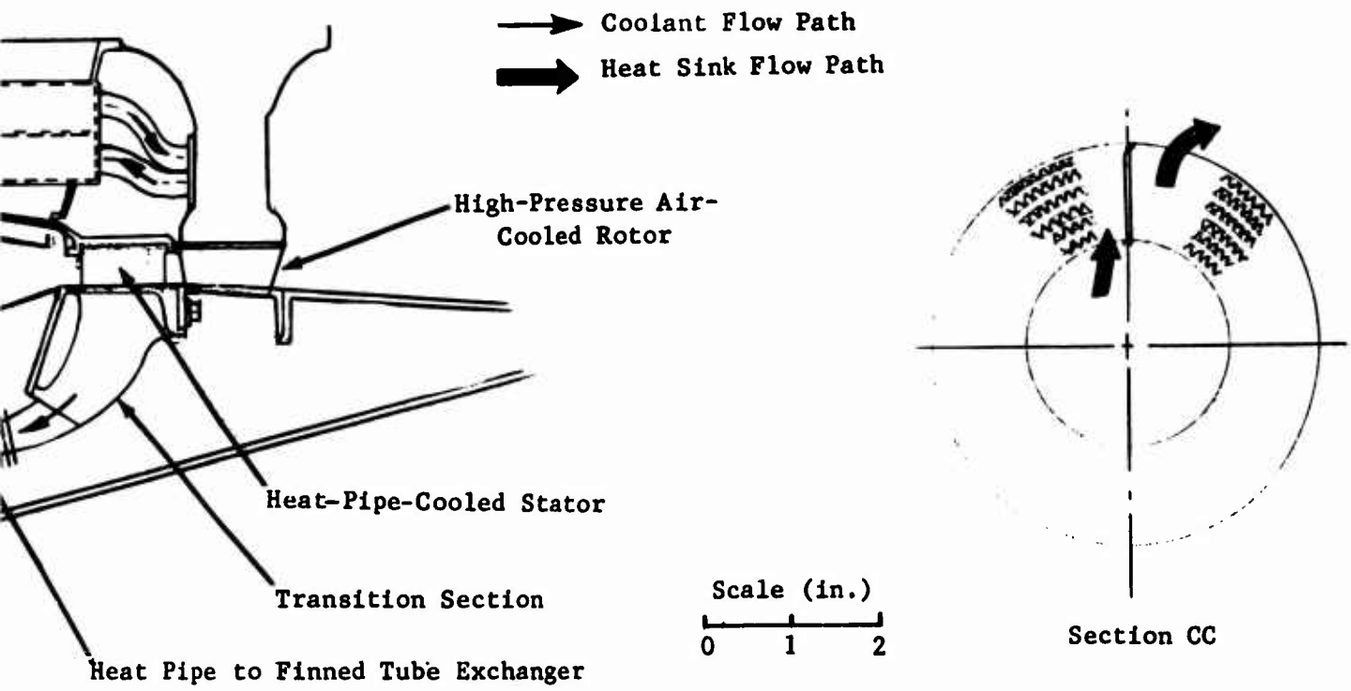
Coolant Flow Path
Heat Sink Flow Path
High-Pressure Air-Cooled Rotor
Heat-Pipe-Cooled Stator
Transition Section
Heat Pipe to Finned Tube Exchanger
Scale (in.)
0 1 2
Section CC

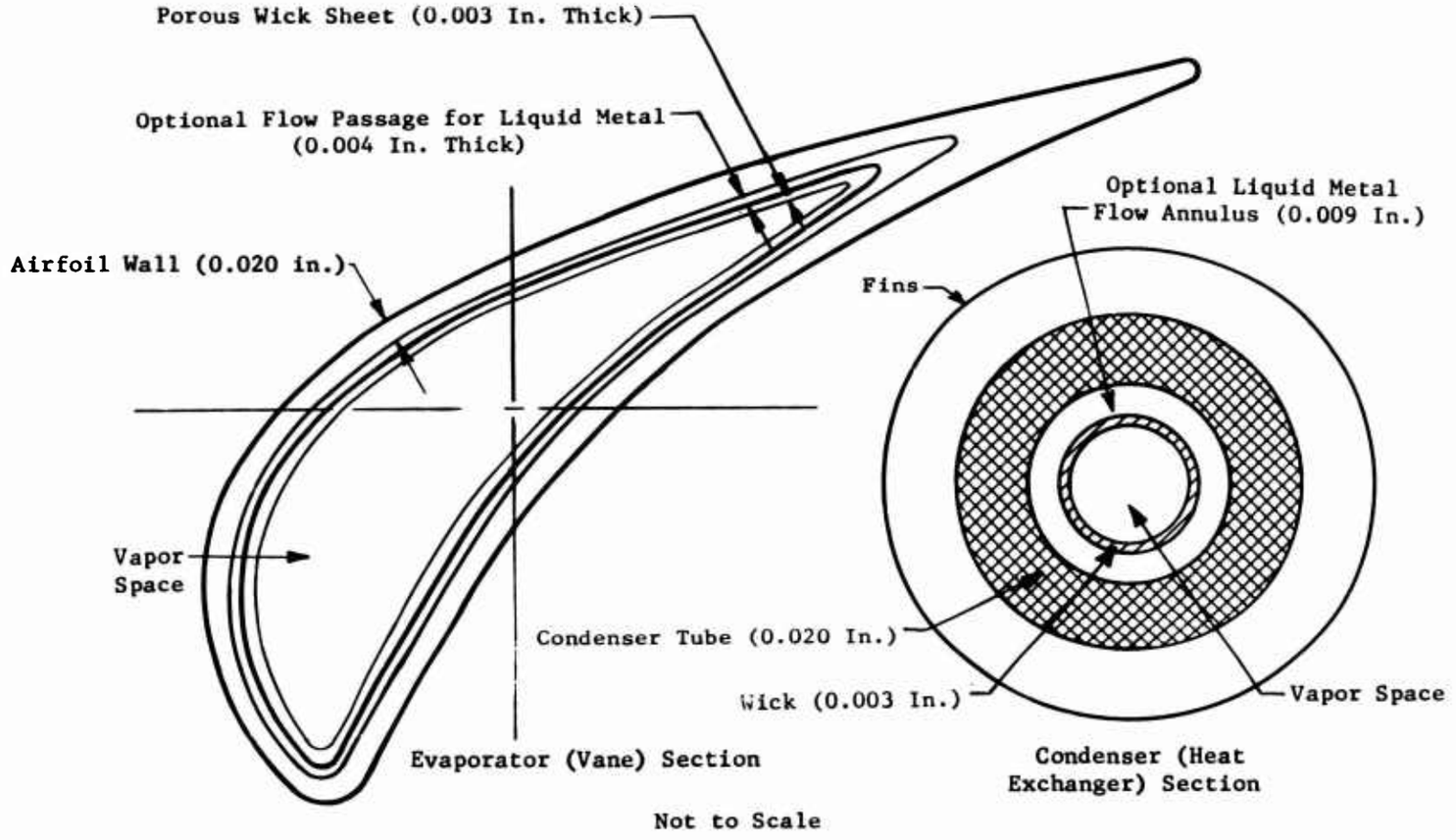

Figure 12. Heat Pipe Concept for Turbine Stator Vanes.

effective thermal conductivity in order to meet metal temperature limits of the trailing edge. This may be done by using an insert of material with a higher thermal conductivity than that of the vane material. If an insert with the conductivity of copper (200 Btu/hr ft^2 °F) can be installed in the trailing edge, enveloped by a 0.020-inch vane wall thickness, the surface temperature may be reduced from 2180°F to about 1800°F.

As an alternate approach, the internal volume of the section of the trailing edge which cannot accommodate a wick may form an extension of the liquid metal flow annulus or a separate artery. Both approaches require detail design study to establish feasibility.

Servicing of the turbine using the heat pipe concept is simple since each heat pipe, consisting of an integral vane and heat exchanger tube, is a separate and discrete component. Also, circulation of the coolant is accomplished without external piping or pumps.

2.2.4 Selection of Five Rotor Cooling Concepts

The thermal design requirements for cooling the turbine rotor are less severe than those for the stator. The rotor is exposed to lower gas temperatures as a result of its rotation. The local hot spots in the combustor are averaged by the rotating blades, resulting in the lower peak temperature profile shown in Figure 5. During exposure to a relative gas temperature of 2185°F, cooling of the turbine rotor is required to maintain an average blade metal temperature of 1500°F. However, performance penalties are associated with direct air cooling of the rotor and are more detrimental to the cycle than the stator, since the rotor cooling airflow is unable to produce useful turbine work. Therefore, internal cooling concepts using a contained coolant system for the rotor offer an engine performance improvement.

The design of a contained coolant system with the coolant circulating force provided by the difference in densities of hot and cold fluids in a centrifugal field offers an additional performance advantage since a coolant pump is not required. Thus, the following natural convection cooling system concepts were initially selected for the rotor investigation:

1. Liquid Metal System
2. High-Pressure Gas System
3. High-Pressure Superheated Stem

In addition, the heat pipe concept was also to be investigated. Finally, the fifth selection was an external cooling concept utilizing modulated transpiration air cooling.

A review of the natural convection criteria for gases in Table V shows that hydrogen and helium would be desirable coolants. However, both of these gases present sealing problems and, in the case of hydrogen, safety

is also to be considered. Of the remaining gases, air and steam have good heat transfer characteristics and their properties are well defined. Therefore, air and steam were selected as blade coolants for conceptual analyses.

Sodium and lithium also have excellent heat transfer characteristics; however, since their melting points are above ambient, some problems with regard to engine starting could be anticipated. Therefore, the sodium/potassium eutectic with a lower melting point was selected.

It was recognized that the use of a high-density liquid metal to cool the rotor blades would present structural problems due to the centrifugal forces imposed by the high rotational speeds. However, the use of a liquid metal coolant reduces the volume and weight of the rotating heat exchanger as compared with gas and steam systems. It was anticipated that the turbine rotor and heat exchanger would be an integral unit, with the heat exchanger supported by the turbine disk. Therefore, the corresponding disk-to-exchanger attachment stresses would be reduced.

The use of compressor discharge air was selected for the heat sink in each of the above systems. To add completeness to the study, methane, a cryogenic fuel, was also specified as an alternate heat sink for the high-pressure air-cooled blade concept.

The selection of the rotor cooling concepts is summarized in Table VII.

TABLE VII. ROTOR BLADE COOLING CONCEPTS

Concept	Coolant	Heat Sink
Gas	Air	Compressor Discharge Air
Gas	Air	Cryogenic Fuel
Gas	Steam	Compressor Discharge Air
Liquid Metal	Sodium-Potassium Alloy	Compressor Discharge Air
Heat Pipe	Potassium	Compressor Discharge Air
Modulated Transpiration	Compressor Discharge Air	Not Required

The following paragraphs describe preliminary design arrangements for each concept.

Modulated Transpiration Cooling Concept

The transpiration-cooled design for the rotor blade is similar to the stator vane design described in the previous section.

Liquid Metal Cooling Concept

A preliminary arrangement of the liquid metal cooling concept for the rotor is shown in Figure 8. Cooling of the blades is accomplished by natural convective circulation of the liquid metal through a thin-wall blade with mutliple coolant passages. Circulation of the coolant is provided by the difference in densities between the hot and cold fluids in the centrifugal field. The liquid metal makes two passes through the blade. For the first pass, liquid metal enters the leading-edge coolant passages at the blade butt and flows radially outward to the tip plenum. For the second or return pass, liquid metal enters the mid-chord and trailing-edge coolant passages at the tip plenum and flows radially inward to the butt plenum.

The rotating heat exchanger is an annular unit which incorporates thin-wall finned tubes similar to the tubes described for the liquid-metal-cooled vane concept. The tubes form a two-pass serpentine configuration to provide cross-counterflow conditions for the liquid metal and compressor discharge air. The finned tubes are positioned on a triangular pitch and attached to the inlet and outlet headers. The headers are incorporated into the front face of the turbine rotor disk, and the blade butt plenum and headers are connected through radial flow passages within the disk.

The system is designed for installation and removal as a completely integral and hermetically welded unit.

High-Pressure Air Cooling Concepts

A preliminary arrangement of the high-pressure air cooling concept using compressor discharge air as the heat sink is shown in Figure 11. The high-pressure air coolant makes two passes in the blade as described for the liquid metal concept. Circulation of the coolant is similarly accomplished by natural convection. To obtain the necessary heat transfer coefficients and coolant flow rates, the closed system is pressurized to 1200 psi. This thermal design requirement to operate at high pressure must be balanced with the blade stress requirement in the detail design.

The rotating heat exchanger is an annular unit which incorporates a compact plate and fin brazed unit. A percentage of compressor discharge air is routed along the shaft, enters at the exchanger I.D., and exits at the exchanger O.D. after flowing circumferentially through the unit. The compressor discharge air returns to the mainstream by entering the combustor inner liner diluent and film cooling holes. The high-pressure air coolant flows from the blade butt plenum radially through passages in the disk to pipes which supply the coolant manifold on the heat exchanger. The coolant makes two axial flow passes through the exchanger before returning to the blades.

A preliminary arrangement of the second high-pressure air cooling concept is shown in Figure 9, utilizing cryogenic fuel as the heat sink. The high-pressure air coolant makes two passes in the blade as described for the other concepts. The coolant flows radially to the blade butt plenum, which is connected to three finned U-tubes. The tubes are radially incorporated in the disk.

Cryogenic methane, which is assumed as the engine fuel for this design, is diverted to enter the disk rear face, and flows through the disk to provide the necessary heat sink for this compact exchanger. The fuel exits the disk to enter the combustor fuel distributors. This concept requires complex sealing arrangements to route the fuel into and out of the rotating shaft. Use of jets and slinger vanes is necessary for transmission of the fuel into and out of the shaft. Use of contact seals or pressure-balanced labyrinth seals is necessary to preclude fuel leakage into oil or air cavities. Detail design studies for fuel transmission are required but were outside the scope of the conceptual analysis.

Superheated Steam Cooling Concept

The preliminary arrangement of a rotor cooling concept using superheated steam as the coolant is shown in Figure 13. The coolant makes two passes in the blade as described for the liquid metal concept. Circulation of the coolant is similarly accomplished by natural convection. To obtain the necessary heat transfer coefficients and coolant flow rates, the closed system is pressurized to 1200 psi. This thermal design requirement to operate at high coolant pressures must be balanced with the stress/life requirement of the blade.

The rotating heat exchanger is an annular unit which incorporates a compact plate and fin brazed unit. A percentage of the compressor discharge air is routed along the shaft, enters the exchanger at the exchanger I.D., and exits at the exchanger O.D. after flowing circumferentially through the unit. The air returns to the mainstream by entering the combustor inner liner diluent and film cooling holes.

The coolant flows from the blade butt plenum radially through passages in the disk to pipes which supply the coolant manifold on the exchanger. The coolant makes two axial flow passes through the exchanger before returning to the blades.

Heat Pipe Cooling Concept

The single most important consideration in the design of a heat-pipe-cooled rotor blade is the centrifugal force on the liquid in the heat pipe wick. A linear pressure gradient will be set up in the liquid, the pressure varying from zero at the center of the rotating shaft to a maximum at the blade tip. The pressure difference between the liquid and vapor at the liquid-vapor interface must be balanced by surface tension forces. The

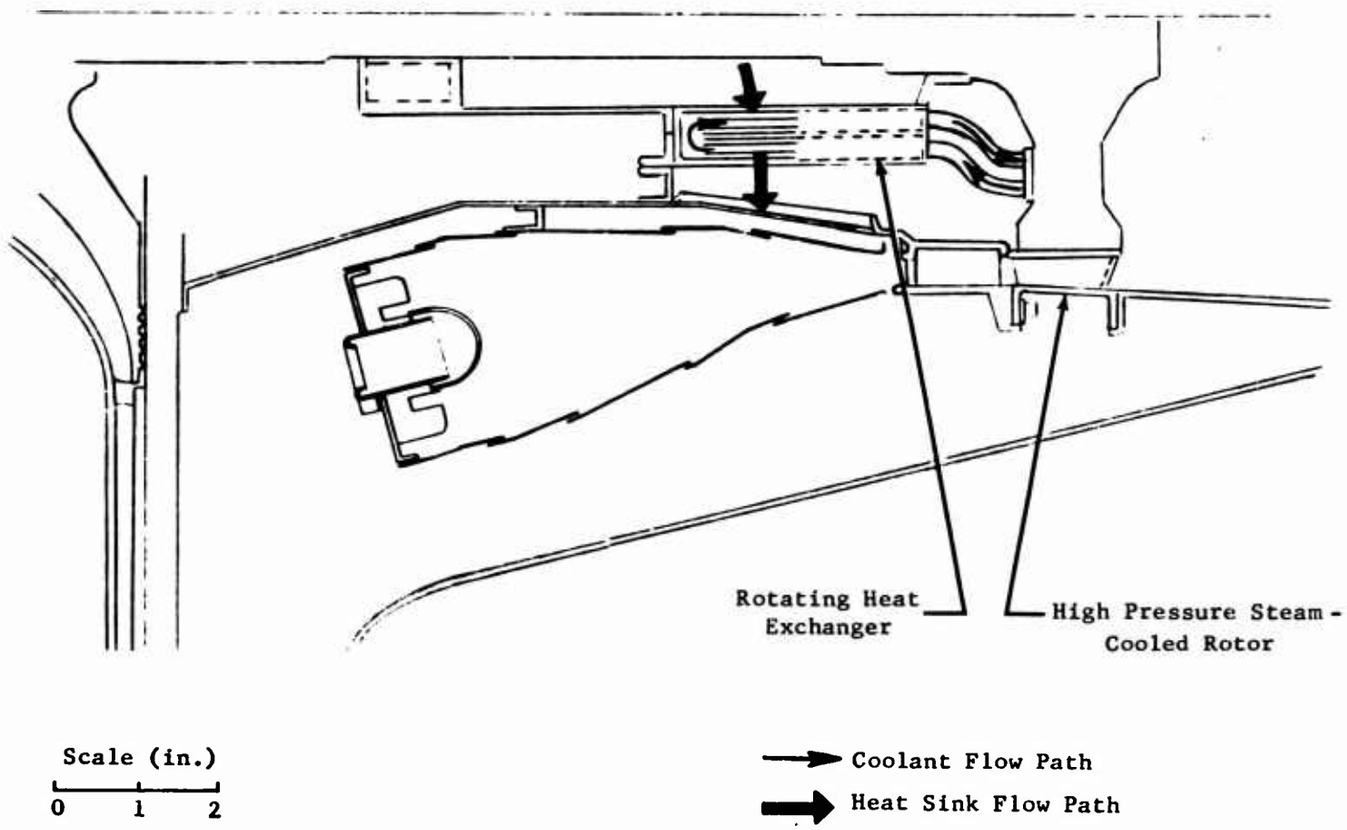

Figure 13. High-Pressure Steam-Cooled Rotor Blade Concept.

maximum pressure difference that can be sustained across the liquid-vapor interface which was calculated during the stator analysis presented in section 2.3 is 2.3 psi using a pore size as small as 20 microns. The maximum coolant pressure in the static liquid is a function of the liquid's specific weight, the height of the liquid column, and the amount of acceleration to which the liquid column is subjected. For this rotating system with 2.44×10^5 g's, the maximum liquid pressure is about 20,900 psi, assuming potassium as the coolant. Since the potassium vapor pressure at the operating temperature is 1.5 psia, the maximum pressure difference between the liquid and vapor is far greater than the maximum value of pressure differential at the liquid-vapor interface which can be sustained by surface tension. Therefore, the liquid cannot be confined in the wick adjacent to the heat pipe wall, but will accumulate in the vapor space at the rotor blade tip. Thus, the heat pipe concept for rotor blade cooling is not feasible.

2.3 PRELIMINARY ANALYSES

2.3.1 Method of Analysis

The general methods for calculating the heat transfer rates in the vanes, blades and heat exchangers are described in Section 3.1 and primarily used for the thermal analysis of the selected vane and blade cooling system in the second phase of the program. A simplified approach for the thermal analysis of five stator vane and five rotor blade cooling concepts was utilized in order to perform a comparative and screening evaluation during the conceptual study phase of the program.

As an example of the simplified analysis, the two-phase water-steam cooling concept using fuel as the heat sink is discussed below.

An estimate of the airfoil heat load to maintain a bulk airfoil metal temperature of 1500°F was made using an assumed average gas-side heat transfer rate of 230 Btu/hr ft^2 °F. The heat transfer rate was obtained from a small turbine design (Reference 3). The bulk metal temperature of 1500°F was selected based on the following: (a) at least a 300°F gradient can be expected in the trailing-edge section of some of the cooling concepts, (b) the trailing edge may be susceptible to low cycle fatigue at the high metal temperatures, and (c) the highly stressed rotor blade may be stress-rupture-life limited at temperatures above 1500°F.

The two-phase fluid temperature is found from the vapor-liquid equilibrium conditions. The maximum steam pressure (1200 psi) and the portion (50%) of the mixture that is vaporized were assumed. The fuel temperatures are found from the heat load fuel flow and fuel properties.

The exchanger configuration and size were approximated by assuming the overall heat transfer rate and fluid velocities. With this exchanger size, the heat transfer and pressure losses are determined. If these are not satisfactory the exchanger dimensions are modified and the heat transfer and pressure losses are reevaluated until suitable values are obtained.

For the high-pressure air and the liquid-metal coolant systems, the coolant temperatures are determined from the heat load, the required vane temperature, and the estimated vane-to-coolant heat transfer rate. The compressor air heat exchanger size and heat sink temperatures are calculated in the same manner as described for the two-phase exchanger.

2.3.2 Results of Preliminary Analysis

Stator

A summary of the thermal and mechanical design characteristics for each of the five stator vane cooling concepts investigated is presented in Table VIII. The table presents the vane coolant conditions, the exchanger heat sink conditions, and the exchanger geometry including coolant side

TABLE VIII. STATOR VANE COOLING CONCEPT PARAMETERS

		Liquid Metal	High Press. Air	Two Phase	Heat Pipe	Modulated Transpiration
Vane (Inco 713)						
Heat Load/Vane	Btu/hr	1644	1644	1644	1644	1644
Coolant Fluid	-	NaK	Air	Water/ Steam	K	Compressor Air
Temperature Out	°F	1400	1240	567	1040	1500
Temperature In	°F	1322	1215	567	1040	871
Pressure	psi	50	1200	1200	1.5	230
Specific Heat	Btu/lb °F	0.21	0.26	649	.2	.24
Flow/Vane	lb/hr	100	253	5.07	-	12
Internal Area/Vane	sq in.	1.108	1.108	1.108	0.92	-
h Vane to Fluid	Btu/hr ft^2 °F	15,350	1232	235	-	-
ΔT Vane to Fluid	°F	14	173	933	230	629
Heat Sink						
Fluid		Compr. Disch.	Compr. Disch.	Fuel JP	Compr. Disch.	None
Temperature Out	°F	1033	936	384	936	-
Temperature In	°F	871	871	80	871	-
Pressure	psi	230	230	Engine	230	-
Pressure Drop	psi	0.5	0.5	1.0	0.5	-
Mass Flow	lb/sec	0.4	1.0	.11	1.0	-
Exchanger Geometry (Total per Stator Row)						
Heat Transfer Area	sq ft	2.7	3.17	10.6	17.0	-
Volume	cu in.	8.2	15.4	24.0	86.0	-
Fluid Side						
No. of Tubes	-	16	-	4	37	-
Face Area	sq in.	1.5	10.44	2.98	3.0	-
Length	in.	3.5	1.526	8.0	10	-
Pressure Drop	psi	1.7	0.10	0.50	0	-
Heat Sink Side						
Face Area	sq in.	5.45	5.24	6.90	138.0	-
Length	in.	3.5	2.94	4.00	4.00	-
Fins per Inch	-	40	Plate	40	40	-
Fin O.D.	in.	0.375	and	0.861	.6	-
Tube O.D.	in.	0.188	Fin*	0.420	0.32	-
Pump Horsepower	hp	0.1	6.2	7.0	0.0	0.0
Reference Figure No.		8	9	-	12	7

*Reference 15, Figure 10-36

and heat sink side configurations. The table shows that for each cooling concept, a thermal design for cooling the vanes to 1500°F average metal temperature at the given heat load is feasible. The coolant flow rates, pressures and temperatures were acceptable, and pumping power is not excessive.

The thermal design of the heat exchanger to accommodate the vane heat load using compressor discharge air as the heat sink is also feasible for each cooling concept. The heat sink airflow rate, pressure loss, and temperature rise for each cooling concept is acceptable, so the air could be returned to the cycle via the combustor outer liner. The exchanger size for each concept can be accommodated within the available volume in the combustor housing aft of the centrifugal compressor.

In the two-phase cooling concept where engine fuel is the heat sink, the flow rate is close to the engine design point fuel requirement. This indicates that a fuel bypass system and pumping heat storage in the fuel tanks may be avoided. However, the bulk fuel temperature at the exchanger outlet is 384°F. This value may present a coking problem since the fuel temperature at the exchanger tube wall will be higher.

The internal operating conditions of the heat pipe vane and heat exchanger section are presented in Table IX.

TABLE IX. HEAT PIPE OPERATING CONDITIONS

Evaporator (Vane)	
L.E. Surface Temperature	1300°F
Vapor Temperature	1050°F
Inner Wall Temperature	1070°F
Vapor Pressure	1.5 psia
ΔP Vapor to Liquid	1.3 psia
Condenser (Heat Exchanger)	
Vapor Temperature	1020°F
ΔT Wick and Liquid Annulus	2°F
Outer Wall Temperature	1013°F

Since the application of the heat pipe, as an advanced cooling concept, to aircraft propulsion systems has been limited and since published literature on this concept has not had the depth of coverage as the other concepts investigated, a detailed discussion of some of the design aspects of the heat pipe is presented below.

Selection of Heat Pipe Fluid

Candidate heat pipe fluids at the 1070°F inner surface temperature are sodium, potassium, and cesium. There are two limits on the maximum axial heat flux (heat transport rate per unit vapor space cross-sectional area). The first limit, called the entrainment limit, occurs when the drag force exerted by the heat pipe vapor on the liquid in the wick is sufficient to entrain liquid and disrupt the liquid-vapor interface.

The second limit, called the isothermal limit, occurs when the temperature drop in the heat pipe vapor along the heat pipe length exceeds some prescribed value. The axial heat flux must not exceed the entrainment limit or the isothermal limit if the heat pipe is to function properly and without excessive temperature drop. The axial heat flux is defined as the heat transport rate per vane divided by the minimum cross-sectional area of the vapor space.

Figure 14 (Reference 14) data extrapolated in the 1000° - 1300°F range shows the isothermal and entrainment axial heat flux limits for sodium (Na), potassium (K), and cesium (Cs) as a function of temperature. The isothermal limit is for a maximum ΔT of 20°F. The entrainment limit is for a wick pore diameter of 20 microns, which represents the minimum size wicks which have been fabricated, although smaller pore sizes may be obtained with special fine-mesh screen and sheets of porous metal.

Using the date of Figure 14, the isothermal and entrainment limits of the candidate heat pipe fluids can be evaluated. Figure 14 shows that the maximum isothermal heat flux for sodium at the 1050°F vapor temperature is below the vane design requirement of 8.9 kw/in.^{2}. Thus, sodium is eliminated from further consideration. Similarly, cesium is eliminated since its entrainment limit is below the design requirement. Cesium's entrainment limit may be increased 15-20% to meet the requirement by reducing the wick pore diameter 25-30%.

Potassium was selected as the most suitable coolant since its entrainment and isothermal limits satisfy the design requirement.

Pressure Drop in Heat Pipe Fluid

The sum of the vapor and liquid pressure drops through a heat pipe cannot exceed the maximum pressure differential across the liquid-vapor interface without disruption of the liquid-vapor interface and subsequent drying out or "burnout" of the wick at the evaporator section. Consequently, the fluid pressure drops are calculated and compared with this ΔP.

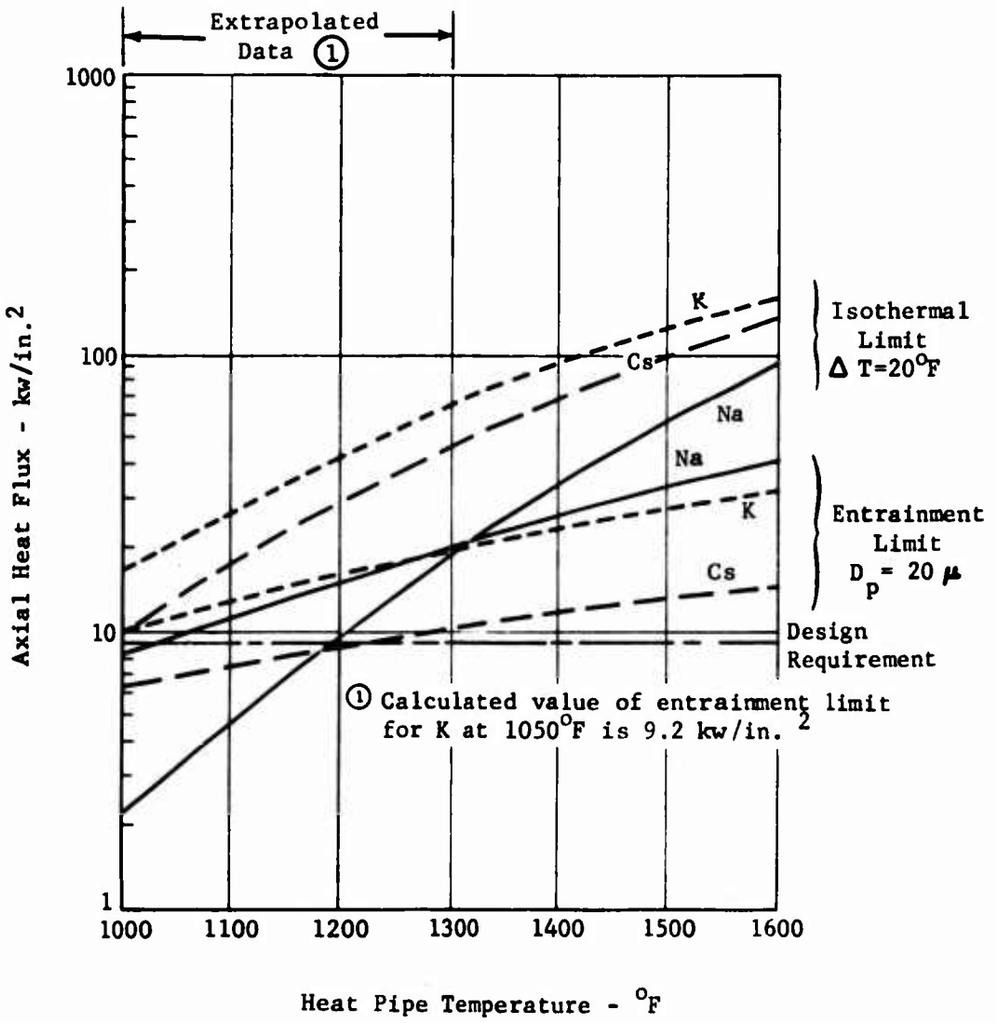

Figure 14. Isothermal and Entrainment Limits for Liquid-Metal Heat Pipes.

The following pressure drops are considered:

1. Vapor momentum pressure drop
2. Vapor friction pressure drop
3. Liquid friction pressure drop
4. Liquid pressure drop due to static head

The first three pressure drops are functions of the maximum fluid velocity, which is related to the heat transport rate.

The fourth pressure drop is a function of the number of g's of acceleration acting on the liquid and tending to keep the liquid in the heat exchanger section and is presented in Figure 15.

Since the vapor pressure of potassium at 1050°F is 1.5 psi, the maximum pressure differential which can be sustained across the liquid-vapor interface if the liquid pressure is not to be negative (i.e., the liquid is not to be in tension) is 1.5 psi. Figure 15 then indicates that for a maximum acceleration of 4 g's, the maximum difference in elevation of 14.5 in. could be sustained between the top and bottom of the potassium heat pipe. The actual permissible elevation difference is smaller, since it is the sum of all the pressure drops which should not exceed 1.5 psi.

Proper selection of the frictional pressure drop terms requires that the laminar or turbulent nature of the flow be known. From Reference 14, it was determined that flow will be laminar in the potassium vapor for a heat transport rate of .47 kw. The total vapor and liquid pressure drop was calculated to be 1.3 psi. Since this figure is equal to the difference between the maximum vapor and minimum liquid pressures, the minimum liquid pressure is 0.2 psi.

Since the liquid pressure at a given point along the heat pipe is not equal to the vapor pressure, the pressure differential at the liquid-vapor interface must be balanced by surface tension forces. The maximum pressure difference that can be sustained across this interface is

$$\Delta P = 8480\, \sigma \,/\, D$$

where

σ = surface tension, lb/ft

D = maximum effective wick pore diameter that will sustain a given pressure difference, microns

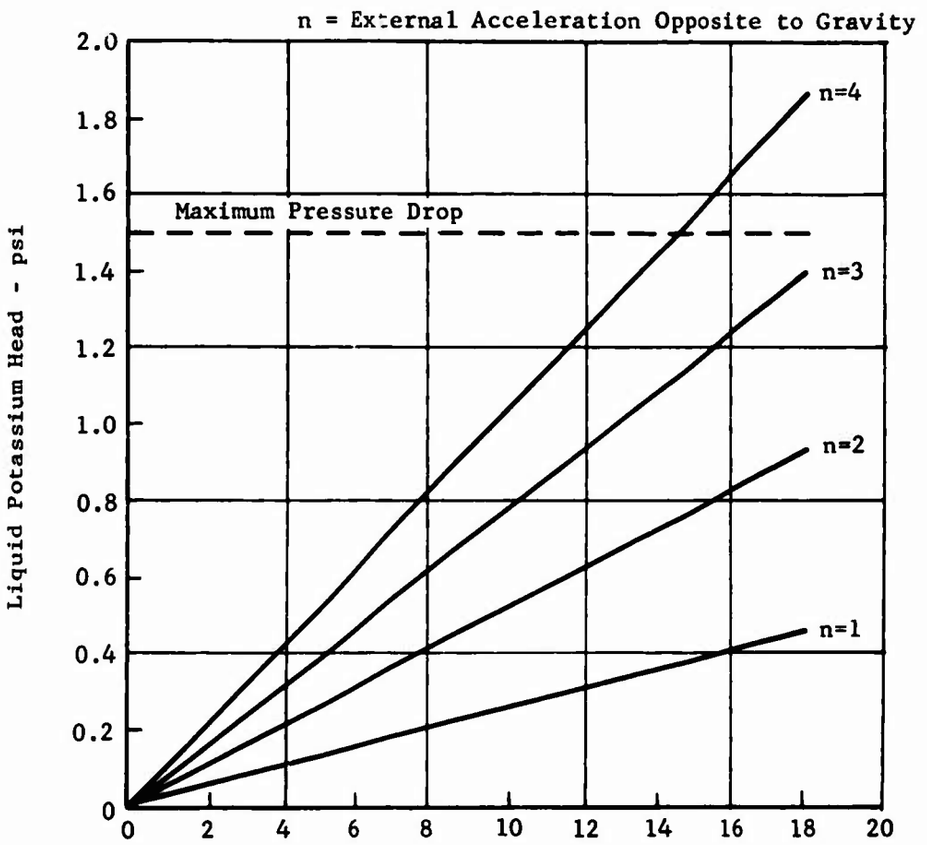

Figure 15. Static Head of Liquid Potassium Versus Heat Pipe Height and External Acceleration.

From this equation, the pore diameter required to sustain the pressure difference is calculated to be 35.2 microns. Since a pore diameter of 20 microns or less has been specified from entrainment limit considerations, the heat pipe design is adequate to handle the specified vane cooling requirement.

Boiling Limit

The heat pipe liquid is superheated in the stator vane. That is, the vapor pressure is greater than the liquid pressure. The superheat is greatest at the heat pipe wall, since the liquid temperature and hence the vapor pressure are highest there. Boiling could disrupt the heat pipe liquid, and should be avoided. Boiling will not occur, despite the fact that the heat pipe liquid is superheated, if the nucleation site diameter does not exceed 23.5 microns based on vapor temperature of 1070°F at the wall and conservatively assuming the liquid pressure equal to zero. Since liquid metal has an excellent wetting property, nucleation site diameters should be smaller than 23.5 microns. Hence, heat pipe operation should proceed without boiling in the wick.

Heat Pipe Start-Up

It is possible that prior to start-up, the heat pipe liquid may have become dislodged from the wick. In this case the capillary force which is developed in the liquid flow space rather than in the pores of the inner wick layer will determine the height of liquid which can be supported. In an annulus, one of the two principal radii of curvature (in the circumferential direction) is essentially infinite, and the capillary force is only one-half that available in a circular pore whose diameter is equal to the thickness of the annulus.

The liquid height which can be supported is presented in Figure 16 as a function of wick annulus thickness. The temperature at which the potassium vapor pressure is equal to the static liquid pressure is also shown in Figure 16. At this temperature the minimum pressure in the liquid cannot be negative, thus insuring that the column will be stable and not in a state of tension.

A thickness of 9 mils for the liquid annulus was selected, resulting in a column height of 4.4 in. that can be supported by the liquid annulus. Since the height of the inclined heat pipe shown in Figure 11 is about 2 in., rewicking capability is assured in the event that liquid is dislodged from the wick. For this geometry the column will be stable when the heat pipe temperature reaches 772°F.

During an engine cold start-up, the potassium heat pipe liquid is frozen. The temperature of the heated (vane) section increases rapidly, approaching steady state within a short time. A portion of the heat which would be rejected to the heat sink during normal operation is then used to raise the temperature of the unheated portion of the heat pipe at a

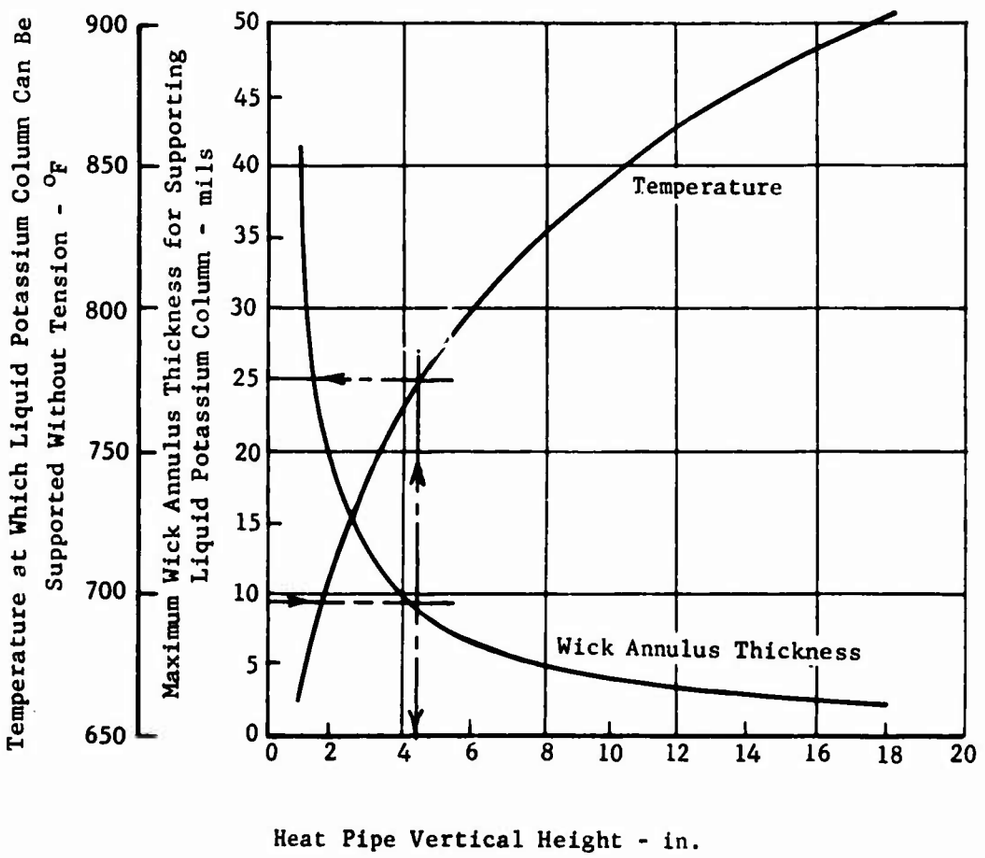

Figure 16. Annular Wick Sizing to Support Liquid Potassium Column.

relatively slow rate. The primary concern is to insure that the vane section of the heat pipe does not exceed the prescribed 1500°F average metal temperature limit during the engine start-up period.

It is important that liquid condensate will always be available at the vane section to replenish the liquid which is lost by evaporation. During start-up of a heat pipe, this may not always be the case. An inadequate supply of liquid to the evaporator section would result in drying out of the wick and "burnout", or overheating, of the vane.

Two factors which can inhibit the return flow of condensate are entrainment of the liquid by the vapor and condensation in the vapor instead of at the liquid-vapor interface. During start-up, the vapor produced in the heated evaporator section expands into the cold condenser section, where the vapor pressure is negligible. The vapor velocity will reach the sonic value at the evaporator exit and will become supersonic in the condenser section before being decelerated by a shockwave-like process. In some instances, the drag of the high-velocity vapor on the adjacent liquid may retard the liquid flow or cause entrainment of the liquid in the vapor.

Also, the expansion process which results in supersonic vapor velocities will subcool the vapor below its saturation temperature. Condensation may then occur spontaneously in the vapor stream. The entrained vapor may then not be able to join the liquid condensate stream at a sufficiently high rate. Also, the heat of condensation will have been released in the vapor stream rather than at the wick surface, thus retarding the rate at which the solidified heat pipe liquid in the cold condenser section can be heated and melted.

The significance of the above factors on start-up capability must be evaluated analytically and experimentally for a particular heat pipe. An estimate of the time required to heat the vanes to operating temperature is approximately 5.4 seconds.

Heat is removed from the condenser section by the flow of compressor discharge air over the heat pipes. Preliminary calculations indicated that each heat pipe would have to be finned in order to provide sufficient heat transfer surface. The heat exchanger design was evaluated on the basis of the methods and data presented in Reference 13 and 15. The heat exchanger used high-density finned (36 per inch) tubes made with continuous fins of copper clad with stainless steel. Initial heat exchanger sizing was established with low-density finned tubes which yielded an exchanger length of about 14 inches and required full compressor discharge flow. This exchanger would have required 2.5 times the heat transfer area, if only about 30% of compressor discharge airflow was used for heat rejection. However, based on simplifying the main airflow path design arrangement and minimizing mainstream air pressure drop, it was desirable to reduce the heat exchanger airflow requirements. This was accomplished with an attendant decrease in heat exchanger length by selecting the high-density copper fin tube.

Rotor

A summary of the thermal and mechanical design characteristics for each of the five rotor blade cooling concepts investigated is presented in Table X. The table presents the rotor coolant conditions, the exchanger heat sink conditions, and the exchanger geometry including coolant side and heat sink side configurations.

The table shows that for each cooling concept, a thermal design for cooling the blades to 1500°F average metal temperature at the given heat load pressure and temperatures is acceptable, although the liquid metal pressure of 8600 psi due to the centrifugal field does introduce a special structural consideration. Coolant pumping for the internally cooled systems is accomplished by the centrifugal field acting on the difference in densities of the hot and cold coolant legs.

The thermal design of the heat exchanger to accommodate the blade heat load using compressor discharge air as the heat sink is also feasible for each cooling concept. The heat sink airflow rate, pressure loss, and temperature rise for each cooling concept is acceptable, so the air could be returned to the cycle via the combustor inner liner. The exchanger size, for each concept using air as the heat sink, can be accommodated within the volume between the combustor inner liner and the turbine shaft, although the high pressure air cooling concept requires a heat exchanger length that precludes a turbine bearing support at the front of the rotor (see Section 4.0).

In the high-pressure air cooling concept using cryogenic fuel as the heat sink, the flow rate is close to the engine design point fuel requirement. This indicates that a fuel bypass system is not required.

2.4 ENGINE PERFORMANCE EFFECTS

To estimate the effects of the cooling concepts on engine performance, the specific fuel consumptions for the combined concepts were calculated and are presented in Table XI. The method of analysis is discussed in Section 4.4. From this data it is apparent that the advanced cooling concepts offer an improvement in engine fuel consumption of at most 5% over a baseline unmodulated transpirational-cooled turbine. The performance decrements associated with each rotor and stator cooling concept are a result of the horsepower of the pump required to circulate the coolant, and the pressure drop the compressor discharge air experiences as a result of passing through the coolant heat exchangers. This data for the various systems is presented in Table XXIV of Section 4.4 and was used for this analysis.

TABLE X. ROTOR BLADE COOLING CONCEPT PARAMETERS

		Liquid Metal	Gas	Gas	Gas	Modulated Transpiration Cooled
Blade (Inco 713)						
Heat Load/Vane	Btu/hr	1644	1644	1644	1644	1644
Coolant Fluid	-	NaK	Air	Steam	Air	Air
Temperature Out	°F	1400	1021	1275	1021	1500
Temperature In	°F	1322	971	1225	971	871
Pressure	psi	8600	1200	1200	1200	230
Specific Heat	Btu/lb-°F	0.21	0.26	0.578	0.26	.24
Flow/Vane	lb/hr	100	126.5	56.9	126.5	112
Internal Area/Vane	sq in.	1.108	1.108	1.108	1.108	-
h Blade to Fluid	Btu/hr ft^2 °F	15,350	530	1418	530	-
ΔT Blade to Fluid	°F	14	404	151	404	629
Heat Sink						
Fluid		Compr. Disch.	Compr. Disch.	Compr. Disch.	Methane	None
Temperature Out	°F	1033	936	936	-240.6	-
Temperature In	°F	871	871	871	-240.6	-
Pressure	psi	230	230	230	32.2	-
Pressure Drop	psi	0.5	0.5	0.5	1.0	-
Mass Flow	lb/sec	0.4	1.0	1.0	.093	-
Exchanger Geometry (Total per Rotor Row)						
Heat Transfer Area	sq ft	2.7	16.9	2.83	0.5	-
Volume	cu in.	8.2	82.1	13.8	24	-
Fluid Side						
No. of Tubes	-	16	-	-	3	-
Face Area	sq in.	2.08	11.2	4.24	0.60	-
Length	in.	3.5	7.3	3.26	3.61	-
Pressure Drop	psi	0.1	0.1	0.1	0.1	-
Heat Sink Side						
Face Area	sq in.	36.2	8.65	5.06	4.95	-
Length	in.	3.5	9.51	2.72	3.6	-
Fins per Inch	-	40	Plate	Plate	8.7	-
Fin O.D.	in.	.375	and	and	1.5	-
Tube O.D.	in.	.188	Fin*	Fin*	1.0	-
Reference Figure No.		8	11	13	9	7

*Reference 15, Figure 10-36

TABLE XI. EFFECT OF COOLING ON SPECIFIC FUEL CONSUMPTION AT 35% MILITARY RATED POWER

	Stator Cooling System						
Rotor Cooling System	"Uncooled"	Heat Pipe to Compr. Disch.	NaK to Compr. Disch.	1200 PSI Air Compr. Disch.	Water/Steam to Fuel	Modulated Transpiration	Transpiration (Baseline)
"Uncooled"	.5500	.5522	.5547	.5585	.5589	.5504	.5520
NaK to Compr. Disch.	.5540	.5592	.5587	.5625	.5628	.5540	.5560
1200 PSI Air to Compr. Disch.	.5542	.5594	.5589	.5627	.5630	.5542	.5562
1200 PSI Air to Methane	.5539	.5590	.5585	.5623	.5627	.5539	.5559
Steam to Compr. Disch.	.5542	.5594	.5589	.5627	.5630	.5542	.5562
Modulated Transpiration	.5615	.5667	.5662	.5700	.5704	.5615	.5635
Transpiration (Baseline)	.5807	.5859	.5854	.5892	.5896	.5807	.5827

2.5 SELECTION OF TWO VANE AND TWO BLADE COOLING CONCEPTS

At the conclusion of this phase of the program,two stator and two rotor cooling concepts were selected as the most feasible for continued heat transfer analysis and incorporation into the engine design. Since the potential performance benefits to be obtained by any one concept were not decisive, a rating system was established to assess the overall value of the concepts for continued analysis and evaluation. The intent of this rating system was to evaluate one concept's overall characteristics with the others. As shown in Tables XII and XIII, the rating system included four equally weighted groups:

1. Nozzle or Rotor Assembly
2. Heat Exhanger Component
3. Overall System Design
4. Engine Performance Effects

As shown in the tables, criteria were specified for each group and each criterion was weighted according to its relative importance within the group. The Engine Performance Effects category was given full weight, since the primary objective of the study was to obtain a cooling system which produced a significant engine performance improvement over the current turbine cooling technique.

The point ratings for each of the five advanced cooling concepts shown in Table XII and XIII are assigned by operating on the criterion weighting factor with a multiplier, from 1 to 5, corresponding to its position relative to other concepts. Increasing the multiplier reflects a more favorable concept. Ratings for the baseline transpiration-cooled concept are also shown as a reference to a current-technology concept.

Rating of Stator Concepts

In the Vane and Support group, the liquid-metal-cooled system has the highest rating because its excellent heat transfer characteristics allow a flexible mechanical design. This is evident from the low operating coolant pressure and high coolant temperature and uniform metal temperature distribution. The heat pipe has the lowest rating in this group due to the geometric controls on wick pore size, wick thickness, etc., necessary to assure successful operation. In addition, it is unable to effectively cool the trailing edge by itself; supplementary cooling is needed. The modulated transpirational-cooled concept rated below the liquid metal primarily because of the complexity of the airfoil fabrication. Finally, the high-pressure air and the two-phase water system were rated below modulated transpiration cooling. The high pressure level of these systems will increase the design and fabrication problems. Also, the reduced coolant temperature level of these systems results in less effective control on vane temperature distribution.

In the rating of the Heat Exchanger group, the modulated transpiration-cooling concept has the highest rating since an exchanger is not required. The high-pressure air, the potassium heat pipe, and the liquid-metal concepts were rated approximately equal in the heat exchanger group. The two-phase water concept scored lowest, primarily because of the exchanger size and the fuel's heat sink capacity.

In the Overall System group, the modulated transpiration-cooled concept showed a slight advantage since coolant pumping power is not required.

In the Performance Effects group, all the concepts were rated equally since the effect of only stator cooling on SFC, as shown in the first line of Table XI, is less than 1% between the five advanced concepts investigated.

Rating of Rotor Concepts

In the Blades and Disc group, the liquid-metal cooling concept has the highest rating because its excellent heat transfer characteristics allow more flexibility in passage location and size. However, this is mitigated by structural problems associated with the high coolant pressure. The high-pressure steam concept has the same point rating in this group as the liquid-metal system. The high-pressure air concepts were rated below the steam and liquid-metal concepts primarily because the lower heat transfer rates complicate the coolant passage design. The modulated transpiration-cooled concept has the lowest rating in this group due to the complexity in fabricating the blades and cooling air seals.

In the Heat Exchanger group, the modulated transpiration-cooled concept has the highest rating since an exchanger is not required. Of the remaining concepts, the liquid-metal exchanger had the highest rating primarily because its small size should reduce fabrication complexity and engine space requirements. The cryogenic fuel exchanger, although smaller, will present design problems associated with introduction of the fuel into the rotating exchanger, sealing of the fuel, and supplying the fuel to the combustor.

In the Overall System group, all the systems rated approximately equal with the exception of the system using cryogenic fuel as the heat sink. The reliability of this system has a low rating because of the high thermal gradients introduced by the very low temperature heat sink and the fuel transfer seals. Also, the fuel flow passages through the disc and shaft will present structural design problems in this highly stressed component.

In the Performance Effects group, the modulated transpiration-cooled concept has the lowest rating because the blade cooling air is ineffective as a turbine working fluid and the engine SFC is adversely affected as shown in Table XI. The other systems were rated equally since the effect of only rotor cooling on SFC is less than .6% among the advanced cooling concepts investigated.

TABLE XII. RATING OF STATOR COOLING

		Weight Factor	Maximum Score	Heat Pipe
I.	Vane and Support			
	A. Fabrication - Complexity	3	15	3
	B. Performance			
	1. Coolant Temperature	2	10	4
	2. Aerodynamic Compromise	1	5	2
	C. Durability			
	1. Coolant Pressure	1	5	2
	2. Thermal Gradient Control	2	10	2
	Total		45	13
II.	Heat Exchanger			
	A. Fabrication - Complexity	3	15	9
	B. Performance - Volume	2	10	4
	Heat Sink Capacity	1	5	4
	C. Durability	3	15	12
	Total		45	29
III.	Overall System Design			
	A. Fabrication - Simplicity, Cost	2	10	4
	Developability	1	5	1
	B. Performance - Power Requirements of Auxiliaries	3	15	15
	C. Durability -			
	1. Metallurgical	1	5	2
	2. Reliability	2	10	8
	Total		45	30
IV.	Performance Effects	9	45	45
	Summary of Points			
	Group I		45	13
	Group II		45	29
	Group III		45	30
	Group IV		45	45
	Total		180	117

RATING OF STATOR COOLING CONCEPTS

Maximum Score	Heat Pipe	Liquid Metal	High-Pressure Air	Two-Phase Water	Modulated Transpiration	Baseline Transpiration
15	3	15	9	12	9	9
10	4	8	6	2	10	10
5	2	2	2	2	1	1
5	2	4	1	1	3	3
10	2	8	4	4	8	8
45	13	37	22	21	31	31
15	9	9	9	6	15	15
10	4	6	6	4	10	10
5	4	4	4	1	5	5
15	12	6	9	6	15	15
45	29	25	28	17	45	45
10	4	6	6	6	4	10
5	1	3	3	3	2	5
15	15	12	9	9	15	15
5	2	2	6	6	6	6
10	8	8	6	6	8	10
45	30	31	30	30	35	46
45	45	45	45	45	45	36
45	13	37	22	21	31	31
45	29	25	28	17	45	45
45	30	31	30	30	35	46
45	45	45	45	45	45	36
180	117	138	125	113	156	158

A

TABLE XIII. RATING OF ROTOR COOI

		Weight Factor	Maximum Score	Liquid Metal
I.	Blades and Disc			
	A. Fabrication - Complexity	3	15	15
	B. Performance -			
	1. Coolant Temperature	2	10	8
	2. Aerodynamic Compromise	1	5	3
	C. Durability			
	1. Stress, Thermal Gradient Control	3	15	9
	Total		45	35
II.	Heat Exchanger			
	A. Fabrication - Complexity	3	15	6
	B. Performance			
	1. Volume	2	10	6
	2. Heat Sink Capacity	1	5	3
	C. Durability - Stress	3	15	6
	Total		45	21
III.	Overall System Design			
	A. Fabrication - Simplicity, Cost	2	10	8
	Developability	1	5	3
	B. Performance - Power Requirements of Auxiliaries	3	15	15
	C. Durability - Metallurgical	1	5	3
	Reliability	2	10	8
	Total		45	37
IV.	Performance Effects	9	45	45
	Summary of Points			
	Group I		45	35
	Group II		45	21
	Group III		45	37
	Group IV		45	45
	Total		180	138

RATING OF ROTOR COOLING CONCEPTS

Maximum Score	Liquid Metal	High-Pressure Air	High-Pressure Air (Cryogenic Fuel)	High-Pressure Steam	Modulated Transpiration	Baseline Transpiration
15	15	9	9	12	3	3
10	8	6	6	8	10	10
5	3	3	3	3	3	3
15	9	12	12	12	6	6
45	35	30	30	35	22	22
15	6	3	0	6	15	15
10	6	4	10	4	10	10
5	3	3	5	3	5	5
15	6	6	3	6	15	15
45	21	16	18	19	45	45
10	8	6	4	6	4	10
5	3	3	3	3	2	5
15	15	15	15	15	15	15
5	3	5	5	3	3	5
10	8	6	4	8	8	10
45	37	35	31	35	32	45
45	45	45	45	45	9	0
45	35	30	30	35	22	22
45	21	16	18	19	45	45
45	37	35	31	35	32	45
45	45	45	45	45	9	0
180	138	126	124	134	108	112

Selection of Concepts

The summary of points in Table XII shows that the modulated transpiration-cooled stator has the highest rating, with 156 out of a maximum possible rating of 180. The feasibility of operating the stator with modulated cooling airflow over a range of 1 to 11% of the compressor airflow was demonstrated during experimental rig engine tests (Reference 16). Since these tests were conducted with nonflight-type valve and control system components, modulated transpiration cooling was still considered as an advanced concept. However, the cascade test of a selected stator cooling concept required for the feasibility test phase of this program would have been conducted on the design aspects which had already been demonstrated earlier had the modulated transpiration cooling concept been chosen. Therefore, this concept was not selected. Of the remaining concepts, the liquid-metal cooling concept and the high-pressure air cooling concept were rated highest and, therefore, were selected for the additional design and analysis efforts in the second phase of the program.

Of the rotor cooling concepts considered, the steam and liquid-metal cooling concepts were rated highest and therefore were also selected for additional design efforts.

3.0 HEAT TRANSFER ANALYSIS OF TWO STATOR AND TWO ROTOR COOLING CONCEPTS

During this phase of the program, the geometry of the airfoil coolant passages and the airfoil metal temperature distribution were established.

3.1 METHOD OF ANALYSIS

To establish the thermal design characteristics of each of the selected internally cooled systems, the following analytical considerations were used:

1. Heat transfer required as determined by:
   a. Hot gas pressure, temperature, and velocity
   b. Allowable metal surface temperatures
2. Metal temperature as determined by:
   a. Metal conduction rate
   b. Hot gas convective rate
   c. Coolant convective rate
   d. Coolant channel configuration
3. Heat exchanger airfoil coolant to heat sink as determined by
   a. Coolant temperature, pressure, and allowable pressure drop
   b. Heat sink fluid temperature, pressure, and allowable pressure drop
4. Materials consistent with operating temperature, pressure, and acceleration forces and compatible with the coolant.

3.1.1 Heat Transfer From the Hot Gas to the Airfoil

The total heat transferred to the blade or to the vane of the cooled turbine is determined by summing the incremental heat additions occurring chordwise along the pressure and suction sides of the blade or vane. Each of the incremental chordwise heat additions to the blade is found from the continued product of the local heat transfer rate, the temperature difference between the local recovered gas and the blade wall, and the local area involved. The local heat transfer rates are predicted by the use of relations corresponding to local flow regimes. The local recovered gas temperature, the temperature affecting the heat transfer, is evaluated from the gas relative total temperature, the local velocity and the recovery factor. The local area is the arbitrarily chosen increment

corresponding to the chordwise distance assumed to be applicable to the local heat transfer rate and temperature conditions. This method of finding the total heat load is used instead of the gross correlations available from other researchers, because it is easily evaluated after finding the local heat transfer rates that are needed for the metal temperature distribution determinations. Comparison of the overall heat loads found by this method shows good correlation with the results of previous analytical-experimental investigations.

Figures 17 and 18 present the design point chordwise local surface gas velocity and static pressure distributions calculated for the mean section of the stator vane and rotor blade profiles that were presented in Figures 3 and 4. The velocity distributions were calculated using the quasi-three-dimensional flow analysis computer program Log 2081. Suction and pressure side velocities were calculated from the mean streamline velocity within the channel formed by the surfaces of adjacent airfoils. The surface static pressure distribution was calculated from the velocity distribution and an estimated linear total pressure variation from inlet-to-throat and from throat-to-exit.

The local gas velocities are used to determine the relative gas temperature between the airfoil and main gas stream as follows (Reference 17):

$$T_{as} = T_{\infty_o} - (1 - R_T) \quad (V_\infty{}^2/2\ Cp\ Jg) \tag{6}$$

The local heat transfer rates are predicted by the use of relationships corresponding to the following flow regimes:

1. Stagnation Region

   At the leading edge and back to the cylinder tangency point with the pressure and suction surfaces, the heat transfer relations for a cylinder are used (Reference 17).

$$h_{c\theta} = 1.14 \frac{k_f}{D} \left(\frac{V_\infty \rho_f D}{\mu_f} \right)^{0.5} \left(\frac{\mu_f Cp_f}{k_f} \right) \left[1 - (\theta/90)^3 \right] \tag{7}$$

2. From the leading edge cylindrical tangency point back to the transition from laminar to turbulent boundary layer flow, the correlation for wedge-type laminar flow is used.

$$h = \frac{k_w}{x} \cdot \overline{F}_{lam} \cdot \left(\frac{\rho_w V_\infty x}{\mu_w} \right)^{0.5} \cdot \left(\frac{Cp_w \mu_w}{k_w} \right)^{0.333} \tag{8}$$

   where F_{lam} is a function of the Euler number, $y/V \frac{dV}{dy}$, found from the chordwise gas velocity distribution.

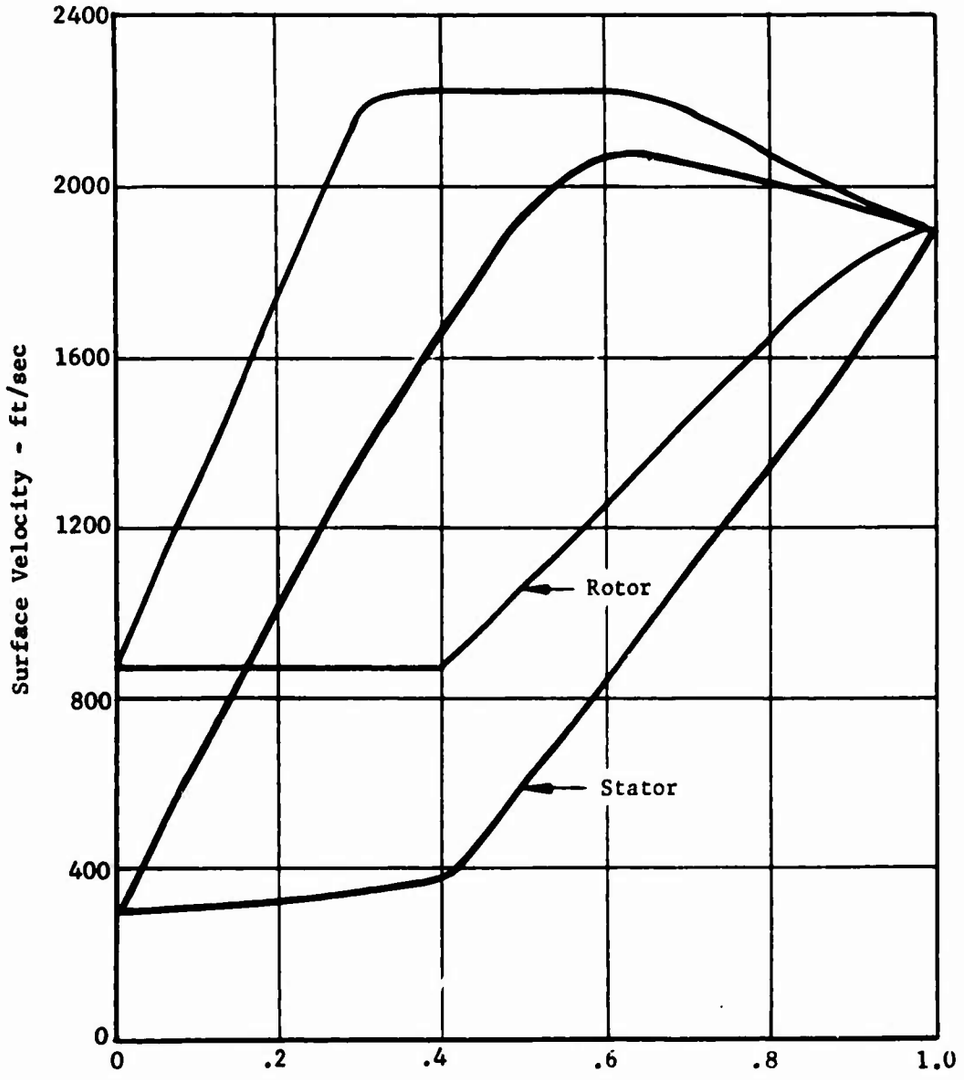

Figure 17. Velocity Distribution at Mean Section.

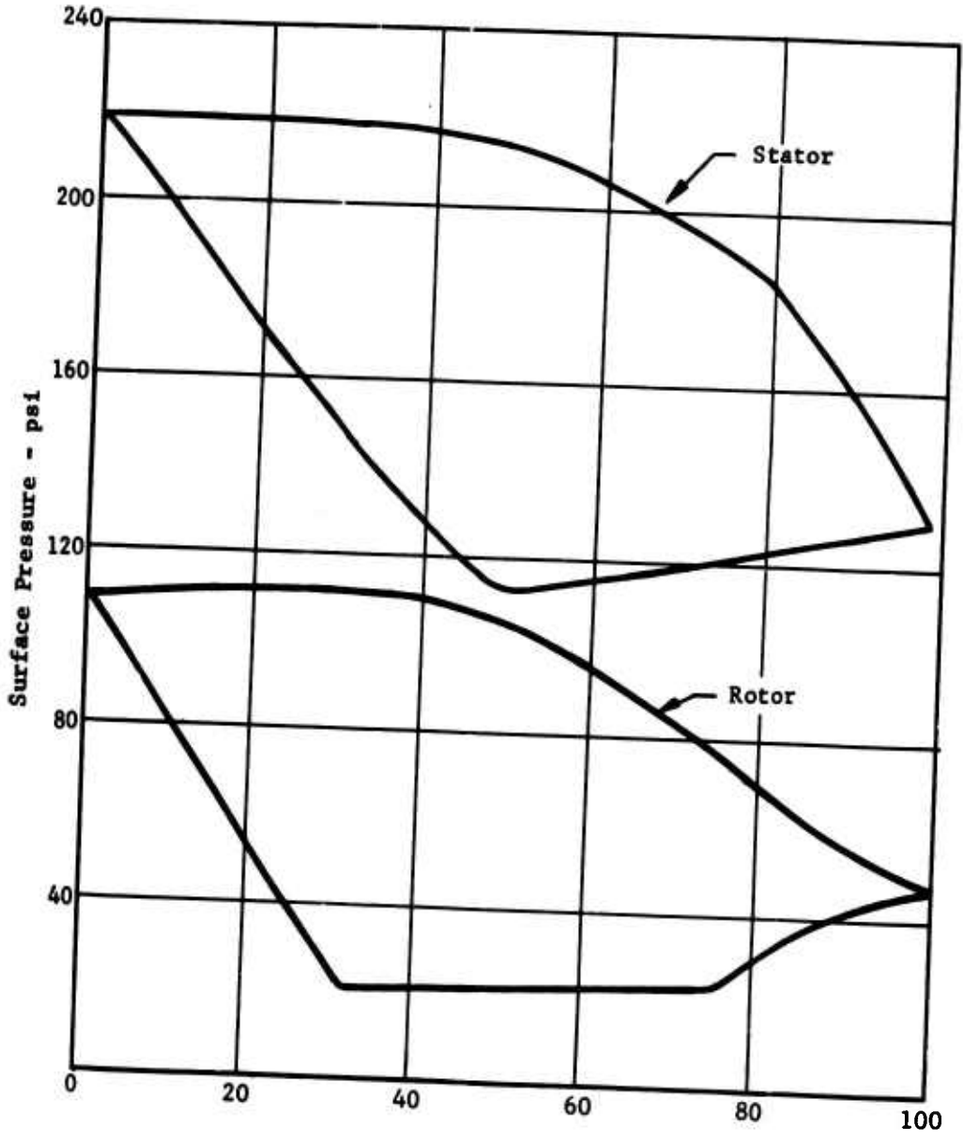

Figure 18. Pressure Distribution at Mean Section.

3. Transition From Laminar to Turbulent Flow

The transition point where the boundary layer changes from laminar to turbulent is determined by either of the following two conditions, whichever is nearest the leading edge:

a. If the Euler number is negative, or

b. If the length Reynolds number ($\rho_w V_\infty x/\mu_w$) is larger than 80,000.

After the transition point, the boundary layer is turbulent over the remainder of the airfoil surface. This method of analysis was used for the stator and rotor airfoils, although it is recognized that flow along the rotor blade surfaces is entirely turbulent. The effect of this method of analysis on the overall rotor blade heat transfer analysis will be small and within the expected accuracy of the procedures.

4. Turbulent Region

From the point where the boundary layer makes the transition from laminar to turbulent flow to the trailing edge, the correlation for turbulent flow over a flat plate is used (Reference 5).

$$h_{c\theta} = 0.0296 \frac{k_f}{x} \left(\frac{V_\infty \rho_f D}{\mu_f} \right)^{0.8} \left(\frac{\mu_f C_{pf}}{k_f} \right)^{0.333} \qquad (9)$$

For each chordal location on the blade where a heat transfer coefficient is evaluated, the incremental amount of heat going to the blade is found as follows:

$$\Delta Q = h \Delta T \; S \left[1/2 \; (X_{+1} - X) + 1/2 \; (X - X_{-1}) \right] =$$

$$h \Delta T \; S \; 1/2 \left[X_{+1} - X_{-1} \right] \qquad (10)$$

where the bracketed term represents the chordal element of the section being considered, and X is the peripheral distance of the element from the leading edge. Finally, the total heat addition to the blade is calculated as follows:

$$Q = \sum_{1}^{n} \Delta Q_n \qquad (11)$$

3.1.2 Heat Transfer Through the Metal

The heat, which flows through the metal of the blade, from the hot gas surface to the intermediate fluid surface is transferred by metal conduction through various paths creating temperature gradients. Based on the local heat transfer rates and metal conductivity values, judicious selection of the locations for the coolant flow channels is required to maintain metal temperatures and temperature gradients within acceptable limits.

The temperatures and temperature gradients are found for the design point steady-state conditions by use of the two-dimensional method of relaxation in which the blade is fragmented into elements which are then interconnected with heat flow paths or conductances. For every one of these elements, in steady state, the heat flow input must just equal the heat flow out to give a net heat retention of zero. Since the conductances are fixed, the heat flows are changed by choosing different temperatures for the elements. When the proper temperatures have been established and all the elements have zero heat retention, steady state has been reached and the temperature levels and the temperature gradients are available for study. The use of a digital computer program was employed to solve the iterative heat balance for each blade element.

3.1.3 Heat Transfer From the Blade or Vane to the Intermediate Fluid

The heat is transferred from the blades or vanes to the compressor discharge air through an intermediate fluid. The intermediate fluid passes through the blade, picking up heat from the inner blade surface by convection. This flow of heat is, as in the case of the hot gas heat flow to the blade surface, the continued product of the heat transfer rate, the temperature difference and the surface area involved. Thus, an increase in any one of these three factors must be accompanied by a decrease in one of the other factors. The blade internal heat transfer rates used here are the values for fully developed turbulent flow in the channels under consideration. Actually, for some of the channels the length/diameter ratio is small enough to indicate consideration of entrance effects, but, since the entrance effects give a less conservative approach, they are not used.

The heat transfer rate inside each coolant channel is determined from the fully developed turbulent flow relations (Reference 18). For nonliquid metal coolants the equation is

$$h = .023 \frac{k}{d} \, (Re)_f^{0.8} \, (Pr)_f^{1/3} \tag{12}$$

For liquid-metal coolants the heat transfer rate from the wall to the coolant is governed by the following equation (Reference 17):

$$h = \frac{k}{d} \left[7 + .025 \, (Re \, Pr)^{0.8} \right] \tag{13}$$

The heat transferred from each element of the blade which contains a portion of the coolant channel is described by the relation $\Delta Q = hA \Delta T$.

3.1.4 Heat Transfer From the Intermediate Fluid to Compressor Discharge Air

The heat exchanger serves to transfer the heat from the blade coolant to the compressor discharge air so that it may be recovered in a useful form. This minimizes the adverse cycle effect of removing heat from the turbine vanes and blades.

The heat is transferred by convection through the films of the coolant and compressor discharge air and by conduction through the metal wall separating them. All of the heat exchangers were designed using conventional procedures (Reference 15). In the cases where high-density finned tubes are used, the required empirical data for Colburn heat transfer factors and Fanning friction factors were obtained from Reference 13.

Factors which affect heat exchanger size are the fluid flow rate, pressure drop and operating temperature. Convection film rates increase with fluid velocity. Therefore, to obtain the required heat transfer rate for a given fluid flow rate, small-diameter, long-length coolant flow passages in the exchanger would be desirable. However, as the coolant channel diameter decreases, friction pressure losses increase with resultant increased pumping power requirements. Another factor affecting the heat exchanger design is the available flow rate and temperature level of the heat sink and airfoil coolant fluids. Increased fluid flow rates result in smaller temperature changes. This increases the mean temperature difference between the fluids, thus reducing the heat transfer area required for given values of heat transfer rate. However, as fluid flow is increased, its effect on increasing the temperature difference diminishes. Thus, the exchanger sizing is performed by balancing these factors to obtain a low-pressure-drop unit which can be accommodated within the available engine space.

3.1.5 Heat Transferred in the Heat Exchanger

The heat transferred through the metal wall separating the cooling fluid from the compressor air is governed by the same conduction relation as that for the flow of heat through the blade material.

For the internal heat transfer rates in the heat exchangers, the equations used were the same as for the internal blade heat transfer rates because in all cases turbulent flow existed.

On the compressor air side of the heat exchanger, the correlation for heat transfer rate for bare tubes is (Reference 18)

$$h = .33 \frac{k_f}{D} (Re)_f^{0.6} (Pr)_f^{.33} \qquad (14)$$

The correlation for the air-side heat transfer rate of finned tubes is (Reference 13)

$$h = J\ G\ C_p\ (Pr)^{-2/3} \tag{15}$$

where J is a function of Reynolds number.

When fins are used to increase the heat transfer capacity of a given square foot of prime surface, the heat transferred is $Q = \eta_s\ h\ A\ \Delta\ T$, where the surface effectiveness (η_s) equation is (Reference 15)

$$\eta_s = 1 - \frac{A_f}{A_f + A_b}\ (1 - \eta_f) \tag{16}$$

and fin effectiveness (η_f) is a function of

$$\left(\tau + \frac{b}{2}\right)^{3/2} \left(\frac{2h}{Kb\tau}\right)^{1/2} \tag{17}$$

3.2 RESULTS OF ANALYSIS

Based on the methods of analysis presented on the preceding pages, the thermal design of the following internal or contained coolant systems was conducted for the high-pressure turbine at the design point gas state conditions described in section 2.1:

1. High-pressure air-cooled stator
2. Liquid-metal-cooled stator
3. Liquid-metal-cooled rotor
4. High-pressure steam-cooled rotor

The thermal design was conducted to establish the heat load, coolant flow rate, coolant passage geometry, airfoil metal temperature distribution, and coolant state conditions. The analysis was based on known physical properties for Inco 713LC, which was considered as a suitable high-strength, high-temperature, nickel-base superalloy commonly used for turbines and compatible with all coolants under consideration for this analysis.

Stator Thermal Design

The equations presented in the Method of Analysis section (3.1) were used to calculate the stator vane external gas film heat transfer rates. Figure 19 presents the heat transfer rates along the chord used for the analysis of this phase. Figure 19 shows that at the stagnation point, due to impact, the heat transfer rate is high. The rate decreases as the boundary layer builds up along the airfoil surface. The layer is laminar until its thickness increases sufficiently to become unstable and then goes through the transition to the turbulent regime. The smallest heat transfer rate on each side of the airfoil occurs at this transition point.

Figure 19 shows that the calculated gas-side heat transfer rate for the stator vane is (on an average basis) almost three times the value (230 Btu/hr $ft^2°F$) assumed in the earlier conceptual analyses (Section 2.3). Consequently, the vane heat load increased approximately 80% to 3000 Btu/hr for the analysis of the selected cooling concepts.

The results of the preliminary design of the two selected stator cooling concepts are presented in Table XIV.

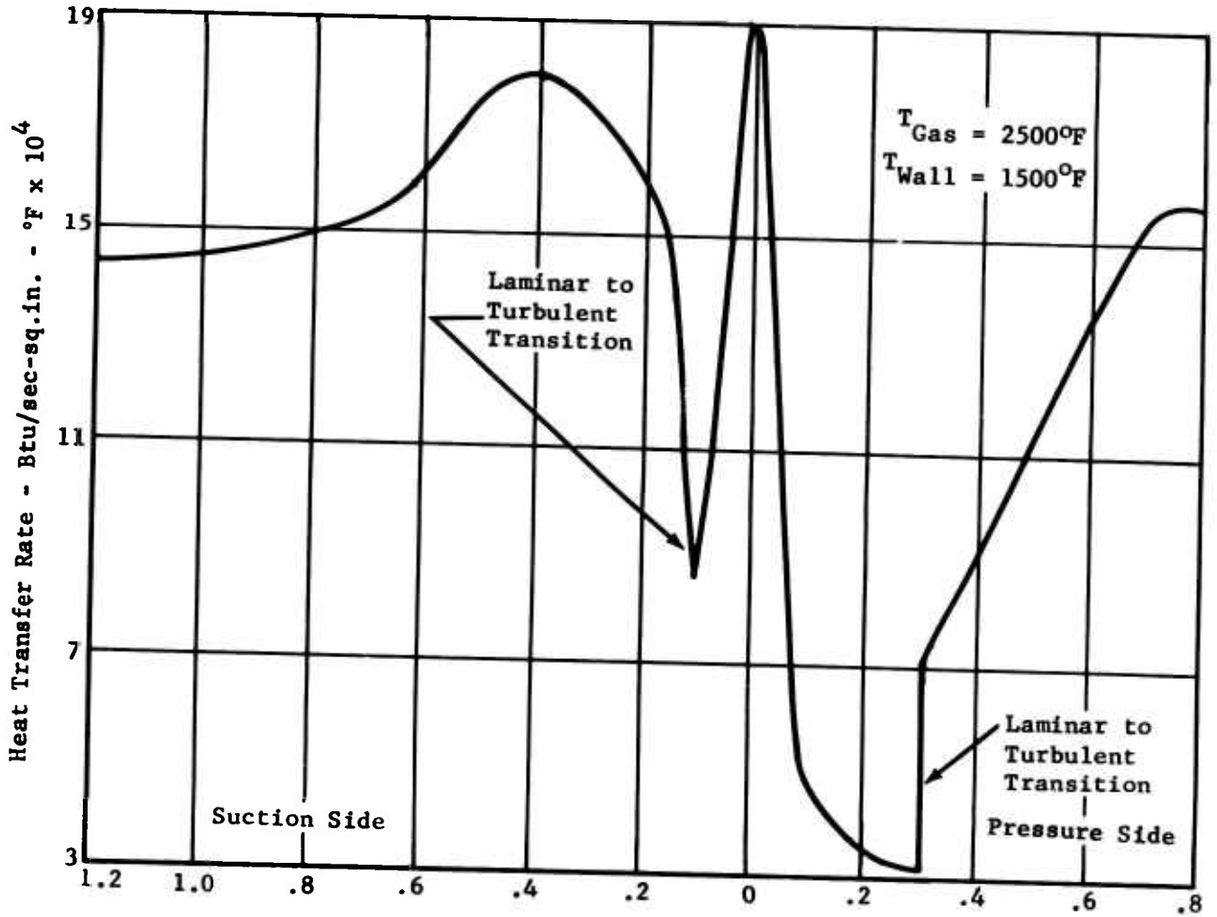

Figure 19. Stator Vane Gas-Side Heat Transfer Coefficients.

TABLE XIV. RESULTS OF THE STATOR COOLING CONCEPTS PRELIMINARY DESIGN

Airfoil Coolant		High Pressure Air	Liquid Metal
Heat Load/Vane	Btu/hr	3000	3000
Coolant Inlet Temperature	°F	1055	1442
Coolant Outlet Temperature	°F	1095	1522
Coolant Pressure	psi	2500	50
Specific Heat	Btu/lb °F	0.26	0.21
Coolant Mass Flow Rate/Vane	lb/hr	303	179
Airfoil Internal Surface Area	sq in.	0.8	0.62
Heat Sink Coolant		**Compressor Discharge Air**	**Compressor Discharge Air**
Inlet Temperature	°F	871	871
Outlet Temperature	°F	961	961
Pressure	psia	230	230
Mass Flow Rate	lb/sec	1.33	1.33

High-Pressure Air-Cooled Stator

The increased heat load for the stator required an increase in the coolant air pressure to obtain an acceptable relationship between the heat transfer coefficient, mass flow rate, coolant flow area and heat transfer surface area. However, the increased coolant pressure required the reduction of the chordal length of the coolant passage to prevent bulging of the coolant passage outer wall. This decreased the heat transfer area, which consequently required an additional increase in coolant pressure. This iterative process was continued until the coolant passage geometry and mid-chord metal temperature distribution of the two-pass high-pressure air-cooled stator as shown in Figure 20 was obtained at a coolant pressure of 2500 psi.

The coolant passage geometry of the vane consists of a series of 0.030-inch-wide channels with a 0.020-inch wall thickness to the vane outer surface. For the preliminary design, these passages were made geometrically the same. The metal temperature distribution shows a large temperature difference between the pressure and suction surfaces. This gradient can be reduced during the final design by resizing the coolant passages for the pressure side to reduce the heat transfer surface area or to reduce the coolant by a metering orifice at the channel entrance.

For the design of the two leading-edge coolant passages, the addition of fins in the passages was required to accommodate the high heat transfer rates associated with the hot stagnation point. This design resulted in an acceptable leading-edge metal temperature of 1713°F.

Special design considerations were necessary in sizing the coolant passages of the trailing edge since this section has a low wedge angle, and a 0.020-inch thickness at the trailing-edge. The design required four 0.007-inch-wide coolant slots. The vane wall thickness adjacent to the slots is also approximately 0.007 inch. The metal temperature of 1795°F at the trailing-edge represents the maximum value on the vane. Current casting technology would have to be extended to provide the necessary accuracy in coolant passage geometry, location and vane profile to incorporate these slots within the span of less than 0.4 inch. The results of a trailing-edge analysis without these four slots showed a metal temperature of approximately 2000°F with a 400°F thermal gradient between the trailing-edge and the large coolant passage.

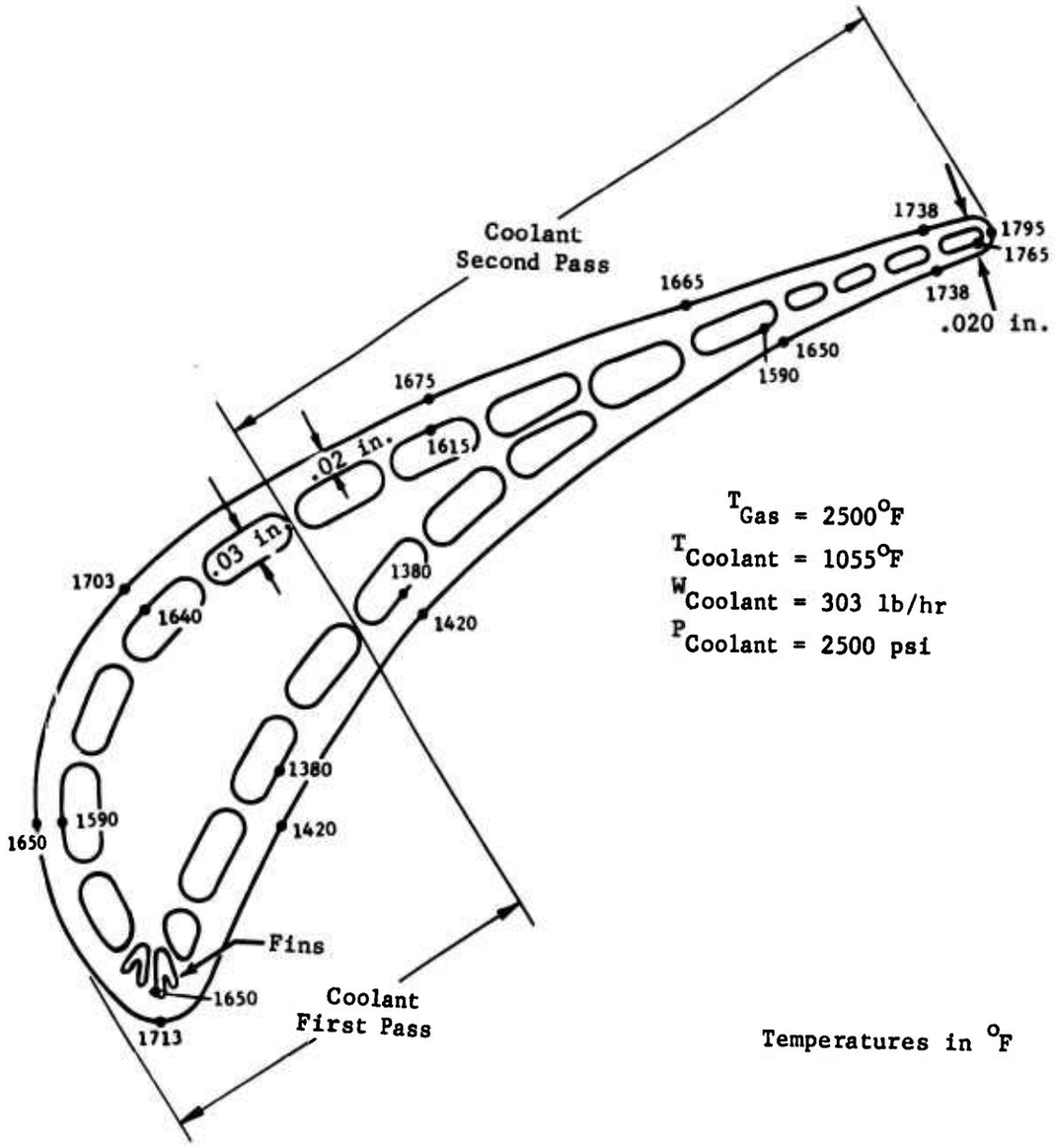

Figure 20. High-Pressure Air-Cooled Stator Vane Temperature Distribution.

TABLE XV. COMPARISON OF VANE METAL TEMPERATURES		
	High-Pressure Air	Liquid Metal
Average Airfoil Temperature, °F	1638	1542
Maximum Airfoil Temperature, °F	1795	1600
ΔT Average Airfoil to Coolant Temperature, °F	563	60

Liquid-Metal-Cooled Stator

The increased heat load for the stator did not present a major problem for the liquid-metal cooling configuration. The increased heat load was accommodated by increasing the coolant flow rate. Since coolant passages were not restrictive, the flow velocity and pressure drop were relatively unaffected.

The coolant passage geometry and the mid-chord metal temperature distribution of the two-pass liquid-metal-cooled stator is presented in Figure 21. The coolant operating pressure of 50 psi did not impose any restrictions on passage sizing. Therefore, the chordal length of the coolant passages was not critical as in the high-pressure air-cooled stator design. The passages were generously sized to maintain .020 inch wall thickness and to minimize the number of passages. The temperature distribution indicates the absence of significant thermal gradients. The high operating temperature of the liquid metal provided good trailing-edge cooling, and an acceptably low thermal gradient was obtained without introducing a coolant passage as close to the trailing edge as in the high-pressure air-cooled stator.

A summary of the significant temperatures obtained from the analysis is presented in Table XV for comparison with the high-pressure air system.

Rotor Thermal Design

The equations presented in the Method of Analysis section were used to calculate the rotor blade external gas film heat transfer rates. Figure 22 presents the heat transfer rates along the chord used for the analysis of this phase. The transition points in the curve are explained in the same manner as the curve for the stator. The heat rate values shown are optimistic since the actual boundary layer of the rotor is entirely turbulent.

Figure 22 shows that the rotor blade average heat transfer rate was approximately two times the value assumed in the conceptual analysis (Section 2.3). However, the blade heat load for the analysis of the selected cooling concepts decreased about 12% to 1439 Btu/hr as a result of the lower relative rotor entrance gas temperature (2185°F) established for this phase. This compares with 2500°F used in the conceptual analysis phase.

The preliminary designs of the two selected rotor cooling concepts and the results are presented in Table XVI.

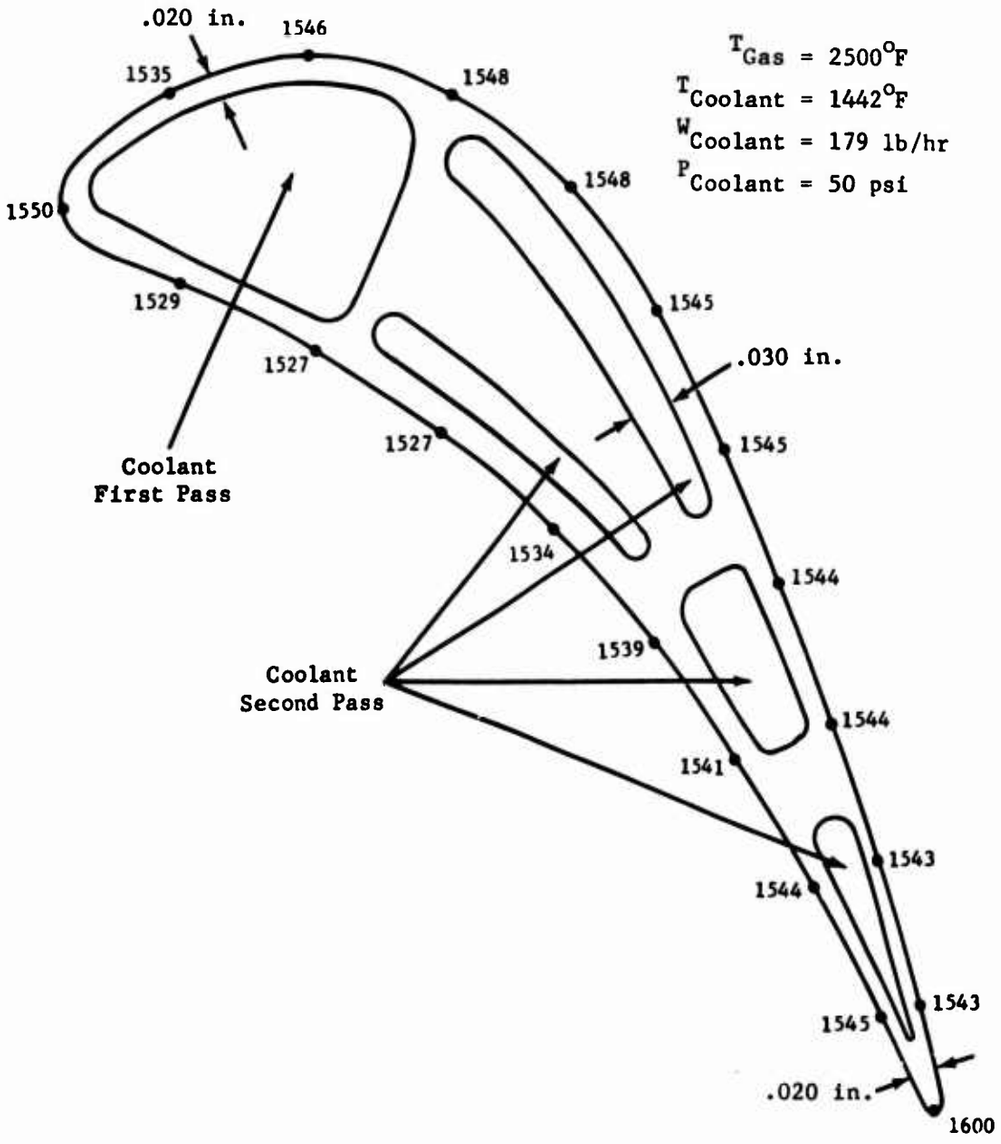

Figure 21. Liquid-Metal-Cooled Stator Temperature Distribution.

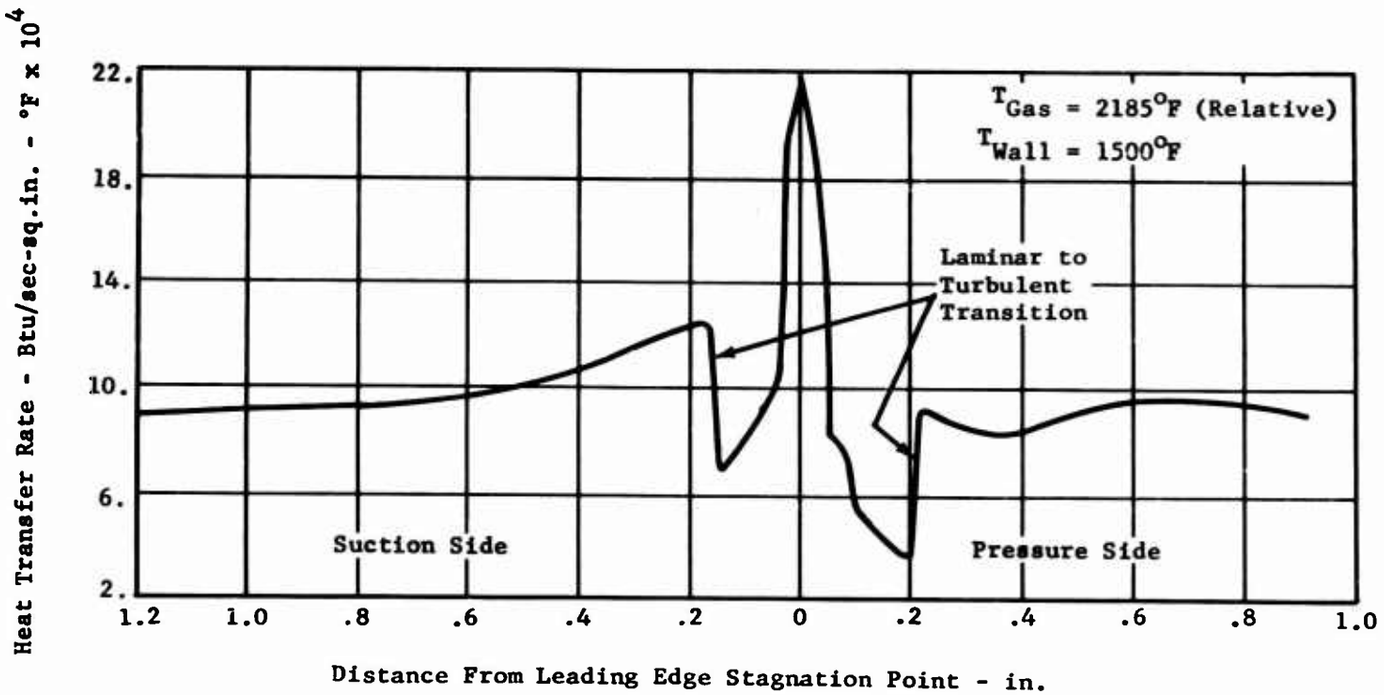

Figure 22. Rotor Blade Gas-Side Heat Transfer Coefficients.

TABLE XVI. RESULTS OF THE ROTOR COOLING CONCEPTS PRELIMINARY DESIGN

Airfoil Coolant	-	Superheated Steam	Liquid Metal
Heat Load	Btu/hr/Airfoil	1439	1439
Coolant Inlet Temperature	°F	1298	1269
Coolant Outlet Temperature	°F	1350	1322
Coolant Pressure	psi	2400	8600
Specific Heat	Btu/lb °F	0.58	0.21
Coolant Mass Flow Rate	lb/hr/Airfoil	47.5	130
Airfoil Internal Surface Area	sq in./Airfoil	0.87	0.56
Heat Sink Coolant	-	Compressor Discharge Air	Compressor Discharge Air
Inlet Temperature	°F	871	871
Outlet Temperature	°F	1009	1009
Pressure	psi	230	230
Mass Flow Rate	lb/sec	0.4	0.4

Liquid-Metal-Cooled Rotor

The coolant passage geometry and the mid-chord metal temperature distribution of the two-pass liquid-metal cooled rotor is presented in Figure 23. The coolant passage geometry was limited primarily to circular passages since the centrifugal field acting on the liquid metal increases the coolant pressure to 8600 psi in the blade tip plenum. The passages were sized to maintain 0.020 inch wall thickness to the blade outer surface and to minimize the number of passages. The temperature distribution indicates the absence of significant thermal gradients except for the trailing edge. The gradient of about 400°F between the trailing edge and the adjacent coolant passage occurred as a result of the non optimized location of this passage. During the final design, displacement of the existing passage toward the trailing edge could reduce the maximum temperature at the trailing edge to about 1600°F and provide uniform pressure and suction side surface temperatures of 1500°to 1600°F near the trailing edge.

TABLE XVII. COMPARISON OF ROTOR BLADE METAL TEMPERATURES

	Liquid Metal	High Pressure Air
Average Airfoil Temperature, °F	1504°F	1654
Maximum Airfoil Temperature, °F	1728	1715
ΔT Average Airfoil to Coolant Temperature, °F	209	330

High-Pressure Steam-Cooled Rotor

The coolant passage geometry and the mid-chord metal temperature distribution of the two-pass high-pressure steam-cooled rotor is presented in Figure 24. The coolant passage geometry was limited for structural reasons to short chordal lengths to prevent bulging of the coolant passage outer wall. The selection of a static coolant pressure of 2400 psi permitted the use of passage surfaces without internal fins except for the leading edge.

The coolant passage geometry of the vane consists of a series of 0.030-inch-wide channels with a 0.020-inch wall thickness to the blade outer surface. For the preliminary design, these passages were made geometrically the same. The metal temperature distribution shows a small thermal gradient between pressure and suction surface. This gradient can be minimized during the final design by passage size optimization.

For the design of the two leading-edge passages, fins had to be added in the passages to accommodate the higher gas-side heat transfer rates associated with the stagnation point. This conclusion was noted from an analysis of the leading-edge temperatures using coolant

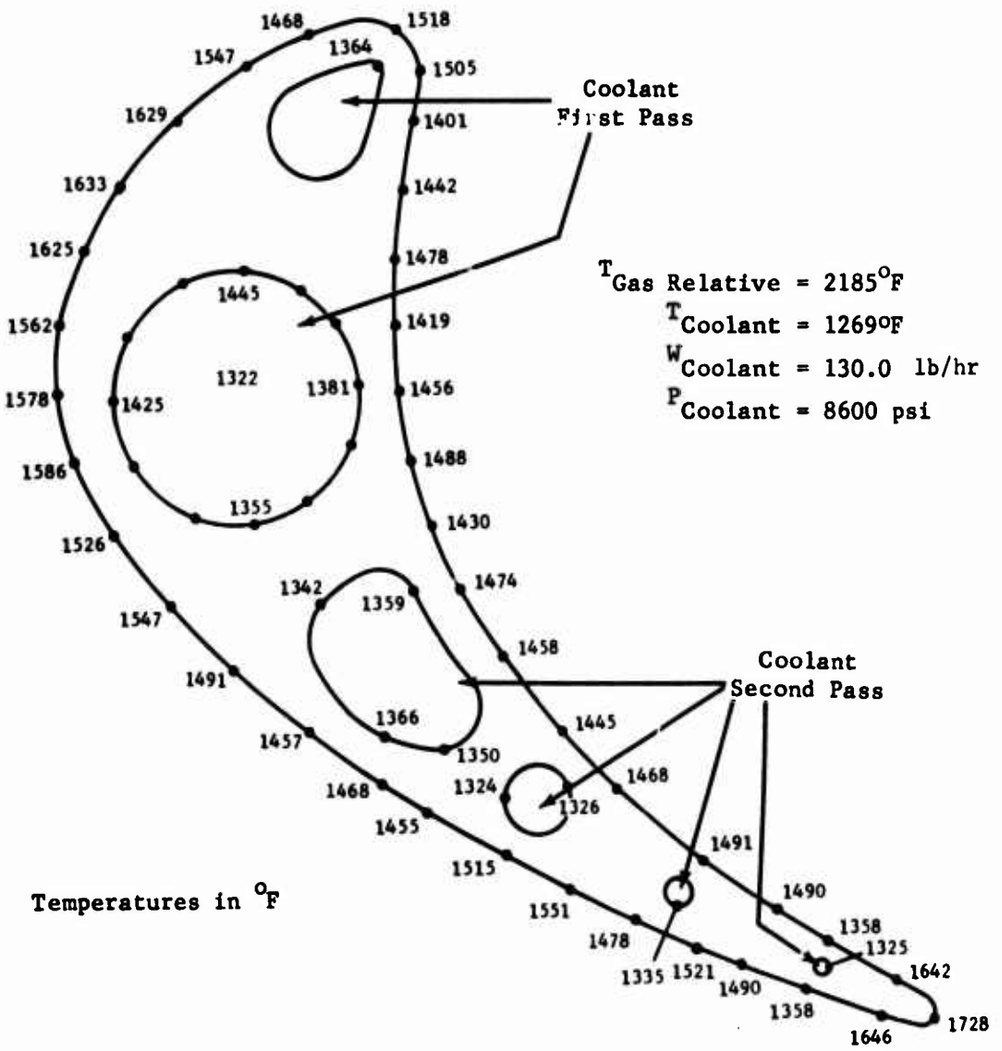

Figure 23. Liquid-Metal-Cooled Rotor Temperature Distribution.

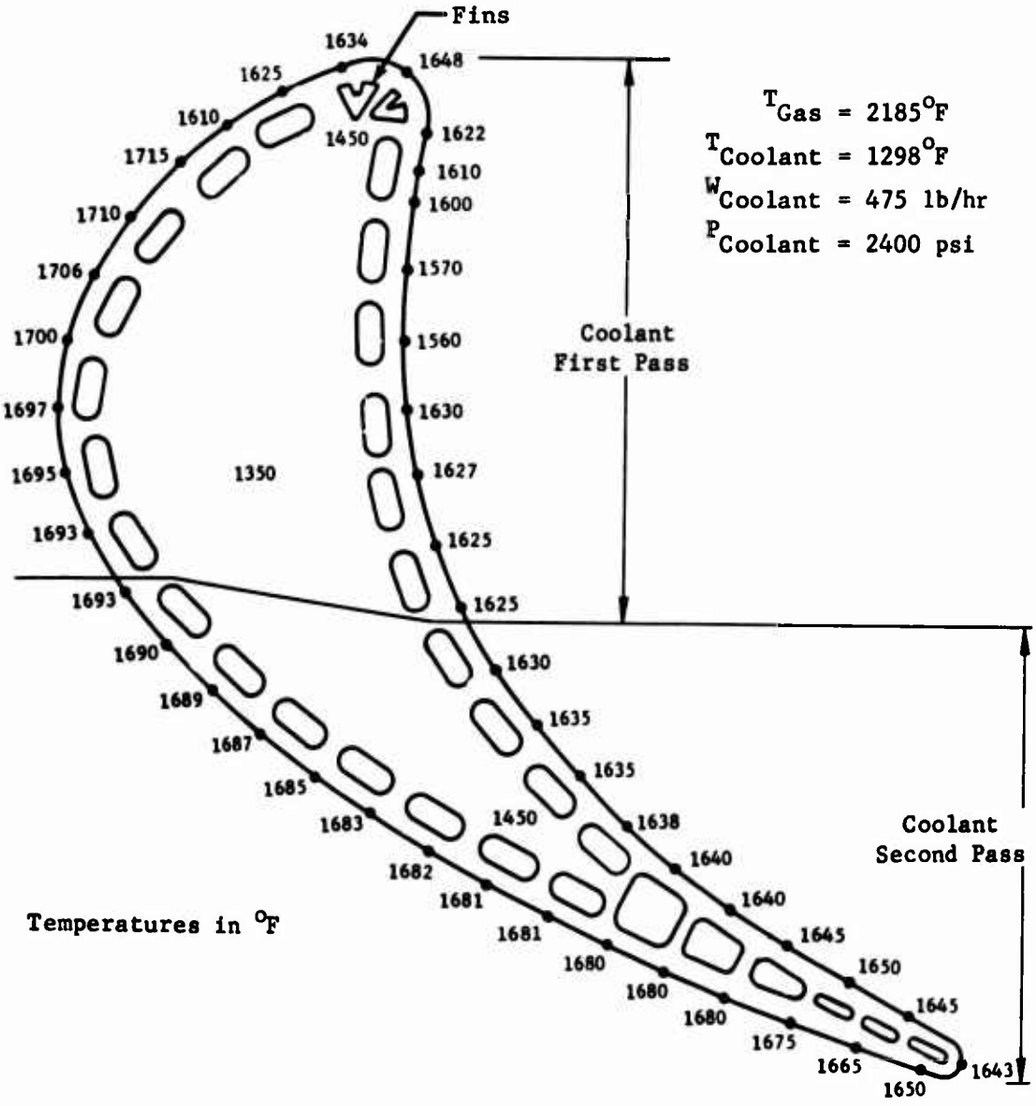

Figure 24. Steam-Cooled Rotor Blade Temperature Distribution.

passages with and without finned internal surfaces. The results are presented in Figure 25. The unfinned configuration provided a leading-edge surface temperature of 1820°F with excessive temperatures extending 0.050 inch along the pressure and suction surfaces. The finned configuration provided an acceptable leading-edge temperature of 1648°F.

Special design considerations were necessary in sizing the coolant passage of the trailing-edge region since this section has a low wedge angle and a 0.020-inch thickness at the trailing edge. The design required in-line coolant slots reducing in width to 0.007 inch at the trailing-edge slot. The blade wall thickness adjacent to these slots is also about 0.007 inch. The metal temperature of 1643°F at the trailing edges provides a low thermal gradient. A summary of the significant temperatures obtained from the high-pressure steam-cooled rotor design is presented in Table XVII for comparison with the liquid metal system.

3.3 Limitations of Analysis

The heat transfer analysis methods which were discussed in this section have certain limitations which are summarized here. The calculation of heat transfer coefficients on the gas side of the airfoil is dependent on the aerodynamic analyses which define velocity and pressure profiles for the turbine airfoil design. If the stagnation point has been incorrectly located, significantly higher leading-edge metal temperatures will result, especially for the steam and high-pressure air-cooled airfoils which require internal fins to sufficiently cool the leading-edge stagnation zone, the location of maximum heat flux. The heat transfer coefficients around the airfoil are also dependent on the local gas velocity. Thus, if the airfoil aerodynamic performance does not match the design predictions, the blade thermal analysis will be affected.

One minor point is noted for the high-pressure air-cooled stator which was based on properties of air for the coolant. After short-term operation, the oxygen in the coolant would be tied up through the oxidation mechanism. Thereafter, nitrogen properties would be more appropriate for the thermal analysis.

Airfoil metal temperatures could be altered by the oxidation mechanism. Oxidation on the gas side of the airfoil will reduce metal temperatures and, conversely, oxidation on the coolant side would increase metal temperatures. Coolant passage plugging affects thermal conditions through changes in:

1. Coolant velocities
2. Coolant-side heat transfer coefficient
3. Coolant flow redistribution or reduction

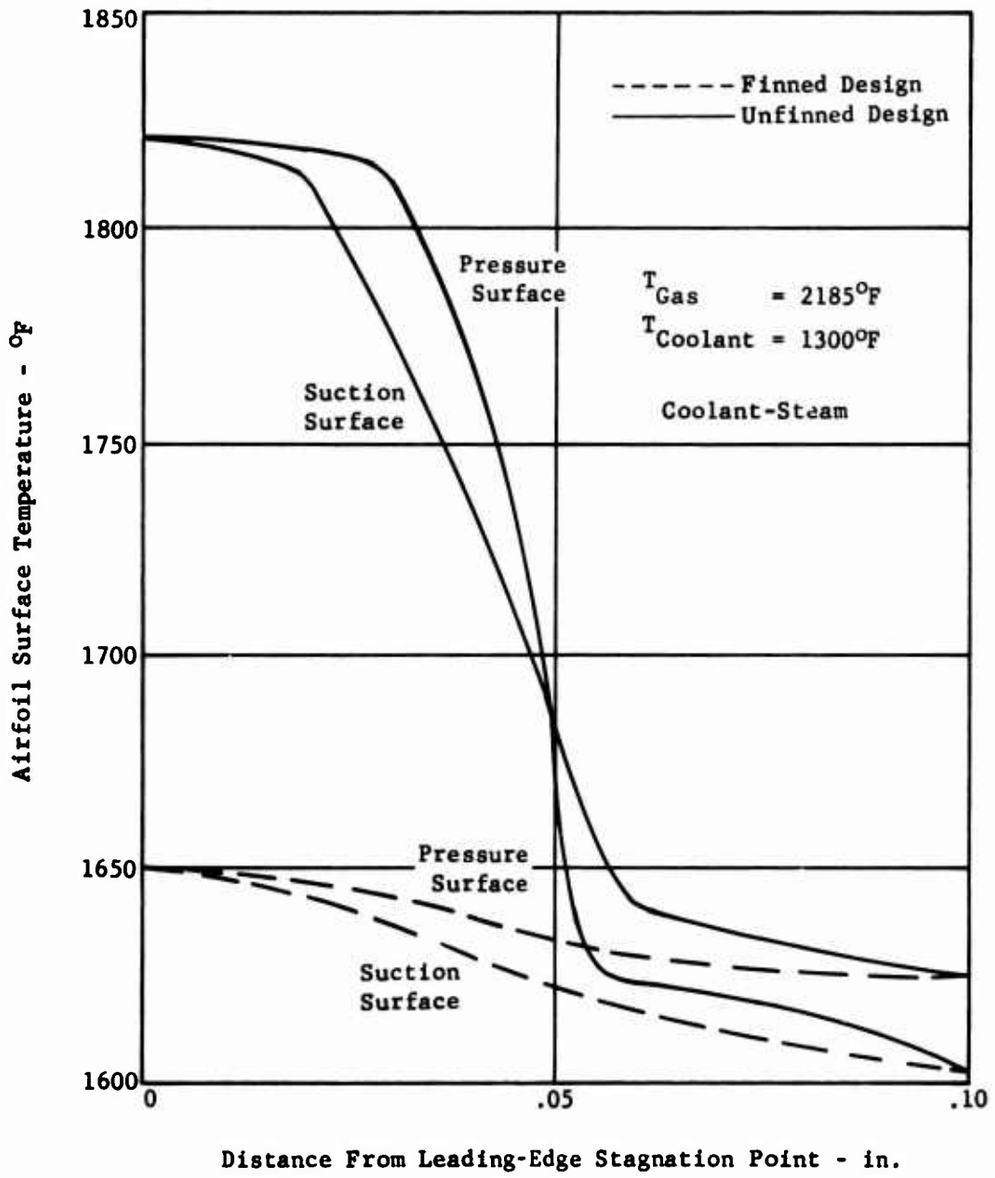

Figure 25. Effect of Coolant-Side Fins on Leading-Edge Temperature.

4.0 PRELIMINARY COOLING SYSTEM DESIGNS AND FINAL SELECTION

The objective of this phase was to conduct preliminary engine design studies to determine the feasibility of integrating the following turbine cooling systems selected for study into a small high-temperature gas turbine engine:

1. High-pressure air-cooled stator
2. Liquid-metal-cooled stator
3. High-pressure steam-cooled rotor
4. Liquid-metal-cooled rotor

The engine preliminary design parameters developed under USAAVLABS Contract DA 44-177-AMC-392(T) were similar to the engine design parameters specified for the turbine cooling investigation and, therefore, were used in this study. The engine general arrangement is shown in Figure 2. The additional design parameters which describe this engine are presented in Table XVIII.

TABLE XVIII. ENGINE DESIGN PARAMETERS

Compressor Design Point Pressure Ratio	15.4:1
Compressor Exit Temperature, °F	870
Engine Airflow, lb/sec	4.0
HP Turbine Stator Inlet Temperature, °F	2500
HP Turbine Rotor Exit Temperature, °F	1984
HP Turbine Pressure Ratio	1.49:1
Outer Liner Est. Diluent and Film Cooling Flow, %	40
Inner Liner Est. Diluent and Film Cooling Flow, %	25

During the design and heat transfer analysis of the vane, a preliminary evaluation of heat rejection systems was made to determine requirements for:

1. Heat transfer area
2. Heat sink capacity

During the system integration study, the selected heat rejection systems were sized to fit within the engine internal space. High-fin-density finned tubes or small-diameter bare tube heat transfer elements were utilized to minimize the required volume.

It was apparent that the turbine front bearing and support as shown in Figure 2 would have to be relocated in order to provide space at the front side of the turbine rotor disc for the heat exchangers associated with the rotor blade cooling concepts. The rotating heat exchanger to be incorporated in the turbine rotor cooling system requires a space preferably located (a) close to the front face of the turbine disk and extending forward and (b) within the annulus formed between the turbine shaft and the combustor inner liner. To obtain this space, the turbine bearing and bearing support shown in the figure would require relocation. Several design approaches for relocation are possible. These approaches include: (a) relocate the bearing aft of the turbine and support it either through the low-pressure turbine stator assembly or on the low-pressure shaft; (b) relocate the bearing forward of the turbine for short-length heat exchangers so that turbine overhang is minimized.

Space was insufficient to incorporate the heat exchangers at the rear of the turbine disk unless axial length was extended significantly. This was unacceptable on the basis that:

1. Engine casings and shaft length would increase with an attendant increase in weight.

2. Compressor discharge airflow used as the heat sink for the turbine cooling concepts would have a more complex path to reach the heat exchanger and return to the combustor.

3. Mainstream gas flow pressure loss between stages may increase.

Similar rearrangements are necessary if cooling of the low-pressure stage rotor is considered. However, since the relative turbine inlet temperature to the low-pressure rotor is 1791°F, little or no cooling air is required. Even at temperatures slightly higher than 1800°F, such a small quantity of bleed air would be required for external cooling that this method appears most feasible. This would avoid the complexities inherent with rearranging for a heat exchanger and associated hardware for the low cooling requirements.

Use of a reverse-flow combustor design generally results in a reduced axial length between the turbine front face and the compressor rear face which would effectively limit the available space for the rotating heat exchanger. However, the reverse-flow combustor was not selected for this 2500°F engine design since it requires a considerable increase in cooling airflow for the combustor exit reverse-flow section.

The system integration was directed at establishing: (a) the turbine cooling system arrangement and (b) the engine performance effects. For the design arrangement, the following was established:

1. Coolant flow path
2. Heat exchanger size
3. Coolant pumping technique
4. Component materials selection and compatibility with the coolant
5. Methods of fabrication
6. Special mechanical design requirements such as turbine rotor shroud cooling, sealing of the coolant and stress levels in critical areas.

To compare the effects of these cooling concepts on engine performance, the following was also established for each system:

1. System and components weight and volume
2. Coolant pumping power
3. Heat sink (compressor discharge air) pressure loss and pumping power
4. Specific fuel consumption at part and full power settings
5. Specific horsepower at full power
6. Turbine inlet temperature at part power
7. Influence of combining dissimilar cooling concepts for the stator and rotor (including utilizing transpiration air cooling for either blade row)

4.1 DESCRIPTION OF STATOR COOLING SYSTEMS

The preliminary design arrangements of the engine hot section incorporating the high-pressure air system and the liquid-metal system for the turbine vanes are shown in Figures 26 and 27, respectively. A summary of the heat exchanger and coolant pump design parameters is presented in Table XIX.

The coolant flow path for each system was designed to provide an appropriate compromise between:

1. Low pumping power requirements
2. Minimum length, volume, weight
3. Low compressor discharge air (heat sink) pressure loss
4. Utilization of compressor discharge (heat sink) air for other cooling requirements
5. Least complexity for installation and removal of the hermetically sealed system for maintenance
6. Ease of fabrication and assembly of system components

Neither cooling system studied required an increase in basic engine envelope (excluding the coolant pump) to incorporate the system heat exchanger and coolant manifolds.

The flow paths of the liquid-metal and high-pressure air coolants are similar. In both systems the coolant is pumped into a supply manifold in the stator outer housing, where it is distributed to each vane inlet exchanger and then into the forward plenum in the vane outer gas shelf. The coolant then makes the first cooling pass through the forward chordal section of the airfoil and into the plenum at the inner gas shelf. The coolant returns through the rear section of the airfoil, making its second cooling pass, and into the rearward plenum in the outer shelf. The coolant in these plenums serves to cool the gas shelves. From this point, the coolant flows radially outward through the vane outlet exchanger, into the return manifold in the stator housing. The coolant is then circulated through the external piping to the pump. To return the heat to the cycle, compressor discharge air is ducted over the outer half of the vane inlet and outlet dischargers and then turned 180 degrees to flow over the inner half of these exchangers. Since the exchanger airflow pressure loss of 2.0 psi is less than the combustor airflow loss, the air then enters the combustion chamber through conventional diluent and liner cooling holes.

The air pressure loss in the 180-degree flow-return bend is negligible due to the low Mach number level even if the air turning vanes are removed. This airflow turn is estimated at .03 psi.

During the 180-degree turn, a small quantity of the compressor discharge air is bled to convectively cool the turbine rotor shroud.

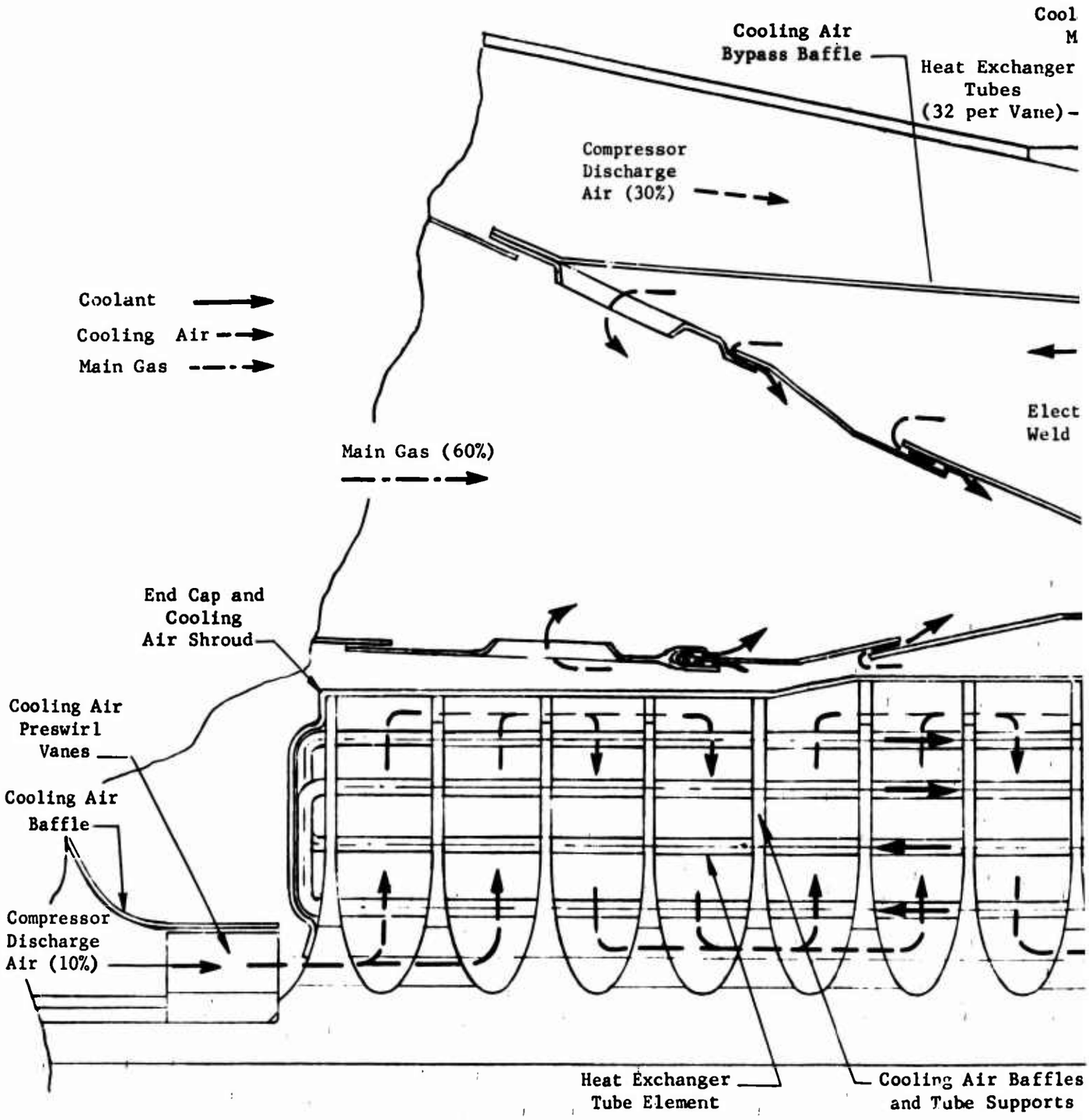

Figure 26. Flow Path of Air-Cooled Stator and Superheated Steam-Cooled Rotor.

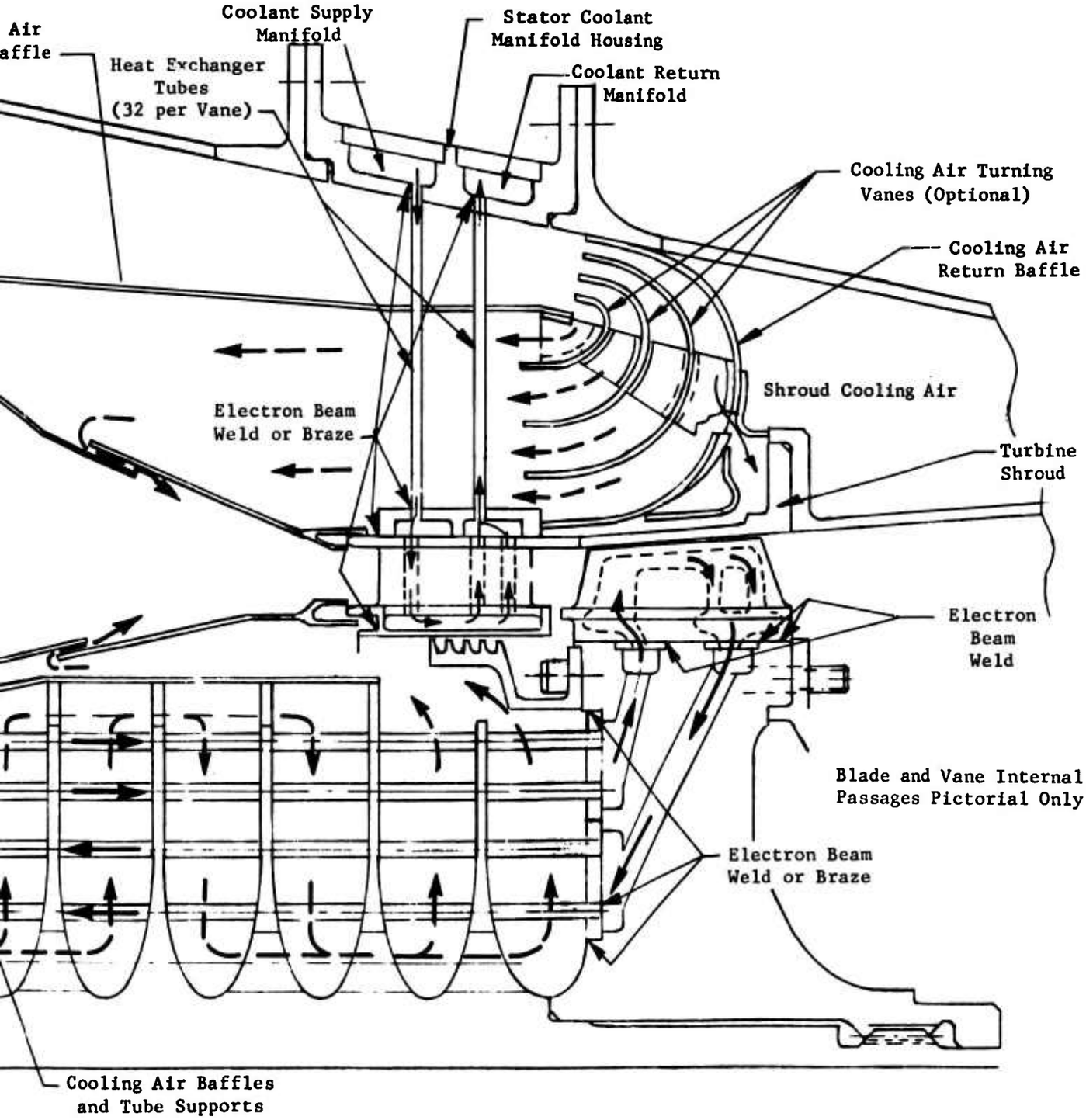
Air
affle
Coolant Supply
Manifold
Stator Coolant
Manifold Housing
Heat Exchanger
Tubes
(32 per Vane)
Coolant Return
Manifold
Cooling Air Turning
Vanes (Optional)
Cooling Air
Return Baffle
Shroud Cooling Air
Electron Beam
Weld or Braze
Turbine
Shroud
Electron
Beam
Weld
Blade and Vane Internal
Passages Pictorial Only
Electron Beam
Weld or Braze
Cooling Air Baffles
and Tube Supports

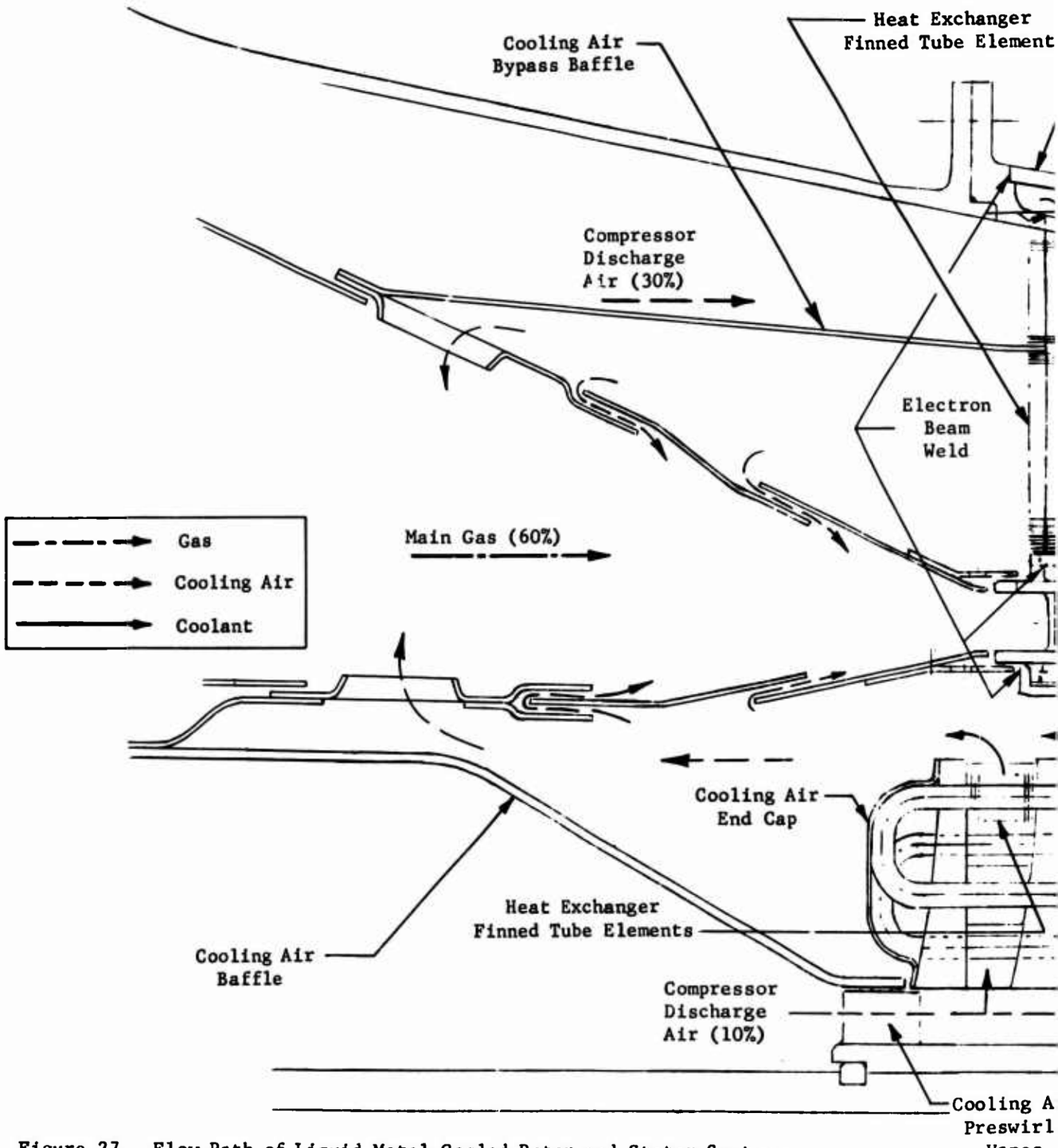

Figure 27. Flow Path of Liquid-Metal-Cooled Rotor and Stator System.

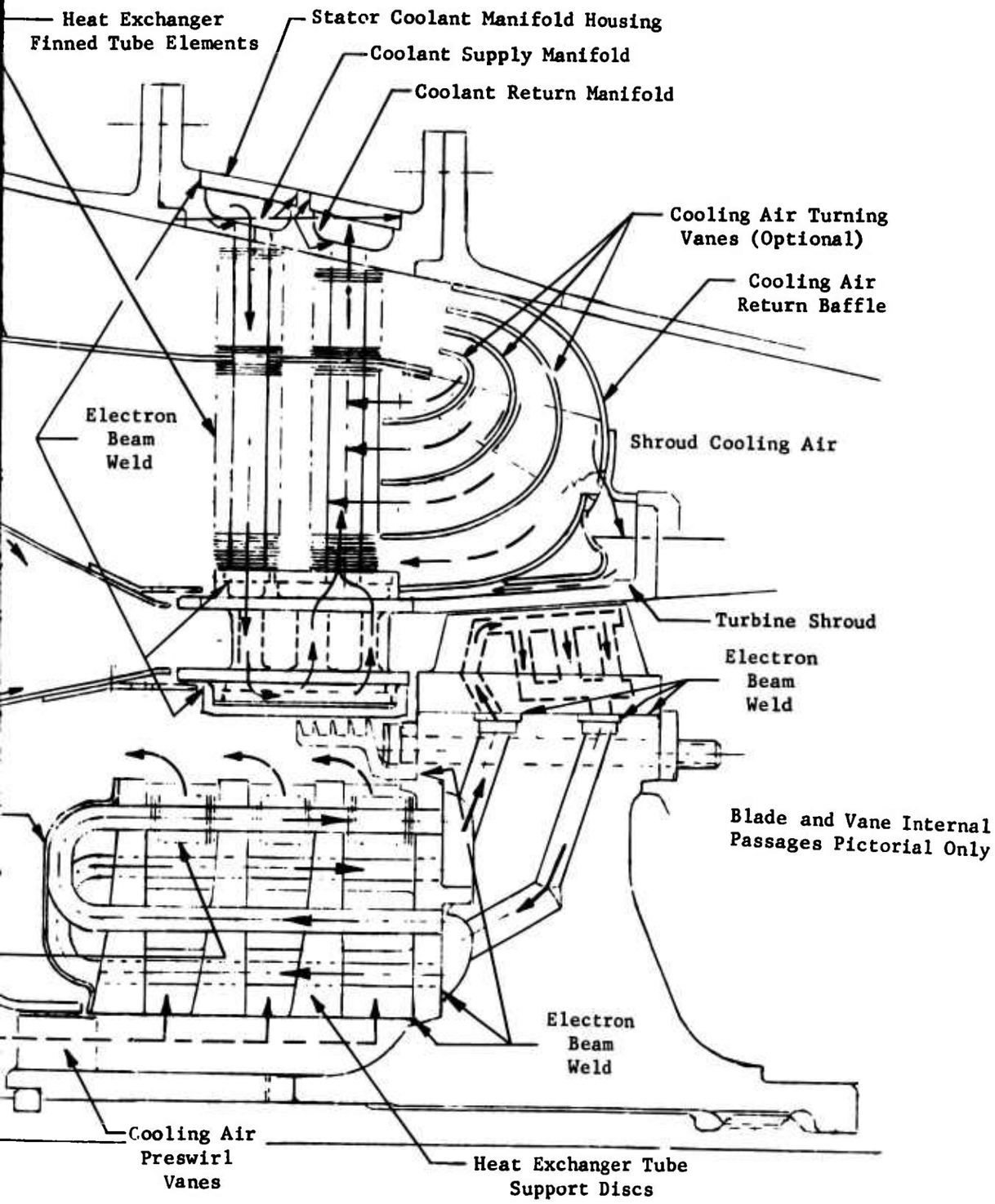
Heat Exchanger
Finned Tube Elements
Stator Coolant Manifold Housing
Coolant Supply Manifold
Coolant Return Manifold
Cooling Air Turning
Vanes (Optional)
Cooling Air
Return Baffle
Electron
Beam
Weld
Shroud Cooling Air
Turbine Shroud
Electron
Beam
Weld
Blade and Vane Internal
Passages Pictorial Only
Electron
Beam
Weld
Cooling Air
Preswirl
Vanes
Heat Exchanger Tube
Support Discs

TABLE XIX. RESULTS OF THE STATOR COOLING SYSTEM HEAT EXCHANGER PRELIMINARY DESIGN

		High Pressure Air	Liquid Metal
Exchanger Geometry	-		
Type OD	in.	Tubes	Finned Tubes
Fin Outer Diameter	in.	-	0.375
Tube Outer Diameter	in.	0.060	0.188
Fin Density	Fins/in.	-	40
Tube Wall Thickness	in.	0.010	0.015
Number Tubes/Airfoil	-	32	2
Heat Transfer Area			
Coolant Side	sq in.	6.83	1.68
Heat Sink Side	sq in.	10.25	22.50
Envelope Volume	cu in.	99.3	104.0
Face Area	sq in.	22.0	22.0
Flow Path Length			
Coolant	in.	3.4	3.4
Compressor Discharge Air	in.	1.3	1.3
Weight (Loaded Including Piping)	lb	10.6	11.5
Circulating Pump			
Type	-	Centrifugal	Rotary Induction
Drive	-	Electric Motor	Accessory Gearbox
Horsepower	-	10.0	1.0
Weight (With Drive Motor)	lb	25	7
Volume (With Drive Motor)	cu in.	245	51
Cooling Required	-	Yes	Yes
Δ P Heat Sink	psi	2.0	2.0

An alternate but more complex arrangement to effect turbine rotor shroud cooling uses the stator internal coolant. The vane outer gas shelf and the rotor shroud are an integral unit. For this design this unit has interconnecting coolant passages. The vane coolant returning to the lower section of the plenum in the outer shelf is diverted through the interconnected axial passages in the rotor shroud. The coolant in the shroud makes two passes, returning the coolant to the upper section of the vane shelf plenum. From this point coolant enters the exchanger tubes as in the initial system.

4.1.1 Liquid Metal Coolant System

Each liquid-metal-cooled airfoil has two 1.2-inch-long finned tube heat exchangers attached to the vane tip. The tube outer diameter is 0.188 inch with a 0.015-inch wall. Stainless clad copper core fins of 0.003 inch thickness and with a 0.025-inch pitch (40 fins per inch) are Nichrobrazed to the tube. The fin outer diameter is 0.375 inch. A typical tube is shown in Figure 28. The finned tube design for this heat exchanger is based on data for Colburn heat transfer factor (j) and Fanning friction factor (f) presented in Reference 13.

The liquid metal pump shown in Figure 29 is a geometric scale of an experimental pump (Reference 13). The pump is a rotary induction (permanent magnet) type which can be driven by conventional means, i.e., electric or hydraulic motor or directly from the engine accessory gearbox as shown in Figure 29. A typical liquid metal pump cross section showing the major components is shown in Figure 30. The nonmagnetic pump cell, which is an annular passage through which the liquid metal flows, is located between a rotating permanent magnet and a stationary flux return path. The lines of flux pass from the north pole of the rotating magnet, through the pump cell and the liquid metal, into the laminated stator flux return path and back through an adjacent section to the south pole of the magnet. Pumping pressure is generated by the force produced on the liquid metal through the interaction of the magnetic flux acting on liquid metal eddy currents. Since no moving parts are in contact with the liquid metal, there are no seals. Therefore, the pump design is inherently leak-proof.

Current permanent magnetic materials are limited to applications where operating temperatures are below 900°-1000°F. Above these temperatures the magnetic strength deteriorates rapidly. Although the 1442°F liquid metal is not in direct contact with the magnetic rotor, it is anticipated that some degree of cooling may be required to maintain magnetic strength or to minimize the heat input to the rotor shaft bearings. This cooling can be accomplished by integrally incorporating air pumping vanes during the casting or machining of the magnets and by venting the pump bearing support housing to ambient air. Use of compressor low-pressure air bleed may be an alternate scheme for pump rotor cooling. (This cooling requirement was not considered in the cycle analysis discussed in Section 4.4).

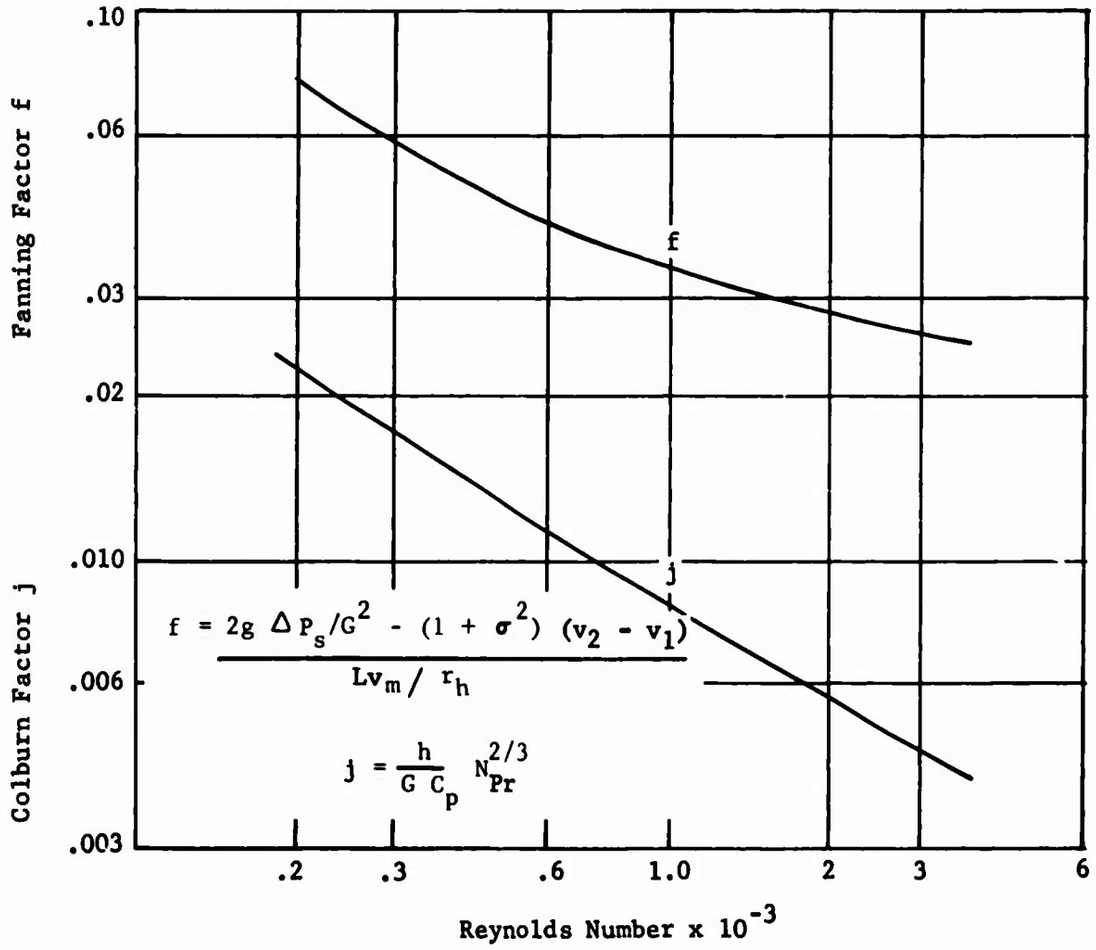

3/16-Inch Tube OD - 40 Straight Fins per Inch

Figure 28. Finned Tube for Liquid-Metal Heat Exchanger.

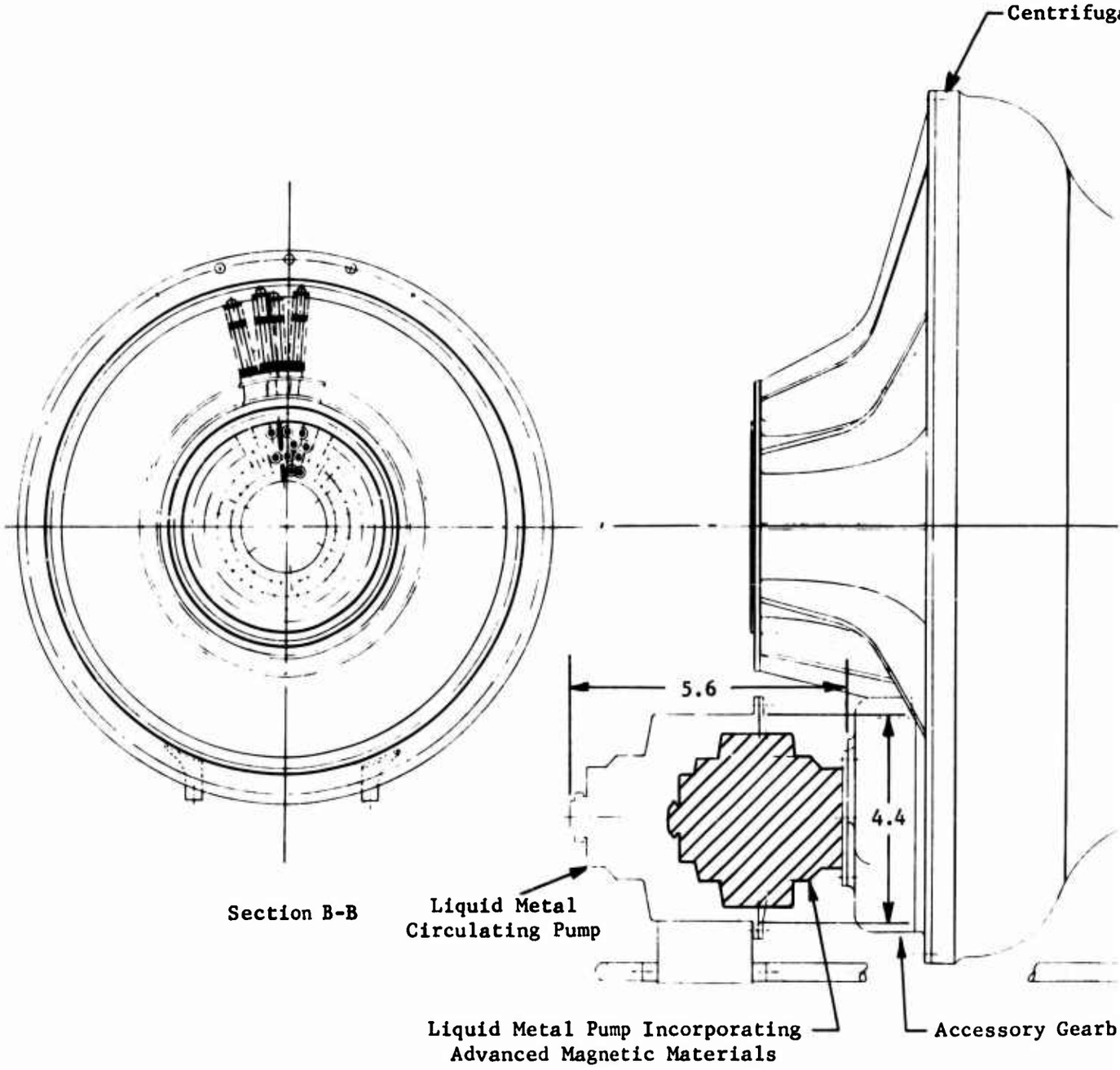

Figure 29. Preliminary Engine Design With Liquid-Metal-Cooled Rotor and Stator System.

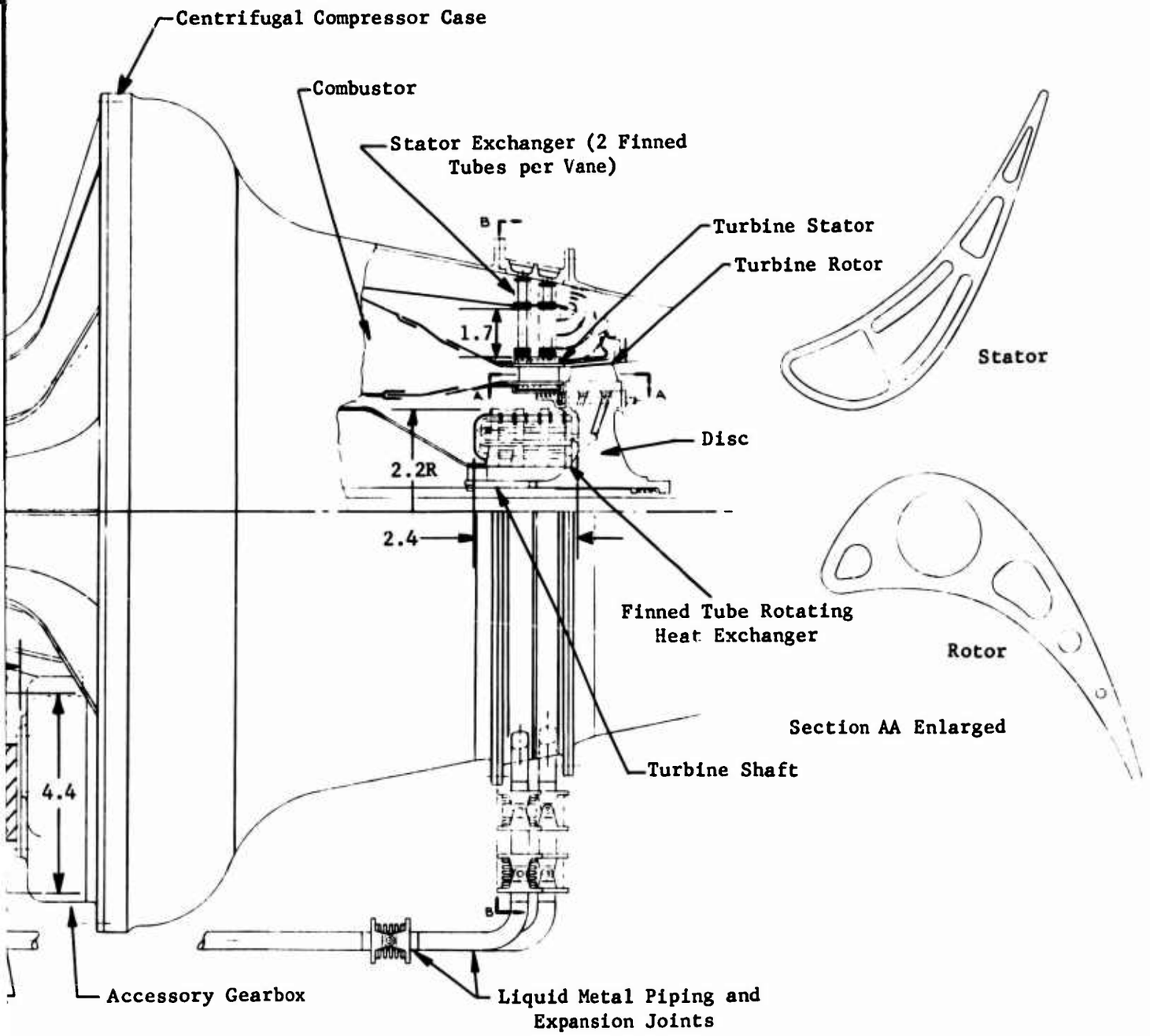
Centrifugal Compressor Case
Combustor
Stator Exchanger (2 Finned Tubes per Vane)
Turbine Stator
Turbine Rotor
1.7
Stator
Disc
2.2R
2.4
Finned Tube Rotating Heat Exchanger
Rotor
Section AA Enlarged
Turbine Shaft
4.4
Accessory Gearbox
Liquid Metal Piping and Expansion Joints

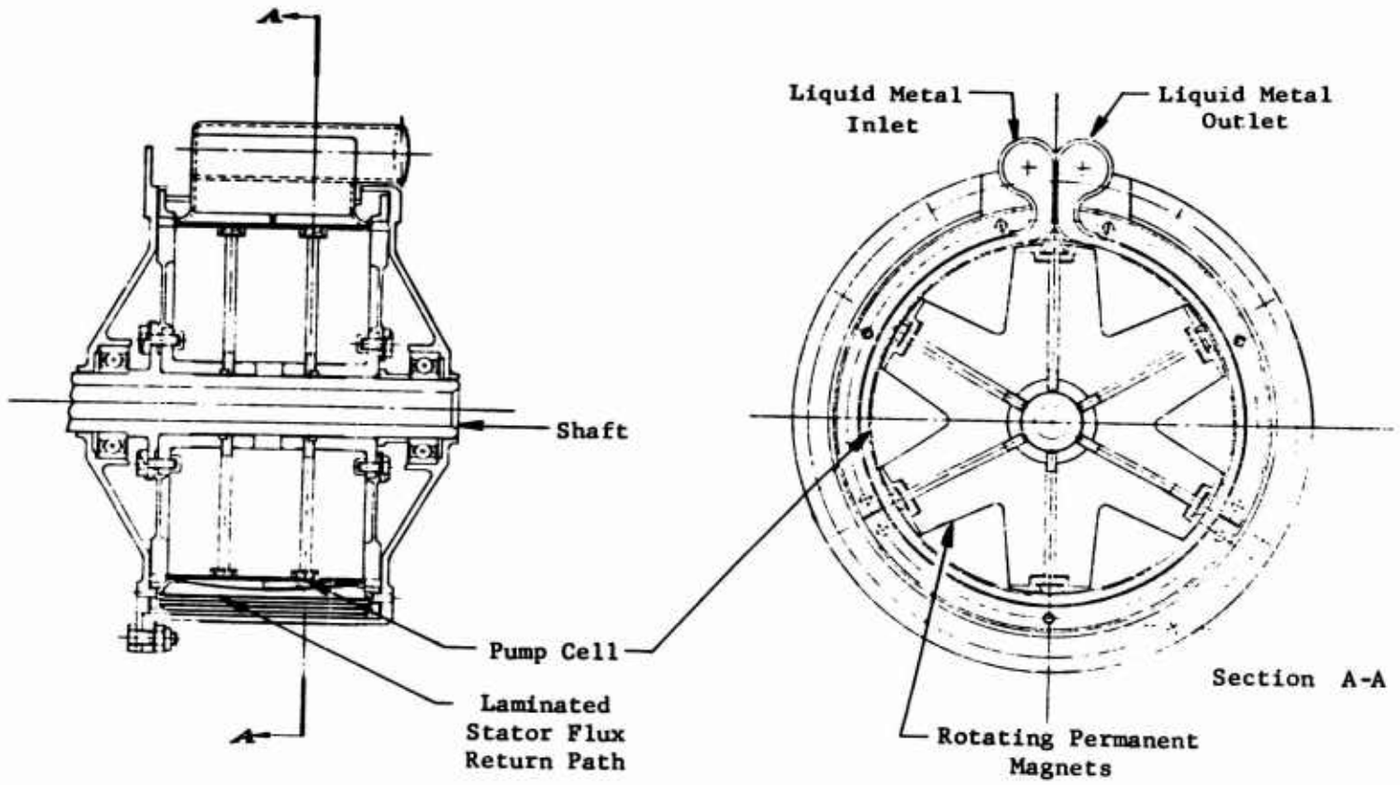

Figure 30. Liquid Metal Pump Design Arrangement.

Advanced magnetic materials have recently been developed. One of these, a samarium-cobalt material, has an energy product which is 3-4 times greater than Alnico V used in current pump designs. Since the energy product is a measure of the magnet volume, the effect of this increased energy product would be to reduce the pump rotor size proportionately; or for the same size as the Alnico material, operation at higher temperature without cooling may be feasible. There are limitations on pump size reduction since (1) minimum shaft diameter is based on torque requirements or pole to hub interface and (2) minimum height of the pump cell flow annulus is based on hydraulic frictional losses and magnetic damping. Furthermore, mechanical and magnetic retention properties of this new material at elevated temperatures are not fully established.

Figure 29 shows the pump envelope using the Alnico magnets. The weight of this pump is 7.0 pounds. Pump design point speed is 6000 rpm. The pump envelope using the advanced magnetic material has been estimated and is also shown in Figure 29. Weight of this pump would be approximately 75 percent of the Alnico magnet pump.

Typical performance of an unmodulated liquid metal system are characteristically presented in Figure 31. These curves are for a pump design which has been optimized for weight and volume for flight requirements rather than for efficiency. The system performance characteristic shows a reduction in flow and pressure with pump rotor rpm. Since the pump is driven off the gas generator accessory gearbox, reductions in liquid metal flow and pressure would occur with an attendant reduction in required pump horsepower. Since the vane heat load is reduced as power and gas generator rpm are reduced, the unmodulated liquid metal system performance characteristic is compatible with gas generator operating characteristics. Since gas generator rpm is 90 percent and 80 percent of design for the 60 percent and 35 percent power settings, respectively, it may be desirable to further reduce liquid metal flow rates at these power settings in order to maintain a constant vane temperature throughout the operating regime. The following alternatives to reduce the liquid metal flow are possible:

1. Three-speed drive for 35 percent, 60 percent and 100 percent power
2. Infinitely variable speed drive
3. Back-pressure valve between the pump and the heat exchanger
4. Bypass circuit around the vanes

The three-speed drive and the variable-speed (mechanical or hydraulic) drive are bulky and add substantially to the system weight. The back-pressure valve and the bypass circuit absorb more horsepower to produce the required flow for part-power conditions. Furthermore, cooling the liquid metal in the bypass circuit to reject the heat input due to pumping work may be necessary at high bypass flow conditions.

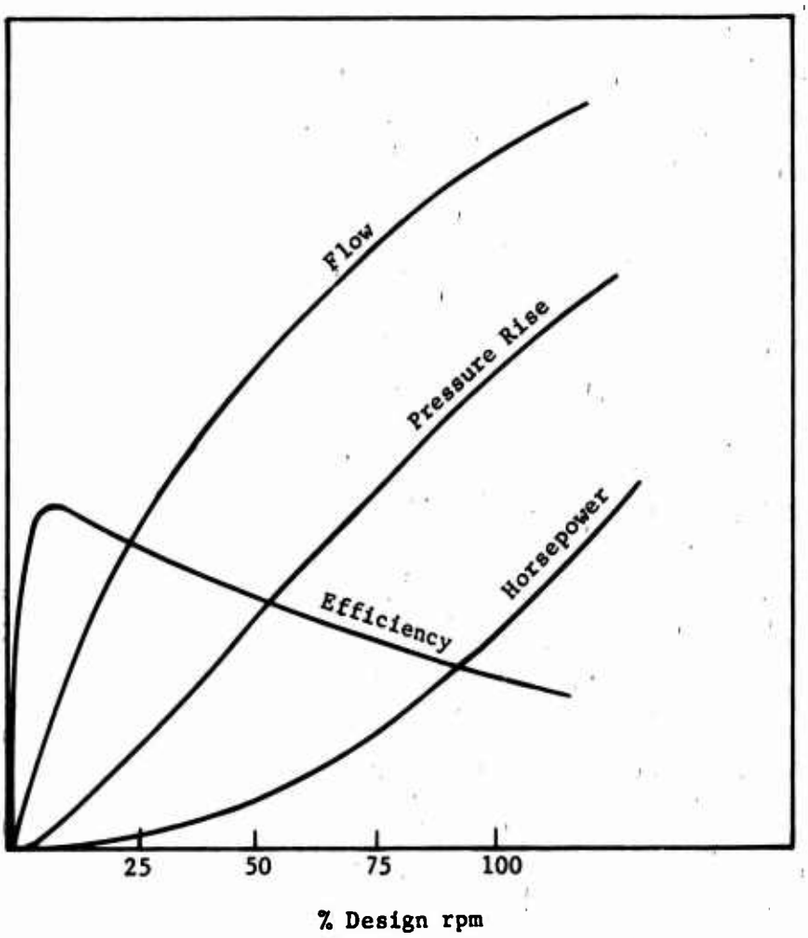

Figure 31. Unmodulated Liquid Metal System Performance Characteristics.

Pumping power extraction is shown (in Section 4.4) to produce up to 2.5 percent increase in SFC per horsepower over the engine operating range. Since the liquid metal system pumping power requirement is one horsepower or less over this range, the additional mechanical complexity and increased system weight associated with modulating liquid metal flow rate at part power do not appear justified.

Bellows-type connections are provided in the piping (a) to minimize thermal stresses due to differential growths between the pump mounting and the turbine support housing, (b) to compensate (as an expansion chamber) for the change in liquid metal volume that occurs between the idle and full power conditions, and (c) to permit flexibility in the piping between the pump and turbine housing during the installation or removal of the integrally welded system.

4.1.2 High-Pressure Air Coolant System

The high-pressure air cooling concept for the vanes utilizes inlet and outlet heat exchangers fabricated of .060-in.-diameter, thin-walled, unfinned tubing. Each air-cooled vane has 32 tubes distributed equally between the inlet and outlet exchangers as shown in Figure 32. Circulation of the high-pressure air is accomplished by a centrifugal boost impeller providing a 1.02 pressure rise ratio to maintain the coolant system pressure level at 2500 psi. To minimize pump horsepower requirements, the system must be initially charged to the 2500-psi operating pressure. Direct drive of the centrifugal impeller from the accessory gearbox was considered unfeasible since the air leakage rate through the impeller drive shaft seals at the 2500-psi level would result in loss of coolant during the mission. Therefore, a "canned" rotor design, consisting of the pump and drive which are encased in a pressure vessel, was selected to effectively prevent coolant leakage. The air pump and drive volume is 245 cubic inches, which is substantially larger than the liquid metal pump, and the estimated weight is 25 pounds.

The pump is driven by a constant-speed 11,800-rpm induction motor which is powered by the 400-cps aircraft electric generator. The 2500-psi coolant air is also used as the impeller shaft bearing lubricant. Oil cooling of the electric motor may also be required due to the high temperature of the vane coolant.

The principal performance disadvantage of this system is that there is no flexibility to vary the coolant flow at part-power operation, and the required pumping power remains essentially constant over the full operating range of the engine. Although the liquid metal system pumping power is small and therefore has no appreciable effect on cycle performance, the 10-horsepower air pump power requirement over the engine operating range does introduce a cycle performance penalty at the part-power condition of up to 2.5 percent on SFC.

Bellows-type expansion connections in the piping between the pump and the turbine housing are incorporated in the high-pressure air system to

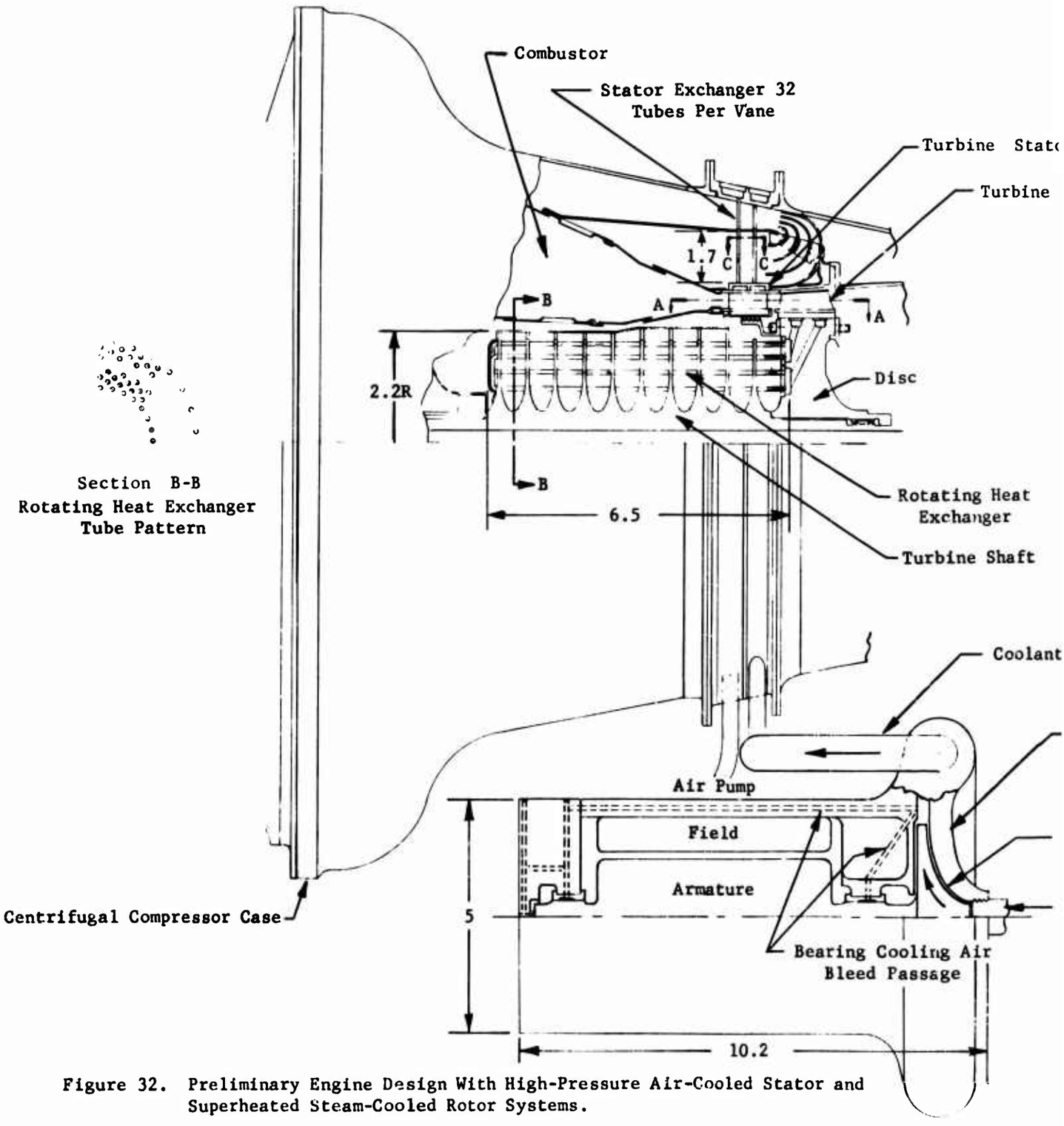

Figure 32. Preliminary Engine Design With High-Pressure Air-Cooled Stator and Superheated Steam-Cooled Rotor Systems.

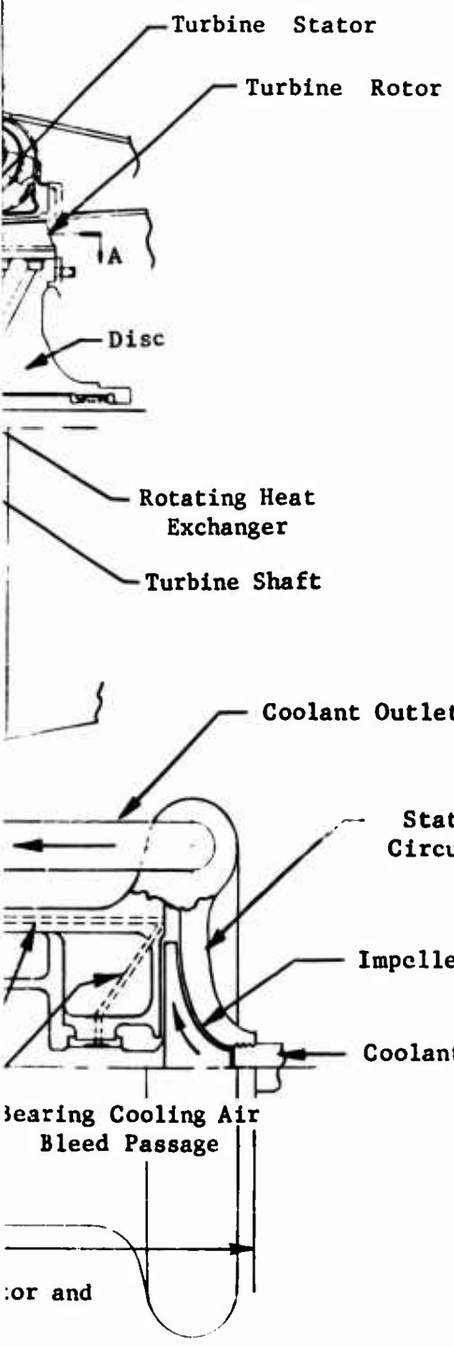

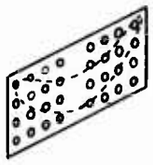

Section C-C
Heat Exchanger
Tube Pattern
Enlarged View

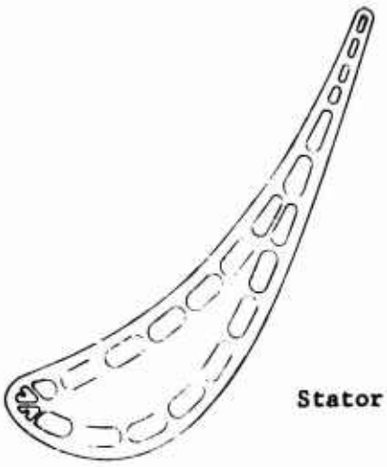

Stator

Section A-A
Enlarged View

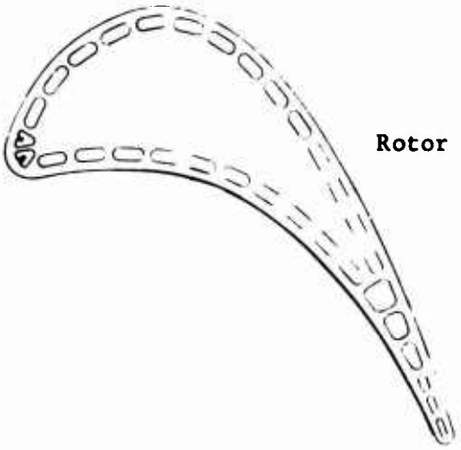

Rotor

minimize stresses due to differential thermal growths and to facilitate installation and removal of the integral system. This piping arrangement and the self-contained drive motor feature offer a degree of freedom in mounting the pump on the engine where effects on engine volume, frontal area, or center of gravity are minimized.

4.1.3 Method of Fabrication

The two vane cooling concepts are fabricated and assembled as follows:

1. The airfoil and gas shelves of the vanes are precision investment castings using Inco 713 LC alloy. The 0.030-inch coolant passages are integrally cast. Electrical discharge-machining of 0.007-inch coolant holes may be necessary if ceramic core problems associated with strength, stability, or removal occur.

2. The parallelogram-shaped Inco 600 inner gas shelf cap is electron beam welded (Figure 27) to the vane to form the hub plenum for shelf cooling and to transfer the coolant from the forward passages in the airfoil to the rearward passages.

3. The exchanger seamless drawn tubes fabricated of thin-wall AISI 316LC material are press-fit and welded into the tube holes in the vane outer gas shelf cap, and this subassembly is weld-attached to the vane to form the coolant inlet and outlet plenums. The plenum also provides cooling of the outer gas shelf.

4. The heat exchanger tubes of each vane assembly are press-fit into the tube holes in the AISI 316LC wrought alloy manifold headers of the turbine stator housing fabricated from forged and machined rings. This is accomplished as the set of vanes is positioned on a hub support fixture.

5. The loosely assembled stator is then fixtured to maintain dimensional integrity during the final welding process which follows.

6. The heat exchanger tubes are welded to the headers in the turbine stator housing.

7. The stator housing inlet and outlet manifolds are sealed by circumferentially welding 180° sector rings to the outer diameter of the housing.

8. The turbine rotor shroud, fabricated from an Inco 718 forged and machined ring, is circumferentially butt welded to the vane outer shelves.

Use of the electron beam welding process is desirable for joining of the vanes to gas shelf caps, manifolds to housings, and rotor shroud to vane

shelves since the low heat input during this welding process results in minimized distortion of the subassemblies. The exchanger tubes for the liquid metal system are electron beam or inert-gas welded to the caps and headers. Fixturing of the subassemblies to position details and to provide chills or heat sinks to minimize thermal distortion during the welding or brazing process is necessary. However, final machining of fore and aft bolting flange and the inner diameter pilots of the stator coolant manifold housing and the radial spline attaching flange of the turbine rotor shroud is required to assure the location of the true position of the stator assembly.

4.2 DESCRIPTION OF ROTOR COOLING SYSTEMS

The superheated steam-cooled rotor blade concept and the liquid-metal-cooled rotor blade concept also represent systems that remove heat from the blades and return it to the engine cycle. In both systems, the difference in densities of the hot and cold fluids in the presence of a centrifugal field is utilized to provide the pumping force necessary to circulate the coolant. Preliminary design arrangements of the two rotor blade cooling concepts are presented in Figures 26 and 27. The rotor coolant systems are independent of the stator coolant systems; therefore, either combination of rotor and stator coolant systems can be utilized for an engine without change to the basic system design.

In both systems the compressor discharge air is used as the heat sink. Table XX summarizes the design of the rotating heat exchangers.

The major system components consist of an integrally cast cored rotor blade, a disc with machined grooves on the outer diameter and the front face, and a rotating heat exchanger.

In both rotor cooling system designs, shown in Figures 26 and 27, the flow paths of the coolant are identical except for blade passages. Cold coolant enters six flow passages in the turbine disc. These passages connect the heat exchanger outlet header on the front face of the disc to the blade supply manifold located on the disc rim. The supply manifold connects to each blade, and the coolant continues an outward radial flow path, making its first pass through the forward coolant passages in the airfoil to the blade tip plenum. From the tip plenum, the coolant flows radially inward through additional blade cooling passages in the rear section of the airfoil to the hub gas shelf plenum and into the return manifold on the disc rim. The coolant flows through six return passages in the disc to the exchanger inlet header on the disc face and enters the heat exchanger. Here, compressor discharge air, used as the heat sink, removes the heat from the coolant and returns it to the engine cycle through delivery to the combustion chamber diluent and liner cooling air slots.

Preswirl vanes are provided to bring that portion of the compressor discharge air required for cooling up to the rotational speed of the heat

TABLE XX. RESULTS OF THE ROTOR COOLING SYSTEM HEAT EXCHANGER PRELIMINARY DESIGN

Exchanger Geometry		Superheated Steam	Liquid Metal
Type	-	Tube	Finned Tube
Fin Outer Diameter	in.	-	0.250
Tube Outer Diameter	in.	.062	0.125
Fin Density	fins/in.	-	40
Tube Wall Thickness	in.	.010	.015
Number Tubes - Total	-	112	60
Heat Transfer Area			
Coolant Side	sq in.	174	43
Heat Sink Side	sq in.	262	424
Envelope Volume	cu in.	98.8	28.4
Face Area	sq in.	3.8	3.14
Flow Path Length			
Coolant	in.	13.0	4.0
Compressor Discharge Air	in.	13.3	1.5
Weight (Loaded)	lb	6	8
Pumping Horsepower	-	16	16

exchanger. Air pumping work in the radial outflow passage of the exchanger is

$$HP = \frac{W}{550} \frac{(V_1^2 - V_2 C)}{g} \tag{18}$$

where V_1 = tangential velocity at exchanger outlet, fps

V_2 = tangential velocity at exchanger inlet, fps

C = tangential component of air velocity into exchanger fps

Therefore, to minimize pumping work, it is desirable to impart a large tangential velocity to the air entering the exchanger. Preswirl vanes accelerate the low-velocity compressor discharge air in the vicinity of the exchanger entrance up to the rotational speed of the exchanger at the hub by converting static head to velocity head and imparting the appropriate air angle to enter the rotating exchanger.

The preswirl vanes are designed to meter the airflow rate to the exchanger. The small pressure losses associated with swirl vanes, heat exchanger tubes and pumping are overcome by the 60-psi pressure rise developed by centrifugal pumping in the rotating exchanger. Therefore, the pressure at the outlet of the exchanger is greater than compressor discharge pressure and thus may enter the combustor as dilution air and film cooling air similar to the stator design.

4.2.1 Liquid-Metal-Cooled System

The liquid metal rotating heat exchanger design consists of sixty 0.125 inch OD finned U-tubes with 0.015 inch wall thickness. The fin diameter has an OD of 0.250 inch and a density of 40 fins per inch. There are three cooling airflow radial passes over the 60 tubes. Air entering the exchanger initially flows radially outward, returns toward the hub on the second pass, and finally exits radially outward. The three air passes in the exchanger are baffled by thin discs which also serve to support the exchanger finned tubes. Cowling at the exchanger OD and at the forward end prevents air bypass or leakage.

4.2.2 Steam-Cooled System

The rotating heat exchanger design for the superheated steam-cooled blade cooling concept consists of 112 U-tubes of 0.062 inch diameter with 0.010 inch wall thickness. Five radial passes are made by the compressor discharge air over each tube section. Again, the tube support discs baffle the air, and cowling at the exchanger outer diameter and forward end prevents air bypass and leakage.

4.2.3 Method of Fabrication

The fabrication and assembly of the liquid metal and steam cooling systems are similar in concept and are described below:

1. The rotor blade, of Inco 713LC alloy, is a precision investment casting with the tip plenum, the coolant passages and the hub shelf plenum integrally cast. The blade tip plenum is open.

2. The disk is machined from forged Inco 718 material. Two grooves machined on the front face form the heat exchanger coolant manifolds, and two channels machined on the OD form the blade coolant manifolds. Six passages are then machined radially and axially to connect each face groove with a corresponding circumferential channel.

3. Inco 718 forged machined rings are welded onto the disk rim to cover the cylindrical coolant supply and return manifolds. This provides an uninterrupted cylindrical surface on the disk OD which is required for electron beam welding of the blade butts to the disk rim.

4. The set of rotor blades is fixtured to the disc and electron beam welded in a single, full-penetration, circumferential weld pass. This type of blade-to-disk weld attachment has been successfully performed for 0.5-inch penetration on typical turbine materials such as Inco 713 or Mar M 302 blade and Inco 718 disc materials (Reference 10) and for 0.8-inch penetration on Inco 713 and Inco 718 combination during subsequent efforts.

5. The blade cooling passages are connected to the manifolds in the disc by electrical discharge machining radial passages through the blade gas shelf and into the blade plenum, through the rings in the disk rim, and into the coolant supply or return manifold in the disk. The hole made in the gas shelf for this operation is then plug welded. A possible alternative to this procedure is to electrical-discharge machine a connecting passage between blade and disk through the open blade tip via the cast coolant passages.

6. The blade tip closure weld is made by electron beam welding an Inco 718 tip cap to the air- 'l.

7. The liquid metal finned tube heat exchanger and the steam U-tube exchanger are assembled and installed as follows:

   a. The liquid metal exchanger is fabricated by alternately stacking the Inco 718 support discs and flat disc fins over the 60 Inco 718 U-tubes. The tubes are positioned in a triangular pitch pattern to form a compact annular unit

along the engine axis. The exchanger assembly is then furnace brazed to provide good heat transfer contact between the tubes and fins, and to attach the tubes to the support disks. The tubes are press-fit into the headers and inert gas arc welded. These headers are electron beam welded in the two grooves in the disk face which form the cooling manifolds.

b. The steam exchanger is fabricated by assembling the 112 Inco 718 U-tubes onto the one-piece tube support disks and shaft component. The tubes are positioned in a triangular pitch pattern to form a compact annular unit along the engine axis. The tubes are also press-fit into the headers. The U-tubes are furnaced brazed to the support disks and shaft component and headers. Finally, the exchanger assembly is furnace brazed to the blade and disk assembly.

4.3 METALLURGICAL AND STRESS CONSIDERATIONS

Materials considered for application to the turbine stator and rotor for the internally cooled systems are based on the turbine design aspects of mechanical and thermal loads. Nickel-base and cobalt-base alloys typically used for turbines are candidate materials. However, in selection of the blade or vane materials for the liquid-metal-cooled system, consideration must also be given to the following in order to limit the corrosion and mass transfer rate of the selected materials:

1. Temperature differential between cold and hot areas
2. Oxygen content of NaK
3. Velocity of coolant
4. Effect of NaK operating temperature on material strength

Studies of the effect of liquid sodium and NaK alloys on high-temperature materials in the range of 1000° to 1650°F have been pursued at the Oak Ridge National Laboratory (Reference 21). The objectives of these studies were to evaluate the mass transfer resistance of nickel - and cobalt-base materials under various conditions of temperature, flow rate, and purity.

The major finding of these studies indicated that the formation of macroscopic cold-region deposits was initially observed in the 1300°F to 1375°F range and that the extent of deposition increased with increasing temperature. The weight changes of nickel-base alloys increased with change in temperature to 1650°F. However, it was noted that the addition of 3% Al to the nickel-base system noticeably lowered the mass-transfer rate. Their investigation included a nickel-base alloy (Inconel X-750) with 0.5% Al and 2.5% titanium, which showed the lowest mass-transfer rate among the alloys tested. In fact, at a temperature of approximately 1350°F, Inconel X-750 indicated a very low weight of accumulated deposits. Above this temperature, however, Inconel X-750 exhibits an increase in mass transfer deposits with increasing temperature. At 1500°F for 1000 hours, Inconel X-750 indicated a maximum hot area attack of 0.001 inch with plain sodium as the circulating fluid and a 300°F change in temperature, at a velocity of up to 7 feet/second. The total weight of deposits at 1500°F showed a linear dependence on both flow rate and temperature difference with time. A minimum threshold ΔT of 60°F was found necessary to give greater than zero mass transfer rate, with the rate increasing with increasing temperature. Changes in oxygen concentration in sodium from 90 to 500 ppm had little effect on the rate of transfer of a material such as Inconel 600. Higher oxygen concentrations increased the mass-transfer rate.

Evaluations similar to those for nickel-base materials are required for cobalt-base materials such as Mar-M-509. Blade and vane materials for cooling by 2400-psi superheated steam @ 1300°F and 2500-psi air @ 1055°F, respectively, will depend largely on the operating stresses. For metal

temperatures up to 1500°F, a material such as Udimet 700 is considered. Above this temperature, cast materials such as Inconel 713 LC and In 100 are applicable. For this turbine application, Inconel 713 LC or In 100 is recommended for rotor and stator blades cooled with sodium-potassium alloy operating at low oxygen content levels, a difference of temperature between hot and cold regions of 100°F, and a flow rate of approximately 10 feet/second. These materials have approximately 6% aluminum and should provide excellent performance based on the reported Inconel X-750 tests.

The preliminary selection of current materials for the highly stressed areas is presented in Table XXI.

TABLE XXI. TURBINE MATERIALS SELECTION

Stator System	High-Press. Air	NaK
Vanes	Inco 713 LC	Inco 713 LC
Heat Exchanger Tubes	316 LC	316 LC
Method of Assembly	Braze	Weld
Rotor System	High-Press. Steam	NaK
Blades	Inco 713 LC	Inco 713 LC
Disk	Inco 718	Inco 718
Heat Exchanger Tubes	Inco 718	Inco 718
Heat Exchanger Support Disks	Inco 718	Inco 718
Method of Assembly	Braze	Weld

The vanes and rotor blades in a turbine experience unique operating loads and temperatures. Therefore, the possible failure mechanisms for each component are different. Table XXII presents a summary of the stress analysis of critical components.

TABLE XXII. STRESS ANALYSIS SUMMARY

	Rotor		Stator	
	NaK Cooled (psi)	Steam Cooled (psi)	NaK Cooled (psi)	Air Cooled (psi)
Blade & Vane Stresses				
P/A Stress @ Root	17,800	17,800	-	-
Gas Bending Stress @ Root	10,000	10,000	1,500	1,500
Thermal Gradient Stress @ Trailing Edge	48,000c	47,000c	12,000c	23,000c
Internal Coolant Pressure Hoop Stress (Mid-Span)	27,200	12,900	6,400	14,300
Design Criteria (Inco 713 LC)				
90% of 1000-Hour Creep Rupture @ 1350°F (Hub Section)	65,000	65,000	-	-
Cyclic Life @ Trailing Edge	(Cycles) 5,000	(Cycles) 10,000	(Cycles) 20,000	(Cycles) 20,000

4.3.1 STATOR VANES

Stator vanes are subjected to the highest temperatures in the turbine. Since they are stationary and their function is to change the direction of the gas stream leaving the combustion chamber, the operating stresses of the vanes are relatively low. The high temperatures, however, may result in internal stresses and corrosion attack. Cracking can cause loss of coolant and lead to gross failure of the vanes. Metal corrosion can cause a significant change in external dimensions of small-size turbines and result in a serious loss in engine performance characteristics. This is aggravated in a small turbine system, such as the one under consideration, where a small change in dimensions will cause a large change in performance. The possible failure mechanisms are discussed below.

Gas bending loads are normally low on a stator vane. The stresses on the subject vanes are 1500 psi and represent no problem to material selection or structural design.

The turbine temperature profile causes an unequal temperature distribution in the vane, with a hot spot normally concentrated at the trailing edge near the midpoint of the vane. Since the metal expands with increasing temperature, the "hot spot" experiences a compressive stress at operating temperature. This can result in buckling or bowing of the vane at the trailing edge.

The tendency to buckle is controlled by the basic geometry of the vane (vane span/trailing-edge thickness) and the material mechanical properties such as modulus of elasticity, yield strength and creep-rupture strength If the amount of thermal distortion is sufficient to exceed the elevated temperature yield or creep-rupture strength, then permanent plastic deformation takes place.

Compressive plastic deformation effectively reduces the vane span so that during cooling the vane develops a residual tensile stress. Repeated application of heating and cooling can then result in thermal fatigue cracking. Uniform thermal distribution can be effected by cooling of the vane, which will reduce the tendency to crack.

Estimates of the expected cyclic life can be made by means of (Reference 19) Manson-Halford equations These equations, while developed for low cycle fatigue, can be used in thermal fatigue by making some conservative assumptions. The major assumption is that all cycling occurs isothermally at the maximum temperature. This is conservative because in reality the maximum stress occurs in the cold period of the cycle when the fatigue strength is greatest.

The equations relate the number of cycles to failure (N_f) to the thermal stress ($\sigma = E \alpha \Delta T$) and mechanical properties (i.e., ultimate tensile strength, percentage of reduction in area and elastic modulus). In general, the equations show that increasing ultimate tensile strength and percentage of reduction in area result in increased life. Figure 33 shows the lower bound values for low-cycle fatigue vs operating stress for Inco 713 LC, the vane material. The vanes provide cyclic lives of 20,000 for each design.

4.3.2 Rotor Blades

Three distinct loads are experienced by the rotor blades. They are:

1. Combined centrifugal, thermal, and coolant hoop
2. Gas bending
3. Vibratory

Gas bending loads may be essentially eliminated in the design by incorporating radial offset or lean in the blade so that centrifugal loads can cancel the gas bending loads.

Vibratory problems normally originate either from pressure pulsations as a result of passing low-pressure regions behind each stator vane or because of other vibrations in the engine which are being transmitted through the mechanical shafting However, the low aspect ratio of the small engine blades results in a high natural frequency which is not easily excited in the engine.

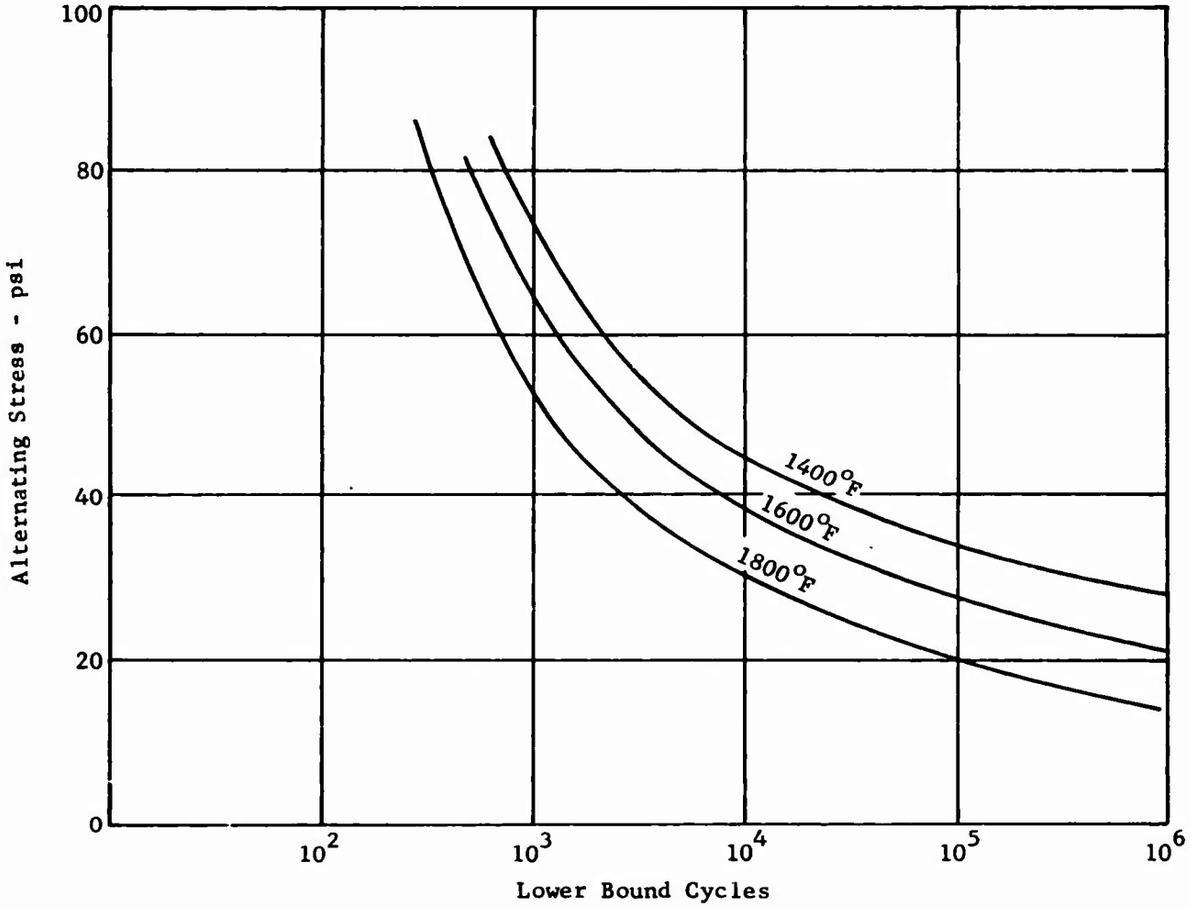

Figure 33. Stress Versus Low-Cycle Fatigue for Inco 713LC Material.

Centrifugal loads are normally quite high and account for life limitation as a result of creep rupture through the airfoil. The combination of the high steady-state centrifugal loads and the high airfoil temperatures causes stretching and eventual failure of the blade. In order to avoid this phenomenon, the blade must be designed to minimize the load by providing an adequate cross section. Metal temperature may be effectively lowered by providing a low gas temperature profile at the highest stressed root section.

In a liquid-metal-cooled rotor blade, additional stress is developed as a result of the coolant being supported by the blade. High centrifugal loads within the blade result in large biaxial stresses. This requires an increase in the wall thickness, which consequently prevents the incorporation of a cooling passage close to the trailing edge. Calculations show that internal coolant pressure hoop stresses at the mid-span will be approximately 27,200 psi on the liquid-cooled blade. The steam-cooled rotor blade will have a hoop stress of 12,900 psi at the same location.

The 1000-hour creep-rupture properties of Inco 713 LC are presented in Figure 34. At the hub section of the blade, which is the critical location for creep rupture, the allowable combined stress is 65,000 psi, which provides sufficient margin for a feasible design.

As mentioned above, the hoop stresses resulting from support of the cooling medium necessitate design of cooling passages away from the thin trailing edge. Therefore, a large thermal gradient will occur within the blade. This gradient results in high thermal stresses. The liquid cooled blade will have a thermal stress of 48,000 psi compression.

Calculation of cyclic life based on these combined stresses shows 5000 cycles of life for the liquid-metal-cooled blade and 10,000 cycles of life for the steam-cooled blade. The major difference in life is due to the higher metal temperature of the liquid-cooled blade. In the subject analysis, a cycle consists of a start-up to shut-down or a major change in power level.

4.3.3 Rotating Heat Exchangers

The design of the rotating heat exchanger is a compromise between minimizing the high centrifugal loads and sizing the tube wall thicknesses for the internal coolant pressure loads. In addition, the weight and volume of the exchanger as related to the tube support discs must also be considered. The allowable and calculated stresses for both rotating exchangers are presented in Table XXIII. The material of construction is Inco 718. From the table, sufficient margin between allowable and actual stresses exists to assure a feasible design.

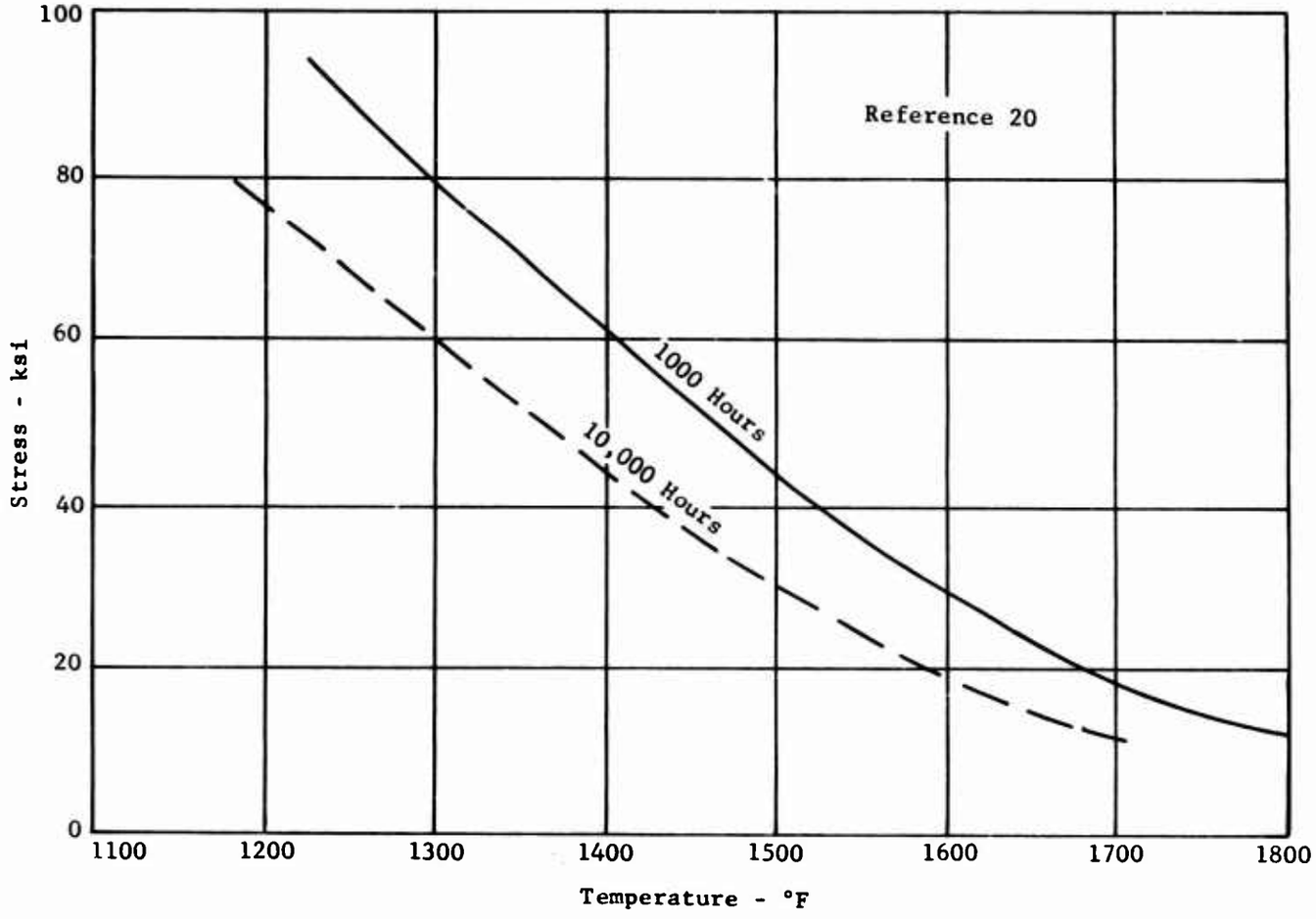

Figure 34. Creep Rupture Data for Inco 713LC.

TABLE XXIII. ROTOR STRESS ANALYSIS SUMMARY

	NaK Cooled (psi)	Steam Cooled (psi)
Rotating Heat Exchanger Stresses		
Disk Stress (Tangential)	53,000	51,000
Tube Stress (Bending)	60,000	50,000
Design Criteria		
1000-Hour Stress Rupture @1200°F (Inco 718)	86,000	86,000

4.4 PERFORMANCE ANALYSIS

To permit a quantitative analysis of the rotor and stator cooling concepts under consideration, a digital computer program for a two-spool turboshaft (with free power turbine) cycle analysis was used to determine the performance effects of the combined and independent turbine cooling concepts. The program utilizes the thermodynamic characteristics of the turbine-shaft cycle which was originated in Reference 1.

The effects of power extraction from any of the three rotating systems, i.e., high-pressure shaft, low-pressure shaft, or power turbine, were included in the analysis to account for the coolant and heat sink pumping power requirements of each cooling system. The relationships between specific fuel consumption, specific horsepower, turbine rotor inlet temperature and turbine stator inlet temperature were determined as a function of shaft power extraction,and these data were provided as program inputs. The relationships are presented in Table XXIV for 35% and 100% military rated power as performance corrections. The data at 60% power was interpolated for the program inputs.

The effect of the heat exchangers located in the compressor discharge air flow path was also included in the analysis by providing the program with a pressure loss in the engine between the diffuser exit and combustor inlet station. This data is also presented in Table XXIV in the form of changes in SFC, SHP and turbine inlet temperature per 1% pressure loss provided by the heat exchanger. The effects of power extraction on specific fuel consumption indicate that driving the cooling system auxiliary equipment off the low-pressure shaft provides the lowest penalty on cycle performance. The increase in SFC using the low-pressure shaft is 20% of the increase associated with extraction from the high-pressure or power turbine shafts. At 35% power, the advantage is still evident but the SFC increase is 50% and 33% of the penalty associated with the high-pressure turbine shaft and power turbine shaft, respectively.

TABLE XXIV. EFFECT OF SHAFT POWER EXTRACTION AND PRESSURE LOSS ON ENGINE PERFORMANCE

100% Military Power, 2500°F Turbine Stator Inlet Temperature

Condition	$\frac{\Delta SFC}{SFC}/HP$	$\frac{\Delta SHP}{SHP}/HP$	ΔT.R.I.T.$/HP$
Power Extracted From High-Pressure Shaft	+.11%	+.05%	+2°
Power Extracted From Low-Pressure Shaft	+.02%	+.04%	+6.3°
Power Extracted From Power Turbine	+.11%	+.13%	+1.0°
	$\frac{\Delta SFC}{SFC} / \frac{\Delta P}{P}$	$\frac{SHP}{SHP} / \frac{\Delta P}{P}$	T.R.I.T. $/ \frac{\Delta P}{P}$
Compressor Exit Air Pressure Loss	+.5%	+.06%	+10°

35% Military Power, Constant Shaft Horsepower

Condition	$\frac{\Delta SFC}{SFC}/HP$	ΔT.S.I.T.$/HP$
Power Extracted From High-Pressure Shaft	+.25%	+4.6°
Power Extracted From Low-Pressure Shaft	+.13%	0
Power Extracted From Power Turbine	.35%	+2°
	$\frac{\Delta SFC}{SFC} / \frac{\Delta P}{P}$	ΔT.S.I.T. $/ \frac{\Delta P}{P}$
Compressor Exit Air Pressure Loss	+.6%	+14°

where: $\frac{\Delta SFC}{SFC} /$ = the change in specific fuel consumption per one horsepower extracted

$\frac{\Delta SHP}{SHP} /$ = the change in specific horsepower per one horsepower extracted

TABLE XXIV - Continued

ΔT.R.I.T./HP = change in turbine rotor inlet temperature per horsepower extracted

ΔT.S.I.T./HP - change in turbine stator inlet temperature per horsepower extracted

and similarly

$/\frac{\Delta P}{P}$ is the change in a performance parameter for a 1% compressor exit airflow pressure loss.

Table XXV, summarizing the horsepower requirements and pressure loss associated with internal cooling systems auxiliary equipment, includes the following:

1. The power required to drive the stator system coolant pump.

2. The unrecovered cooling air pumping power absorbed in the rotating heat exchanger. The unrecovered pumping horsepower charged to the rotor blade cooling system is a result of acceleration of the compressor discharge cooling air up to the system rotational velocity as it passes through the next exchanger. Conversion of this increase in kinetic heat to thermal energy at the exchanger exit is an inefficient process with usually only 30% of the energy recovered as temperature rise. The pumping work is minimized by utilizing preswirl vanes upstream of the exchanger inlet, but was not considered in this analysis.

3. Compressor discharge air pressure loss which occurs across the vane heat exchangers.

The stator coolant pump horsepower requirements are calculated from the coolant flow rate, pressure rise, and pump efficiency. The overall efficiency of the high-pressure air boost pump and electric motor was estimated at 60%. Typical efficiencies for liquid metal rotary induction pump designs range from 10% to 40% in larger pumps. The lower efficiensies are related to pumps designed to meet weight rather than high performance requirements. A conservative estimate of 10% was used for the efficiency of the flightweight pump with requirements to operate over a wide flow range.

Table XXV shows the effect of reducing engine power level on the cooling system power requirements. The electrically driven pump for the high-pressure air-cooled system is independent of engine power level. Its horsepower requirement is therefore constant at all engine power levels. The low horsepower of the liquid metal coolant pump is constant at all engine power levels since the design complexity to modulate the liquid metal was not warranted.

The unrecovered pumping horsepower associated with the rotor cooling concepts is related to the high-pressure shaft speed. At reduced engine power requirements, the speed of the high-pressure shaft is reduced, and therefore the pumping work through the rotating exchanger decreases.

The compressor exit airflow pressure loss in the vane heat exchangers is small at the design point and is expected to decrease at reduced engine power levels. However, to simplify the analysis, the pressure loss was assumed constant over the operating range.

The data presented in Tables XXIV and XXV were then used to predict the effects of cooling on engine performance.

TABLE XXV. INTERNAL COOLING SYSTEM POWER REQUIREMENTS

	% Military Power		
	35	60	100
Steam-Cooled Rotor			
Unrecovered Pumping Horsepower (taken from H.P. shaft)	8	12	16
Liquid-Metal-Cooled Rotor			
Unrecovered Pumping Horsepower (taken from H.P. shaft)	8	12	16
Air-Cooled Stator			
Exchanger Pressure Loss (psi)	2	2	2
Horsepower of Circulating Pump	10	10	10
Liquid-Metal-Cooled Stator			
Exchanger Pressure Loss (psi) (1/3 of engine airflow)	2	2	2
Horsepower of Circulating Pump	1	1	1

Included in the engine performance analysis were the following assumptions:

1. Compressor airflow used for the blade and vane heat exchangers returns to the main gas flow, upstream of the turbine stator. For the transpiration-cooled concept, the cooling air which effuses through the porous airfoil was considered to enter the main gas flow downstream of the blade row in which it was used for cooling.

2. Compressor airflow is a constant for all systems.

3. Turbine efficiency is a constant for all cooling concepts. This assumption implies that there is no aerodynamic design compromise for any concept. In reality, internally cooled airfoils which show excessive metal temperature or high thermal gradients at the trailing edge may require thicker trailing-edge sections to incorporate addition of coolant passages. In addition, the transpiration cooling concept has a loss associated with the porous airfoil's surface finish or profile contour and a momentum loss resulting from the cooling air effusion process.

For the baseline transpiration-cooled concept, the cooling airflow presented in Table XXVI as a percentage of main airflow was kept constant at the part-power operating conditions, although decreased turbine inlet temperatures would allow a cooling airflow reduction.

TABLE XXVI. TRANSPIRATION-COOLED TURBINE ENGINE CYCLE AIRFLOW DISTRIBUTION AT 100% MILITARY POWER

Engine Station	% Flow
High-Pressure Turbine Vane Cooling	5.0
High-Pressure Turbine Blade Cooling*	3.0
Low-Pressure Turbine Vane, Housing, and Shroud Cooling	4.0
Low-Pressure Turbine Disk Cooling*	1.5
Bearing and Power Turbine Disk Cooling*	1.0

*Coolant enters main flowpath downstream of engine rotor component.

The results of the performance analysis are presented in Tables XXVII and XXVIII. The tables are arranged (1) to show the engine performance parameter on the basis of any selected combination of stator and rotor cooling system, (2) to show the influence of stator or rotor cooling on an absolute basis, by including the hypothetical case of an uncooled stator and rotor which operates at the same turbine inlet state conditions and incurs zero penalties for airfoil cooling, and (3) to show the effects of the advanced internal cooling systems studied herein with the current state-of-the-art transpiration cooling system.

At 100% power level, the SFC is presented for each cooling system combination based on a constant turbine stator inlet temperature of 2500°F. The SHP shown as a percentage of the hypothetical uncooled turbine configuration reflects the reduced power output of each cooled turbine configuration for a given size engine.

At maximum rated power and 2500°F turbine inlet temperature, the liquid-metal-cooled rotor and stator concept shows a 5.8% improvement in SFC and 10.7% improvement in output shaft horsepower when compared to the transpiration cooling system. The combined high-pressure air-cooled stator and superheated steam-cooled rotor show a 4.5% SFC improvement and 9.8% improvement in output shaft horsepower when compared to the transpiration-cooled system.

The data reveals that the most significant penalty to the cycle occurs in air cooling the rotor by external methods (i.e., transpiration, film, etc.). This is partly based on Reference 16, which indicates that the rotor cooling air does no work on the high-pressure turbine but the air for externally cooling the stator does mix in the gas-stream and does useful work in the rotor blade row.

Table XXVIII presents the increase in SFC and the increase in turbine stator inlet temperature to maintain 35% of maximum rated output shaft horsepower, for each cooling concept. The data shows that the indirect cooling concepts have a 2.4 to 3.4% lower SFC when compared to the transpiration cooled system. For the transpiration cooled system, the 150°F increase in gas temperature is adequately compensated for by the characteristic constant percentage of cooling airflow of this concept, since at the reduced turbine stator inlet temperature, blade and vane cooling requirements are correspondingly reduced. The increase in gas temperature for the indirect systems would be accomodated by the coolant which is near design flow rates at part power.

The specific fuel consumption at 60% of maximum rated power is also presented in Table XXVIII. The steam, air and liquid metal concepts have a 3.3 to 4.5% improvement in SFC, when compared to the transpiration-cooled system at this power level.

TABLE XXVII. EFFECT OF TURBINE COOLING ON ENGINE PERFORMANCE

Specific Fuel Consumption at 100% Military Rated Power and 2500°F Turbine Stator Inlet Temp.

	Stator Cooling System			
Rotor	Uncooled	NaK	Air	Transpiration
Uncooled	.430	.431	.437	.434
NaK	.438	.439	.445	.442
Steam	.438	.439	.445	.442
Transpiration	.444	.445	.451	.466

Percent of Specific Horsepower of Uncooled (Theoretical) Rotor and Stator At 2500°F Turbine Stator Inlet Temp.

	Stator Cooling System			
Rotor	Uncooled	NaK	Air	Transpiration
Uncooled	100	99.4	98.6	95.2
NaK	98.1	97.5	96.7	94.2
Steam	98.1	97.5	96.7	94.2
Transpiration	95.0	94.7	94.3	88.1

TABLE XXVIII. EFFECT OF TURBINE COOLING ON ENGINE PERFORMANCE

Specific Fuel Consumption at 35% Military Rated Power

	Stator Cooling System			
Rotor	Uncooled	NaK	Air	Transpiration
Uncooled	.550	.552	.558	.552
NaK	.561	.563	.569	.563
Steam	.561	.563	.569	.563
Transpiration	.581	.583	.589	.583

Increase in Turbine Stator Inlet Temperature (°F) to Obtain 35% of Military Rated Power

	Stator Cooling System			
Rotor	Uncooled	NaK	Air	Transpiration
Uncooled	0	10	50	50
NaK	37	47	87	87
Steam	37	47	87	87
Transpiration	100	110	150	150

TABLE XXVIII - Continued

Specific Fuel Consumption at 60% Military Rated Power

	Stator Cooling System			
Rotor	Uncooled	NaK	Air	Transpiration
Uncooled	.480	.481	.487	.481
NaK	.491	.492	.498	.492
Steam	.491	.492	.498	.492
Transpiration	.514	.515	.521	.515

4.5 SELECTION OF SYSTEM

From the foregoing, it is evident that modest improvement in fuel consumption of a given engine size can be made by application of the internal coolant concepts to turbine cooling. These benefits must be evaluated with other system characteristics such as manufacturability, reliability, weight, mechanical integrity, cost, etc. Therefore, a rating system and selection criteria were established in order to select, among the systems studied, the stator and rotor system which offers the most promise for advanced cooled turbine development.

The following four major groups were included in the rating of each system:

1. Vanes and Support or Blades and Disc
2. Heat Exchanger
3. System
4. Engine Performance

All of the above groups were considered to have equal weight in the rating. Within each of the first three groups, there were the following three equally weighted general criteria:

1. Fabrication
2. Performance
3. Durability

Special considerations within each criterion were reviewed with respect to

establishing their relative significance within that criterion. Thus, a weighting factor entered into the rating system at this point.

The category of engine performance effects was given full weight as a group since this represents the primary reason for utilizing the internal coolant system for the turbine.

Tables XXIX and XXX summarize the selection criteria weighting factors and point ratings for the stator and rotor coolant systems, respectively.

Stator Cooling System Rating

In the Vane and Supports group the liquid-metal-cooled vane rated higher than the high-pressure air system. In this group, the liquid-metal-cooled vane has:

a. Reduced fabrication cost and complexity because coolant passages are larger in size and fewer in number.

b. Higher overtemperature capability due to the high coolant operating temperature.

c. Greater durability since the coolant operating pressure is much lower, and overall temperature gradient control is better because of the greater flexibility available in locating the coolant passages.

In the Heat Exchanger and Pump group, the two cooling concepts were rated equal. In this group:

a. Fabrication of the air-cooled system's equipment was rated higher as a result of using unfinned exchanger tubes and a conventional coolant pump design as compared to the liquid metal systems advanced rotary induction pump and high-density finned-tube heat exchanger.

b. For performance effects, the liquid metal system was rated higher since the coolant pump is lighter and requires less space.

c. The durability and reliability of both concepts were rated equal. Both concepts use current state-of-the-art design and fabrication techniques.

In the System group, the liquid-metal concept rated slightly better. In this group:

a. The air-cooled vane achieved a higher rating for production cost criteria since furnace brazing techniques can be used.

b. The liquid-metal system was rated higher for the performance criteria since it has the lower horsepower requirement for the

TABLE XXIX. STATOR COOLANT SYSTEM SELECTION CRITERIA AND RATING

	Weight Factor	Maximum Score	NaK	Air
I. Vane & Supports				
A. Fabrication - Cost & Complexity	3	6	6	3
B. Performance				
1. Overtemperature Capability	2	4	2	1
2. Aerodynamic Compromise	1	2	2	2
C. Durability				
1. Trailing-Edge Cooling	1	2	1	2
2. Temperature Gradient Control	1	2	2	1
3. Stress Levels	1	2	2	1
Total		18	15	10
II. Heat Exchanger & Pump				
A. Fabrication - Cost & Complexity	3	6	3	6
B. Performance - Volume & Weight	3	6	6	3
C. Durability & Reliability	3	6	6	6
Total		18	15	15
III. System				
A. Cost				
1. Production Considerations	1	2	1	2
2. Developability	2	4	4	4
B. Performance Pump HP & Air	3	6	6	3
C. Durability				
1. Reliability	1	2	2	2
2. Materials Compatibility	1	2	2	2
3. Overall Design Simplicity	1	2	2	2
Total		18	17	15
IV. Engine Performance				
A. Effect on SFC	9	18	9	9
Point Summary				
Group I		18	15	10
Group II		18	15	15
Group III		18	17	15
Group IV		18	9	9
Total		72	56	49

TABLE XXX. ROTOR COOLANT SYSTEM SELECTION CRITERIA AND RATING

	Weight Factor	Maximum Score	NaK	Air
I. Blade & Disc				
A. Fabrication - Cost & Complexity	3	6	6	3
B. Performance				
1. Overtemperature Capability	2	4	4	2
2. Aerodynamic Compromise	1	2	2	2
C. Durability - Stress Levels	3	6	3	6
Total		18	15	13
II. Heat Exchanger				
A. Fabrication - Cost & Complexity	3	6	3	6
B. Performance - Volume & Weight	3	6	6	3
C. Durability - Stress Level	3	6	6	3
Total		18	15	12
III. System				
A. Cost				
1. Production Considerations	1	2	2	1
2. Developability	2	4	2	2
B. Performance - Pumping Power	3	6	3	3
C. Durability				
1. Reliability	1	2	2	2
2. Materials Compatibility	1	2	2	2
3. Overall Design Simplicity	1	2	1	1
Total		18	12	11
IV. Engine Performance				
A. Effect on SFC	9	18	18	18
Point Summary				
Group I		18	15	13
Group II		18	15	12
Group III		18	12	11
Group IV		18	18	18
Total		72	60	54

coolant pump.

c. The overall system durability for both of the concepts was considered equal. The reliability of both systems depends on good design and manufacturing practice. Although there are some materials compatibility problems associated with liquid metals, adequate knowledge exists in this area to avoid these problems.

Rotor Cooling System Rating

In considering the Blade and Disk rating group, the liquid metal concept rated slightly better. In this group:

a. The fabrication cost and complexity will be lower for the liquid-metal-cooled concept because fewer and larger airfoil coolant passages are required.

b. The higher overtemperature capability of the liquid-metal system is due to the high operating temperature of the coolant. This advantage can be further improved if the number of coolant passsages are increased to bring the coolant closer to the airfoil surfaces.

In the Heat Exchanger rating group, the liquid-metal-cooled rotor blade scored slightly higher than the steam-cooled blade concept. In this group:

a. The cost and complexity of the steam cooling concept heat exchanger scored higher than that of the liquid metal concept because of the latter's requirement of finned tubes, and an all-welded assembly.

b. Performance of the liquid-metal-cooled concept was rated higher because of the lower weight and smaller size.

c. The stress levels in the liquid-metal-cooled exchanger supports are lower due to lower weight.

The liquid-metal-cooled concept again rated slightly better than the steam concept when the overall system was considered. In this group:

a. The fabrication complexity of the steam-cooled blade coolant passages was considered to be more critical than the liquid-metal-cooled concept.

b. Both concepts scored equally in the system performance effects category because effects on power extraction were equal.

c. Both concepts were rated equally for the durability criteria. Materials compatibility and design simplicity of both cooling

systems can be assured through current state-of-the-art information.

The liquid-metal-cooled stator system and the liquid-metal-cooled rotor system each attained a higher point rating than the high-pressure air and the steam-cooled system, respectively. Since the spread in rating points was not large and the rating for each criterion required a qualitative judgment of many design and development aspects, each system design was reviewed again with regard to areas of design and performance which can be compared in quantitative terms (i.e., system weight, horsepower absorbed, etc.). This review also yielded the same results as in the tables, and the liquid-metal-cooled vane was selected as the cooling concept to be evaluated in the test phase of the program. With the selection of the liquid-metal cooling concept, consideration is given below to aspects of reliability, maintainability and special operating conditions.

4.6 SYSTEM CONSIDERATIONS

4.6.1 Mechanical Integrity

The mechanical integrity of the cooling systems designed herein is of prime importance, since failure of any single detail part containing the coolant would result in turbine failure if operating at high gas temperatures. Several highly stressed areas of the mechanical design which require special consideration are:

1. Blade-to-disk attachment
2. Tube-to-header attachments

Blade-to-disk weld attachment evaluations have been conducted by several investigators, and the results are reported in References 5 and 13. Based on this work, it was concluded that welding and brazing parameters can be established to produce the desired joint strength and quality for this turbine application. The key design elements required to provide a good weldment for selected materials are:

1. Uninterrupted mating surfaces

2. Minimum width for thorough penetration of the weld

3. Accessible for inspection

The tube-to-header joint geometry and welding parameters are critical since this area may be susceptible to a fatigue failure mode. Designs which load the weld zone are to be avoided since the weld zone fatigue strength may vary considerably from joint to joint. Therefore, design geometry parameters (including tube and header thickness and tube length supported in the header) must insure that the tube which has repeatable mechanical properties is the loaded and limiting element. This also has been successfully shown in Reference 13.

4.6.2 Reliability and Maintainability

The indirect cooling system components present some special problems with regard to maintainability. Therefore, all the closed cooling concepts have been designed so that the entire system can be removed from the engine and visually inspected or replaced as necessary.

Repair or replacement of a damaged airfoil in the liquid-metal-cooled system requires special procedures which could be done at overhaul facilities. Current liquid metal repair procedures for larger systems where removal is cumbersome involve locally freezing the area to be required, cleaning the affected area, removing contaminated liquid metal, and providing the repair weld in an inert atmosphere. Similar but simpler procedures can be adopted for repair of a liquid metal system at an overhaul facility.

Total loss of stator or rotor coolant during engine operation would naturally preclude operating at gas temperatures above that for noncooled turbines. However, in the case of partial loss of coolant, the following conditions determine the effects on engine operation:

1. Reduction in coolant mass flow
2. Change in coolant-side heat transfer coefficient
3. Chemical reaction of the coolant (i.e., NaK) in the gas stream

For the first two conditions, engine shutdown is required or operation at a lower gas temperature may permit the completion of the flight. The third condition involves the chemical reaction when NaK is exposed to oxygen above 250°F. The possibility of damage to downstream components is expected to be quite small for the following reasons:

1. The system's quantity of coolant is small.
2. The liquid metal pressure in the stator vane is lower than the external gas pressure.
3. NaK tends to form oxides in small crevices which inhibit further leakage.
4. NaK has a very low heat release rate, in case of combustion.

4.6.3 Special Operating Considerations

Starting an engine at low ambient air temperatures must be given special consideration for liquid metal coolant systems. The NaK coolant selected must be liquid after start-up (a) in order to be pumped through the coolant passages, (b) to preclude an unbalance in the rotating system, and (c) to prevent thermal stresses in the finned tubing or blade passages due to large volumetric changes in the coolant as it locally melts. Several options are available to resolve this problem:

1. Select a low-freezing-point liquid metal alloy. For instance, NaK-78 has a freezing point around 10°F. However, a ternary alloy can be produced by the addition of up to 40% by weight of cesium to retain fluidity down to -65°F (Reference 13).

2. Preheat the coolant system by an external heat source such as an electric heater or gas bleed from the APU starter.

5.0 FABRICATION AND TEST OF A LIQUID-METAL-COOLED STATOR

5.1 STATOR VANE DESIGN AND FABRICATION

The stator vane airfoil contour and internal passage geometry designed and analyzed in the previous phase of the program were utilized in this test phase except for modifications which were introduced at this time to facilitate manufacture. The design of the long trailing-edge coolant passage shown in Figure 21 was based on casting the vane with the coolant passage. Since the casting process involves a long procurement cycle and expensive tooling for molds and cores, a decision was made to machine the vanes and coolant passages for the requirements of the test phase of this program. The material selected for the stator vane is Inco 713LC, which is very difficult to machine. Therefore, the electrical discharge machining process was selected to provide the airfoil contour and the coolant passages. The vane design was then reviewed to establish coolant passage modifications which would be appropriate for the selected machining process and would not significantly affect the thermal design. Based on simplifying the electrode design and development, two rectangular-shaped trailing-edge coolant passages shown in Figure 35 were substituted for the single triangular-shaped passage of the original design to minimize the manufacturing complexities.

The airfoil is cooled by the two-pass coolant flow arrangement shown in Figure 21 and 36. Coolant enters the leading-edge passage and flows radially inward to the vane hub plenum. From the hub plenum, the coolant returns radially outward through passages in the suction, pressure, midchord, and trailing-edge sections of the vane. Section B-B of Figure 36 is a view of the hub plenum where the liquid metal turns after cooling the leading edge. This plenum also serves to cool the hub gas shelf. Section AA of Figure 36 details the geometry of the coolant inlet and outlet plenums at the tip section. The complexity of this section is increased by the addition of three thermocouple bosses and the plenum separating wall. To complete the vane assembly, two liquid metal inlet and outlet tubes 0.188 inch in diameter are electron beam welded to a parallelogram-shaped header which, in turn, is welded to the vane tip plenum along the four sides of the outer perimeter. In addition, a seal weld is provided across the top of the header along the separating wall to seal the inlet and outlet coolant plenums from each other.

The vane was electrical discharge machined from small cast blocks. The EDM process was used to finish-machine all internal and external surfaces, including airfoil, coolant passages, gas inner and outer shelves, and coolant plenum sections. The most critical element in the fabrication was the incorporation of a 0.007-inch-wide coolant slot in the 0.020-inch-thick trailing-edge region. The 0.020-inch trailing edge thickness was originally selected for high nozzle efficiency. The 0.007-inch coolant passage was selected to provide coolant as close to the trailing edge as possible, within structural limitations and advanced manufacturing capability. This design resulted in a 0.007-inch wall thickness adjacent to the slot. Although the vane has a constant section from hub to tip, the electrode tool

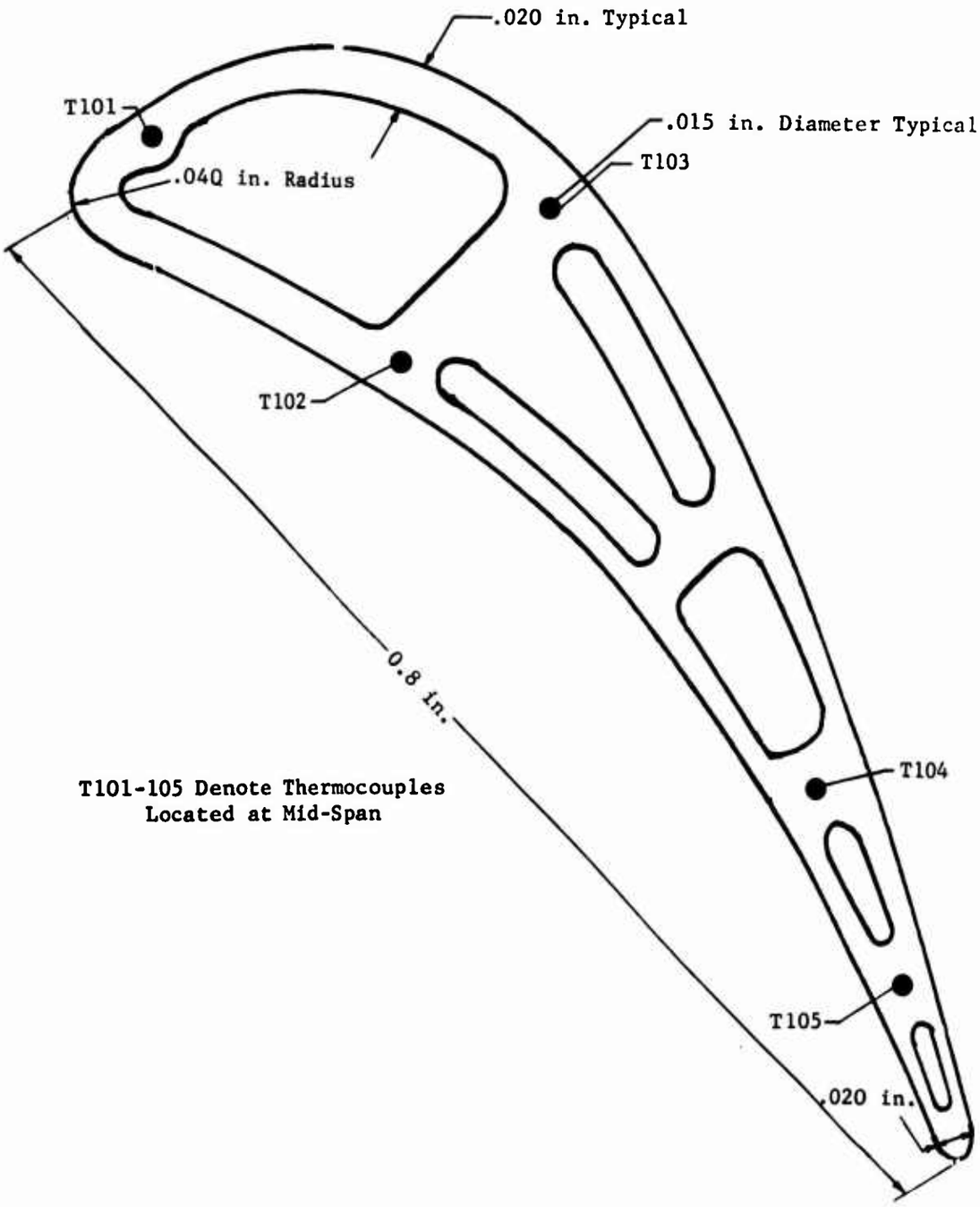

Figure 35. Liquid-Metal-Cooled Turbine Vane Configuration - Test Phase.

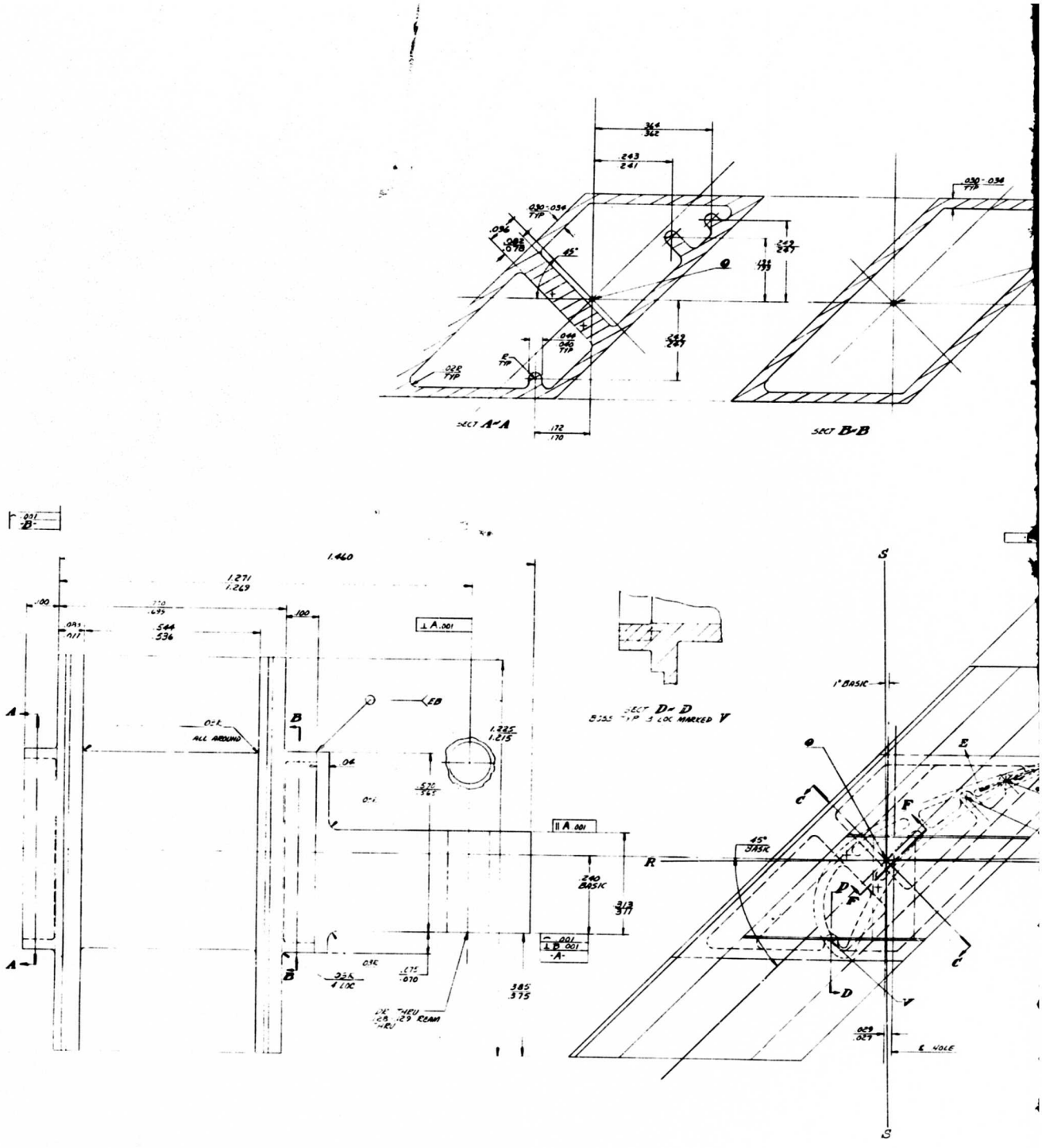

Figure 36. Liquid-Metal-Cooled Turbine Vane Design.

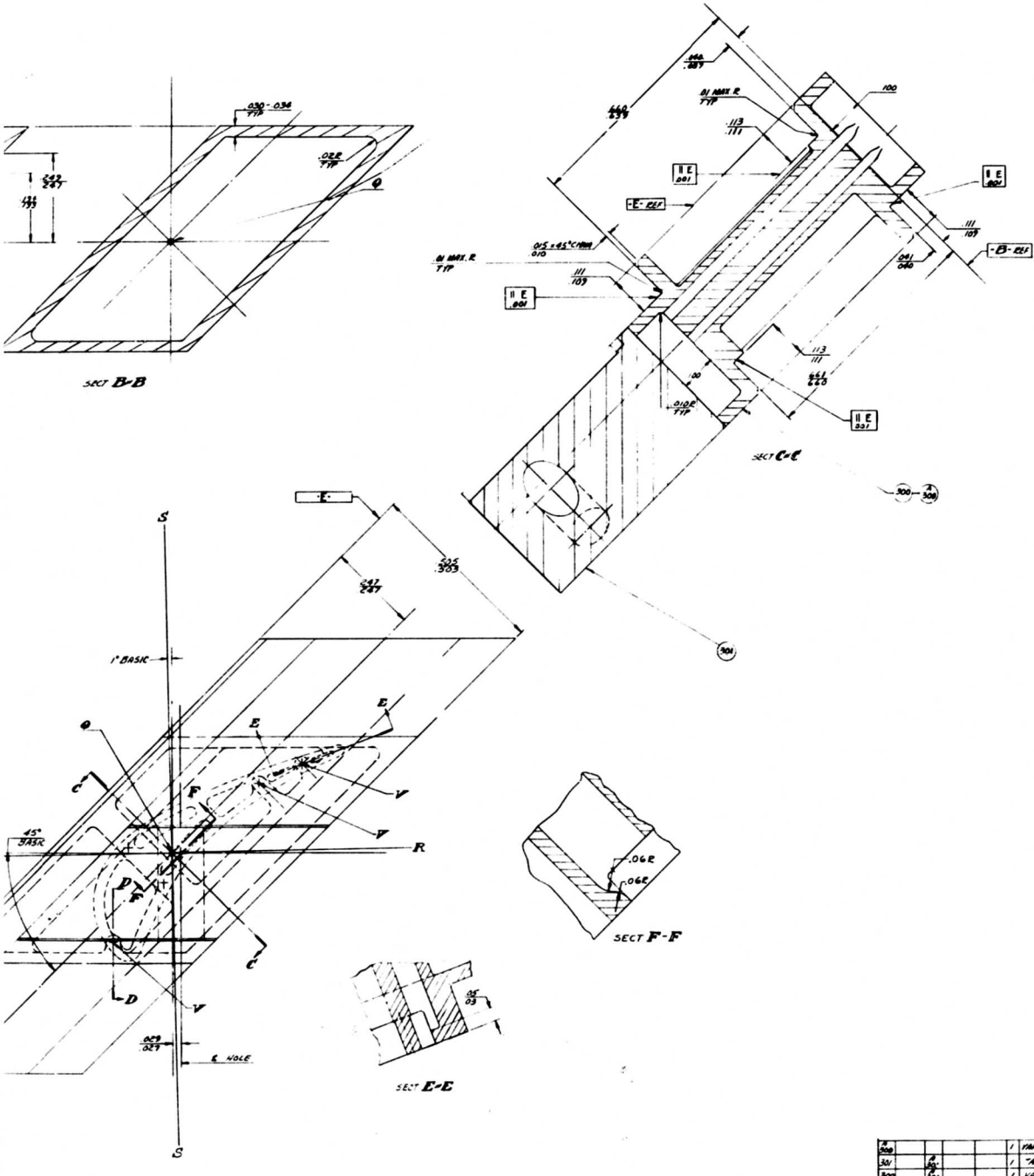

300				1	VANE - ASSY OF		5797
301	300			1	VANE -		
500	301			1	VANE -		

139b

design to provide this 0.007-inch slot through the 0.5-inch span and still maintain constant wall thickness was very difficult. The electrode cross-sectional dimensions must be sized (a) to meet the required slot dimension, (b) to incorporate the electrolyte inlet flow passage, and (c) to provide the clearance around the electrode to discharge the electrolyte. The accumulation of these dimensions and tolerances resulted in an electrode wall thickness which buckled or deflected during machining. This resulted in reduction of the vane wall thickness. This problem produced a manufacturing development effort beyond the scope and schedule of the program. Therefore, a modification was made to the vane design which increased the trailing-edge thickness to 0.030 inch and increased the coolant slot width to 0.010 inch. The values are representative of current manufacturing capability, and fabrication of the vanes was completed with this redesign.

Figures 37 and 38 show the vane details and the coolant passages after machining.

All welding on the vane assembly is performed by the electron beam method. The hub support tang is welded to the vane at the hub plenum. Crack-free welds were made by displacing the beam slightly to the Inconel side of the weld line (established by the ductile Inconel tang and the crack-sensitive Inco 713LC mating surfaces). Welding was completed with the following parameters:

Accelerating voltage	30 kilovolts
Beam current	2.0 milliamps
Travel speed	30 inches per minute

Inspection of all welds was made by binocular (10X) magnification and a mass spectrometer helium leak detector.

Figure 39 shows the electron beam weld joints on the vane, and Figure 40 shows the complete vane assembly.

Provisions were made in the airfoil design for incorporation of five 0.015-inch-diameter holes as shown in Figure 35 for insertion of thermocouples to measure the mid-span vane metal temperature. Prior to machining these holes, seal welds were required to create a fused surface between the header and vane details at the thermocouple boss locations. Subsequent EDM machining of these bosses to provide the thermocouple hole was located so that a leakage interface between these details would not exist. This design was provided to prevent liquid metal from reaching the airfoil thermocouple.

During the vane fabrication, the four peripheral welds attaching the Inconel tube header to the vane plenum were made successfully, but the subsequent seal welds across the top of the header and at the thermocouple bosses produced local cracks in the peripheral welds near the weld intersections. Weld repair of these cracks was not completely successful

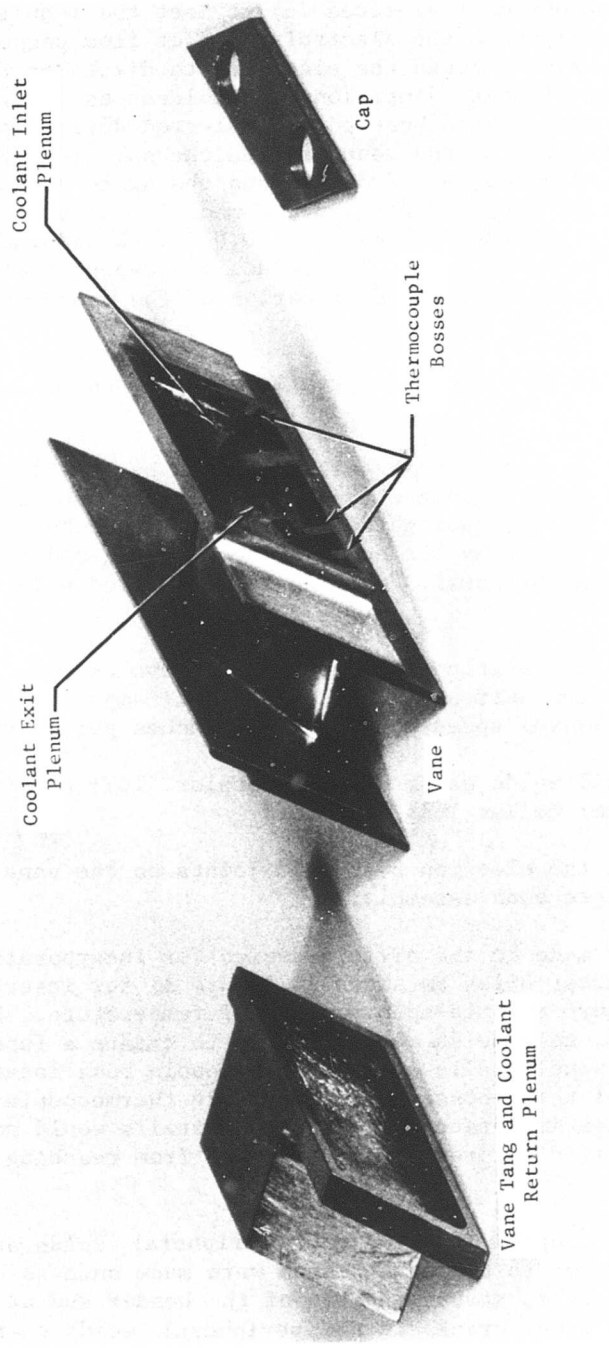

Figure 37. Liquid-Metal-Cooled Vane Details.

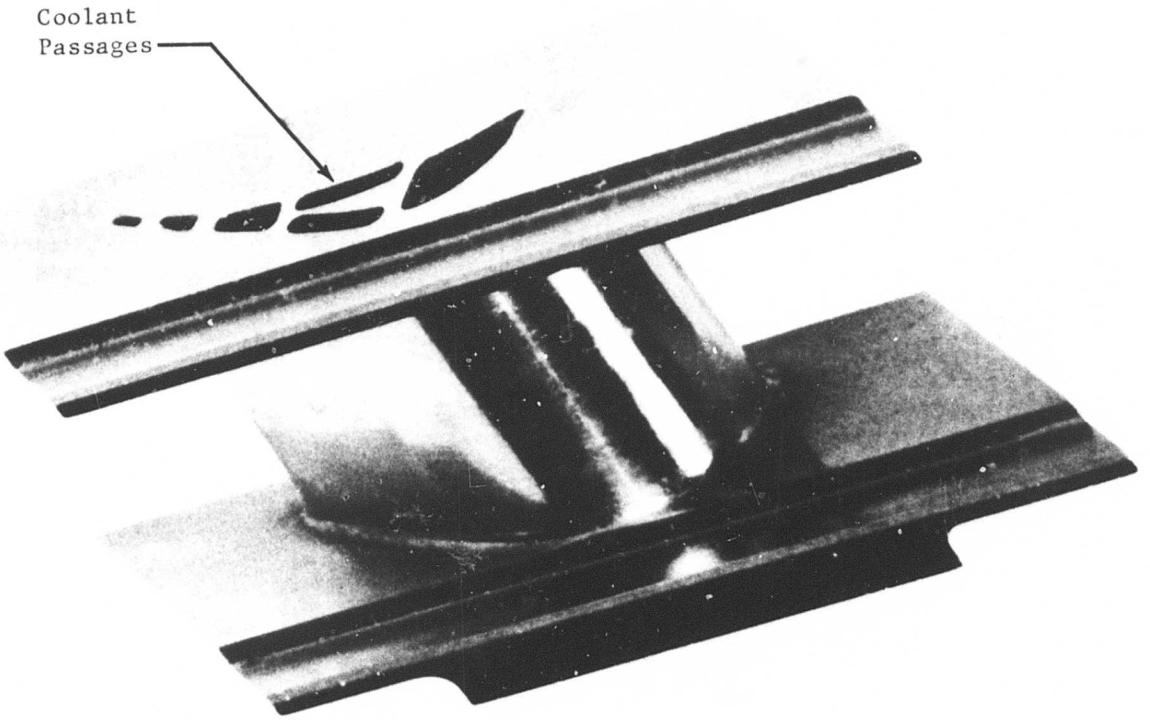

Figure 38. Liquid-Metal-Cooled Vane Showing Electrical Discharge Machined Coolant Passages.

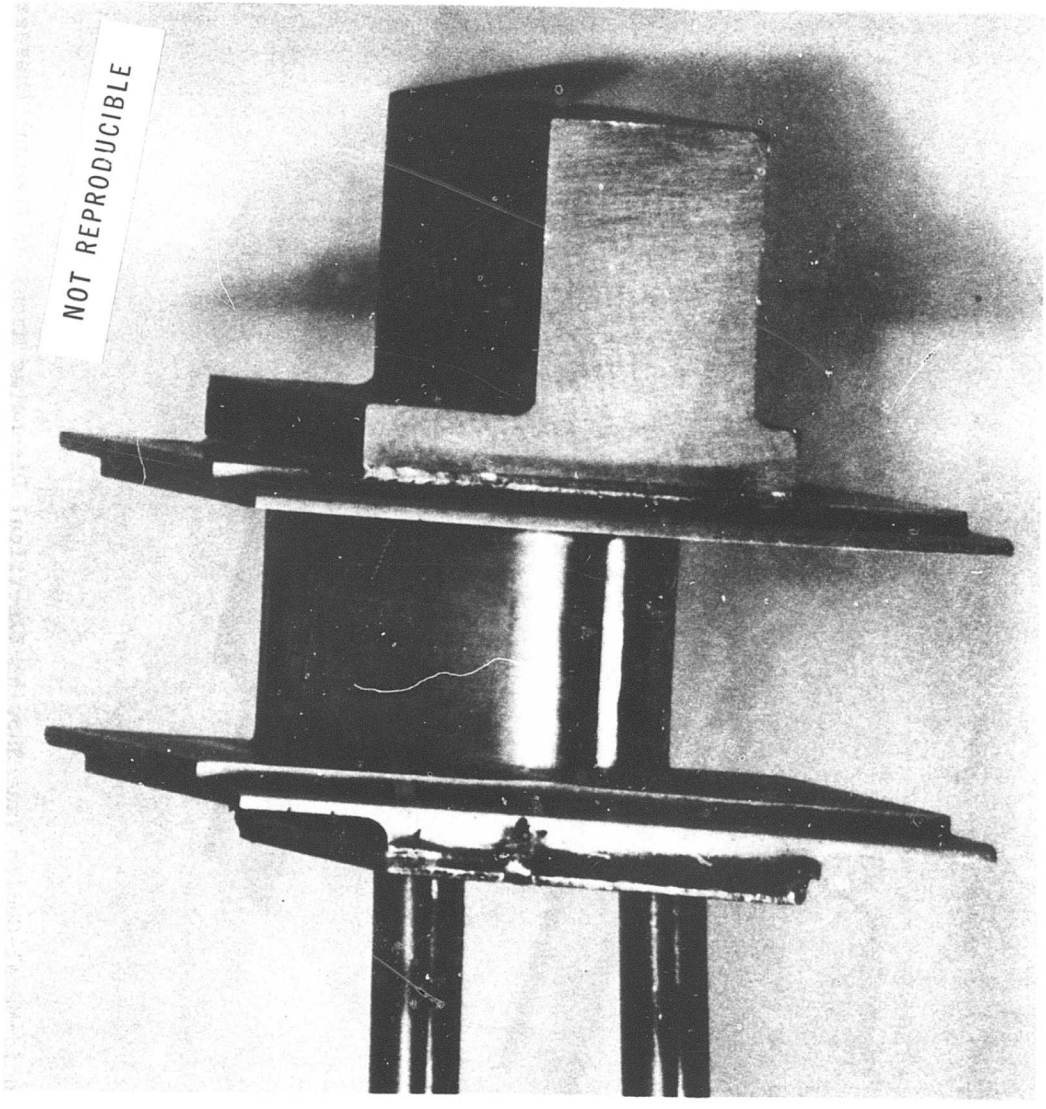

Figure 39. Liquid-Metal-Cooled Vane Electron Beam Welded Assembly.

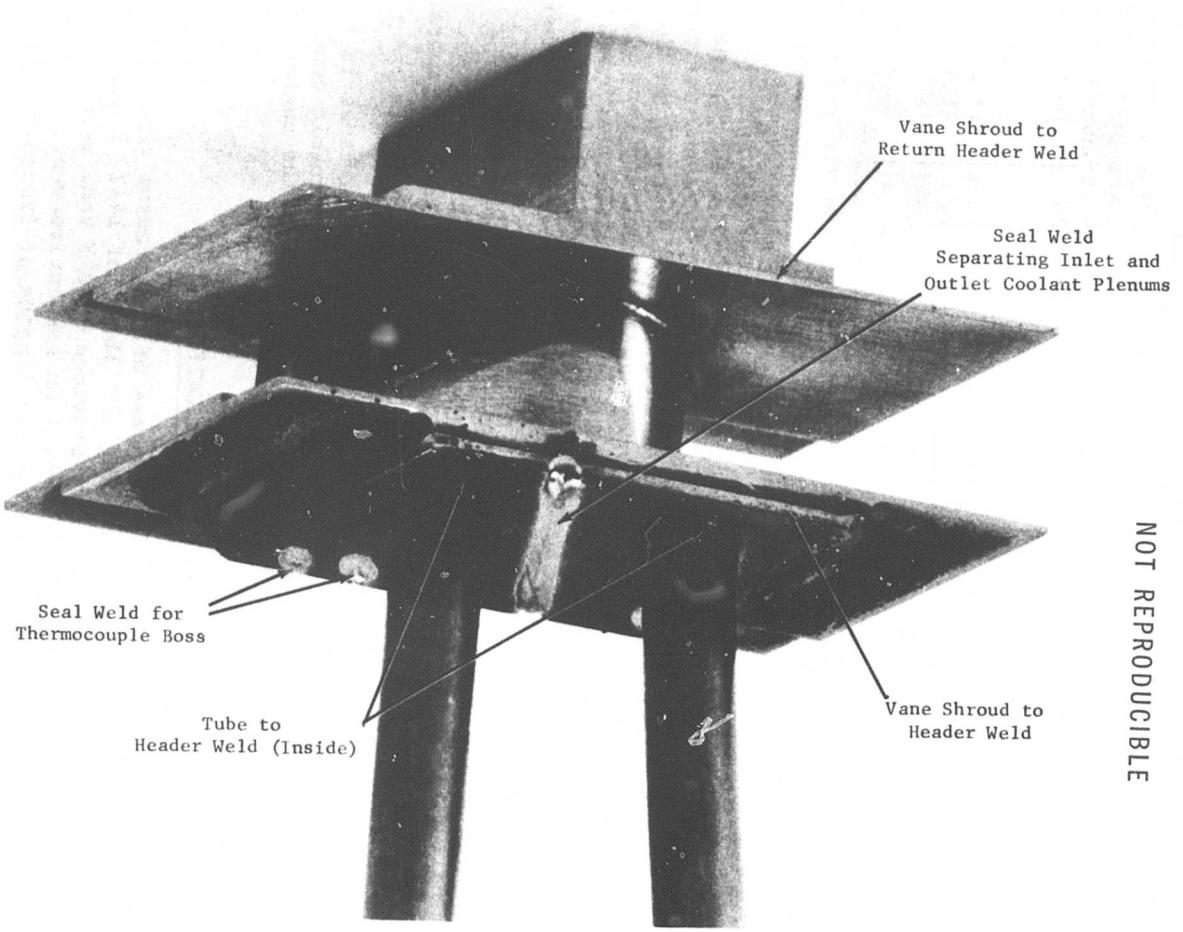

Figure 40. Liquid-Metal-Cooled Vane Electron Beam Welded Assembly.

within the time available, and a nickel-braze alloy was employed to assure sealing of the tip plenums.

5.2 CASCADE RIG DESIGN AND FABRICATION

The two-dimensional combustor and turbine stator cascade rig assembly shown in Figure 41 and described in Reference 10 was fabricated and tested under USAAVLABS Contract DA 44-177-AMC-182(T). This rig was utilized for the test program. The original design incorporated eight transpiration-cooled vanes for testing downstream of a 2500°F fuel (JP4) vaporizing combustion chamber.

Redesign of this rig was required to replace the two center transpiration-cooled vanes with three liquid-metal-cooled vanes as shown in Figure 42. The aerodynamic design of the liquid-metal-cooled vane was to be based on providing 83 to 85% turbine stage efficiency. Thus, the airfoil contour was modified, the chordal distance was reduced, and the number of vanes per assembly was increased from the earlier transpiration-air-cooled vane design. As a result, three liquid-metal vanes physically displaced two transpiration-cooled vanes.

In addition to the performance benefits from reducing the chord, there was also a significant reduction in cascade rig redesign. The shorter chord requires a smaller hub plenum to feed all the coolant passages in the vane. Therefore, the hub fits within the existing front and rear piston ring type seal elements, which seal the cooling air plenum feeding the transpiration-cooled vanes. Thus, the cooling air plenum feeding the slave vanes on right- and left-hand sides remained as a common chamber.

To accommodate the liquid-metal vane tubing and instrumentation, the bottom half of the vane holder was redesigned as shown in Figure 42. The holder was made up of separate front and rear sections to allow installation of the liquid-metal-cooled vanes.

The transpiration-air-cooled vanes were included as slave vanes in the cascade to preclude end wall effects on the aero-thermodynamic conditions of the gas flow through the three test vanes located in the center of the rig.

5.3 LIQUID METAL SYSTEM DESIGN AND FABRICATION

The vane designed during the earlier phase of the program removed 3000 Btu/hr from the airfoil by circulating 179 lb/hr of 1442° liquid metal through each vane. These conditions provided 1542°F vane metal temperature while operating in a 2500°F combustion gas environment. In the preliminary engine design, each vane has two lengths of finned tubing to reject the heat from the airfoils to the compressor discharge air flowing over the finned tube exchanger. The exchangers for the cascade test are shown in Figure 43 and 44. The purpose of these finned tube exchangers was to simulate the method by which the heat removed from the airfoils could be returned to the engine cycle.

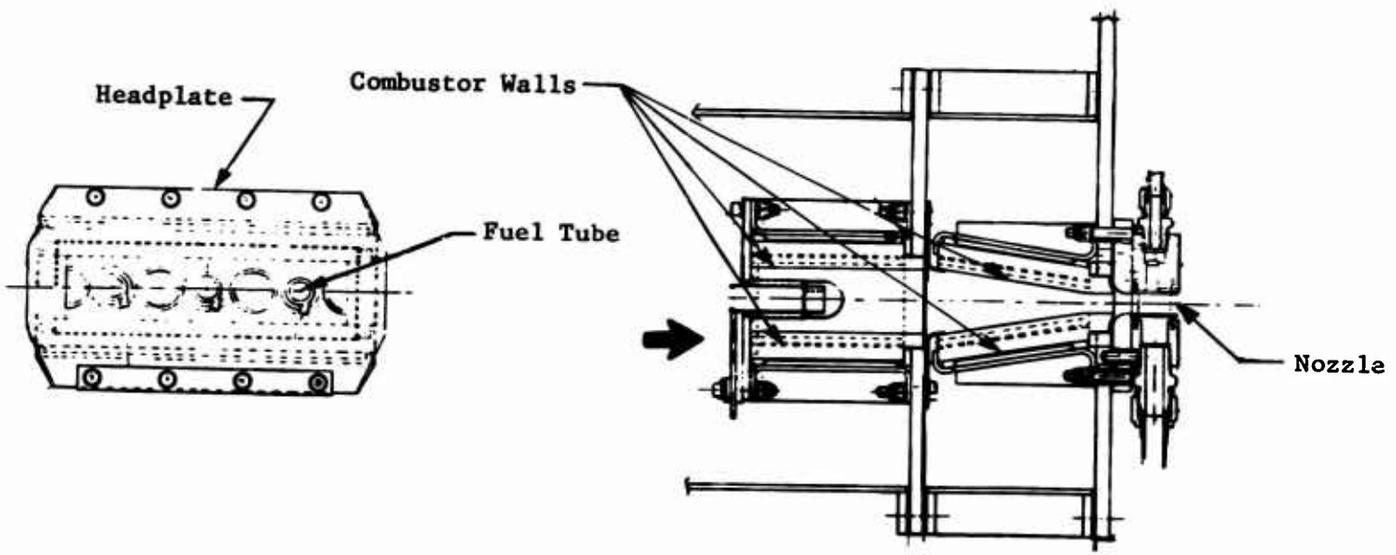

Figure 41. Combustor Cascade Rig.

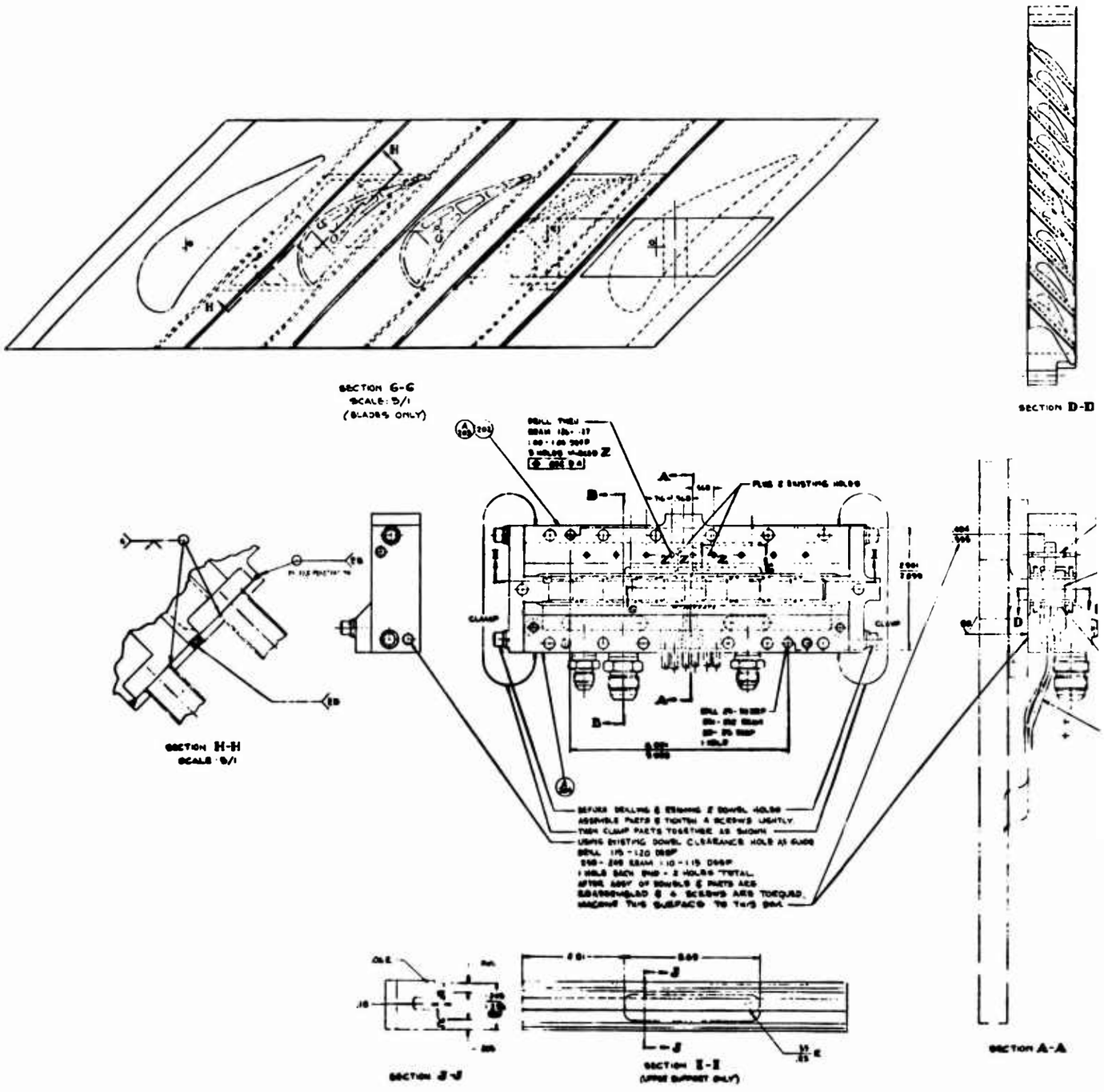

Figure 42. Transpiration-Air-Cooled Turbine Nozzle Assembly Redesign to Incorporate Liquid-Metal-Cooled Vanes.

1 B

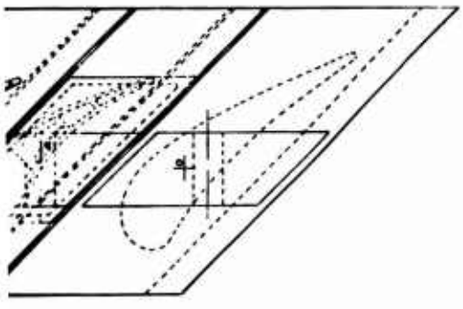

SECTION D-D

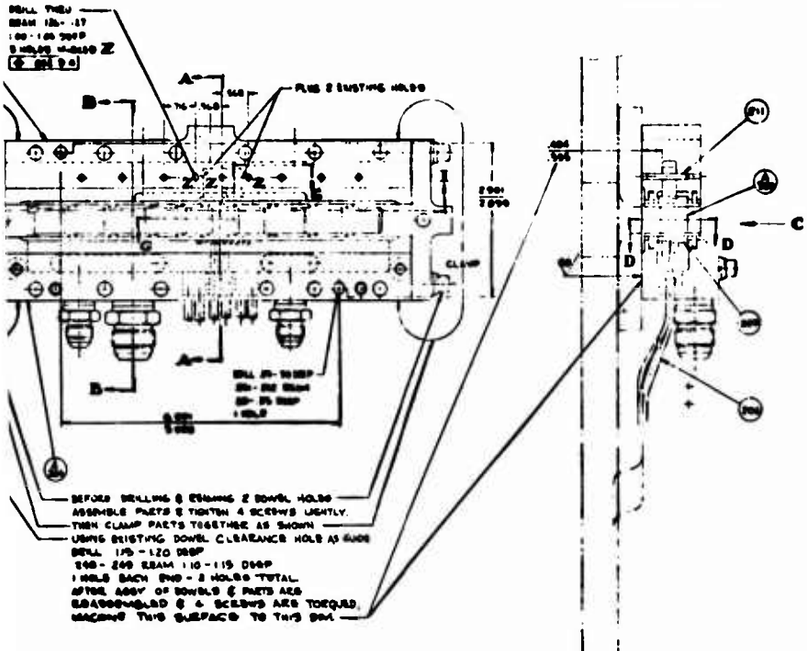

SECTION A-A

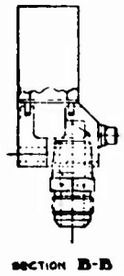

SECTION B-B

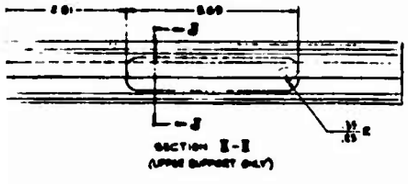

SECTION E-E
(UPPER SUPPORT ONLY)

zle Assembly Redesign
anes.

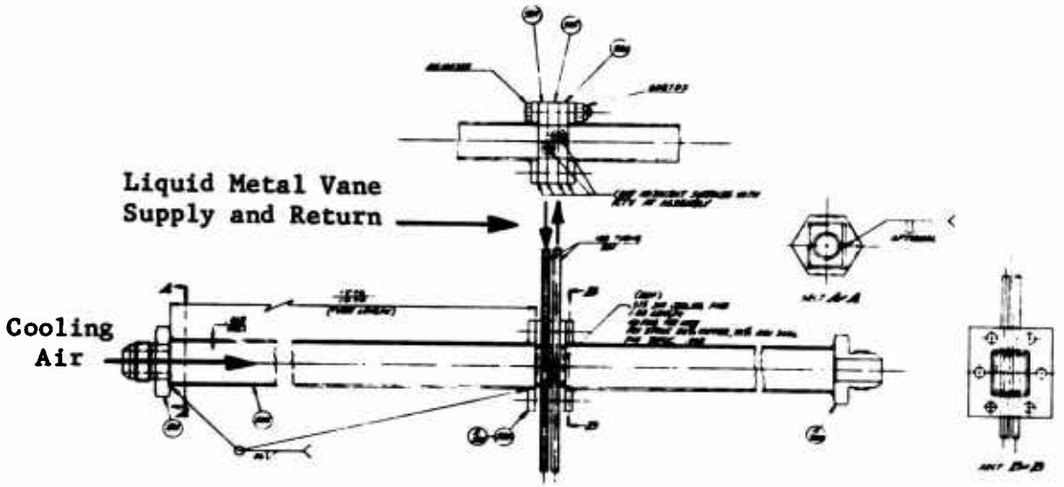

Figure 43. Liquid-Metal-Coolant-to-Compressor Discharge Air Heat Exchanger.

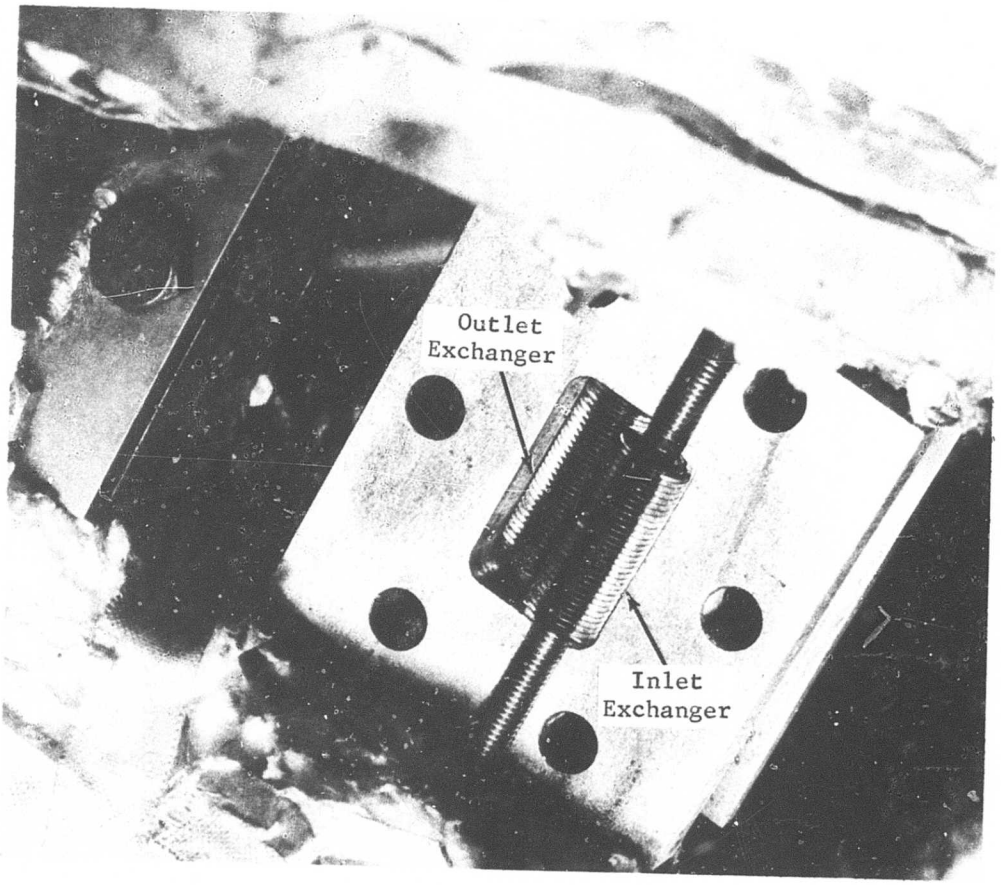

Figure 44. Finned Tube Vane Exchanger.

In the engine design, the finned tubes are installed adjacent to the vanes to minimize pumping losses and to facilitate fabrication and installation. For the rig test, these finned tube exchangers were displaced from the vanes to provide a means for encasing each tube group in order to obtain measurements and establish heat exchanger effectiveness.

The liquid metal system for the cascade test was designed as a breadboard arrangement. The design provides a system with:

1. Flexibility for setting test conditions
2. Fast response time
3. Instrumentation
4. Use of existing liquid metal supply tanks and liquid metal pump
5. Provisions for purging, filling, filtering, pressurizing, etc.

Figure 45 presents the liquid metal flow system schematic. The flow of liquid metal is regulated by the argon cover gas pressure on the two liquid metal tanks. A rotary induction pump is used intermittently to return the liquid metal to the supply tank to maintain the required level in each tank. The flow path of the liquid metal coolant and the design outlet temperatures at key stations are presented in Table XXXI.

TABLE XXXI. LIQUID METAL SYSTEM DESIGN OPERATING TEMPERATURES

Flow Path Station	Exit Temperature (°F)
Supply Tank	160
Cold Side LM/LM Heat Exchanger	1400
Electric Heated Tube	1440
Upstream Vane Exchangers	1400
Vanes	1480
Downstream Vane Exchangers	1440
Hot Side LM/LM Heat Exchanger	200

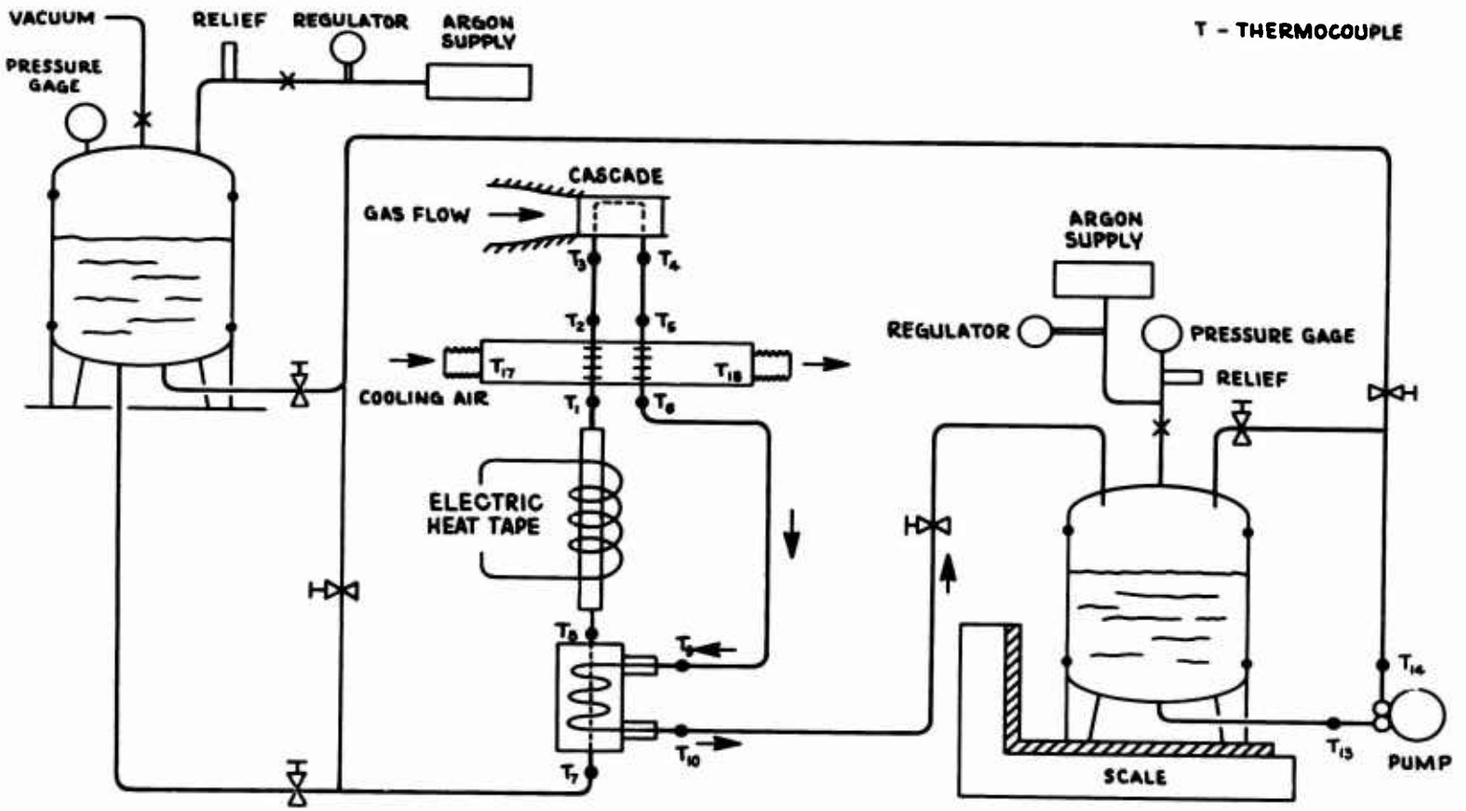

Figure 45. Liquid-Metal-Cooled Cascade System Schematic.

The concentric tube liquid-metal-to-liquid-metal heat exchanger design presented in Figure 46 was provided to use the heat of the liquid metal exiting the vanes to raise the temperature of the liquid metal entering the vanes. This approach had two advantages. It precluded the need for a large electrical heating source. This exchanger also reduced the design complexity of the balance of the liquid metal loop since the section of the liquid metal system containing the supply and collection tanks, the pump, etc., could then operate at temperatures slightly above ambient (200° - 250°F). Furthermore, by utilizing this exchanger concept, the time required to reach a steady-state test condition was greatly reduced, since the bulk of the coolant is maintained at ambient temperatures and only that liquid metal circulating directly through the short length of the system containing the vanes and the vane exchangers is affected by changes in operating conditions.

To determine performance during the test, each component was instrumented to measure liquid metal inlet and outlet temperatures as shown in Figure 45.

5.4 ASSEMBLY OF THE LIQUID METAL TEST LOOP

The system components were assembled and installed in accordance with the system flow schematic. Each of the three liquid-metal-cooled vanes was instrumented with five thermocouples to record the airfoil mid-span metal temperature during test. The thermocouples were located in the vane wall midway between the airfoil gas and coolant surfaces. Figure 47 is a photo of the instrumented vanes installed in the nozzle support.

The liquid metal system is required to be clean and have leak-tight components and interconnecting piping. This is important to avoid liquid metal external leaks during rig operation or to prevent the formation of liquid metal oxides. System filling is performed with a vacuum of 10^{-6} mm Hg in the system. This procedure prevents the formation of oxides which could plug the smallest coolant passages in the vanes. Achieving the required vacuum in the system is relatively easy if established procedures for welding and brazing are introduced and followed. However, difficulties were encountered with this system because a breadboard system was provided in order to include the following non-engine requirements:

1. Instrumentation
2. Secondary flow path for system filling, purging, filtering, etc.
3. Parallel flow paths for flexibility in the operation of the rig
4. Test equipment components for heating, collection, etc.

These requirements necessitated the use of over 100 feet of tubing in addition to the system components and numerous dry-seal, brazed and welded connections. For an engine system design, the majority of these components, tubing, and connections are eliminated, thereby reducing problems in achieving the required system vacuum prior to filling with the liquid metal.

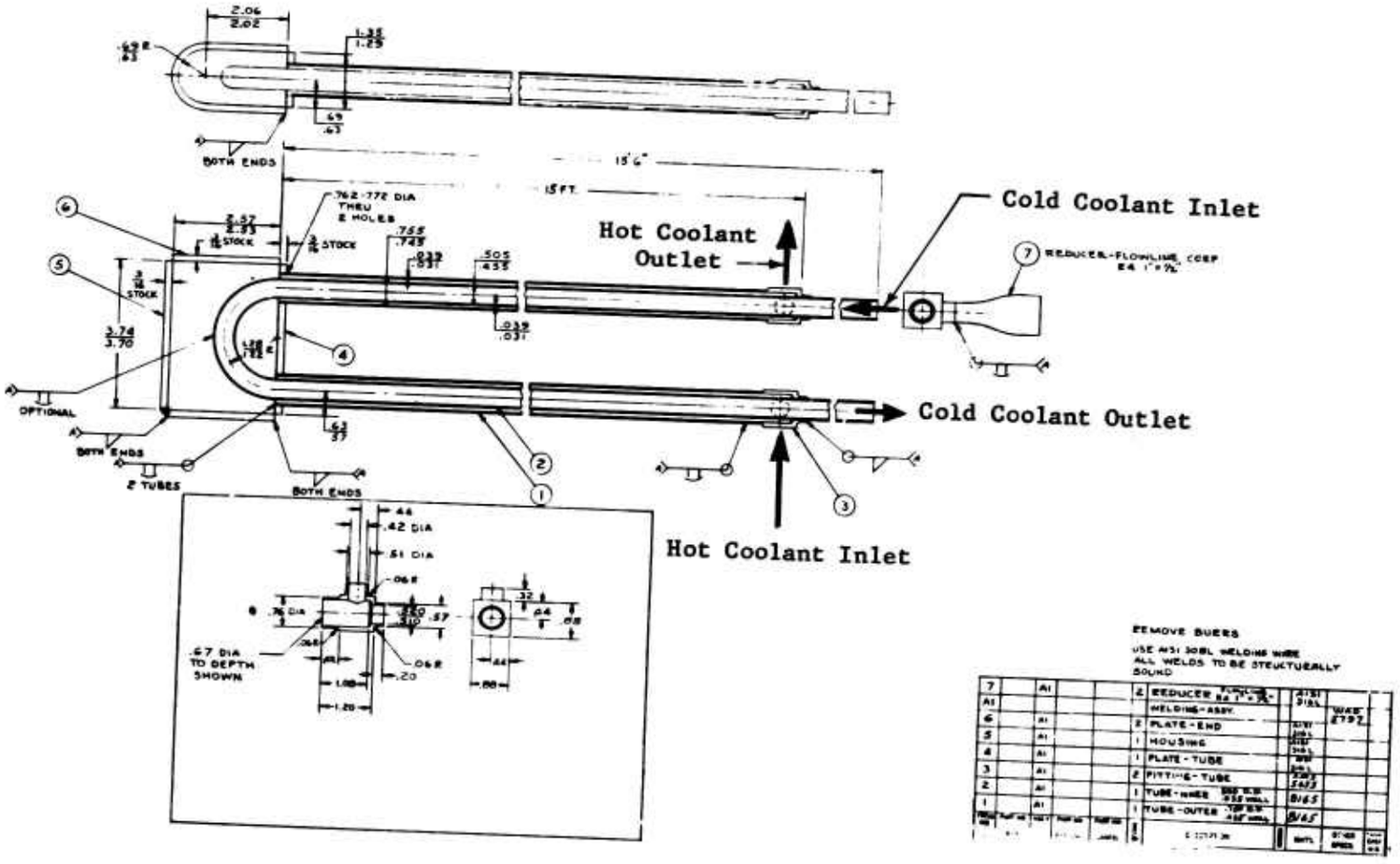

Figure 46. Liquid-Metal-to-Liquid-Metal Heat Exchanger.

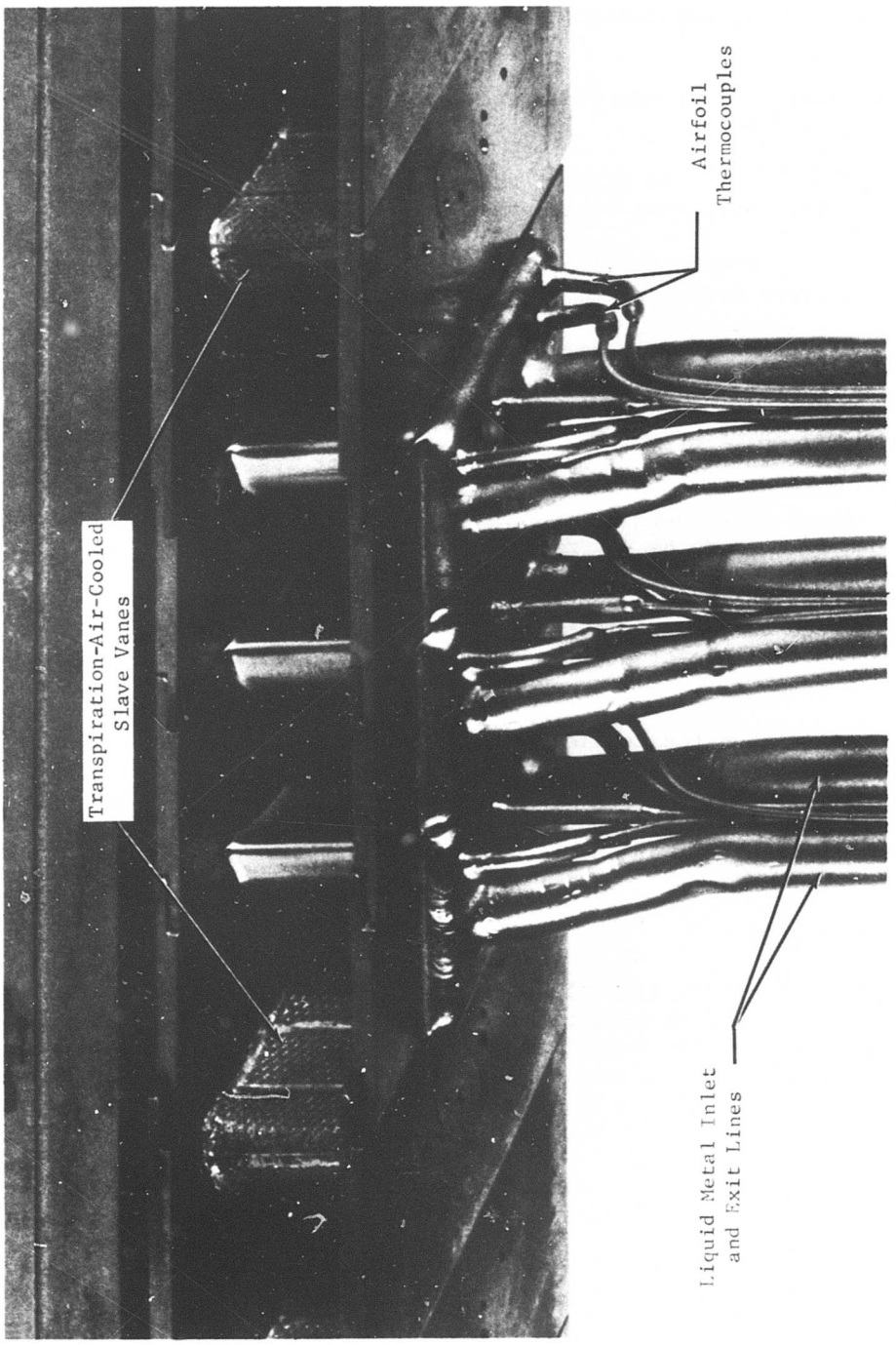

Figure 47. Liquid-Metal-Cooled Vane Installation, Leading-Edge View.

The breadboard system was segregated into four major sections for the purpose of leak checking and isolating problem areas. These sections consisted of:

1. The vanes, the finned tube vane exchangers, and the inlet and outlet manifolds

2. The tubing and cold side of the liquid-metal heat exchanger from the supply tank to the vane exchanger inlet manifold

3. The tubing and hot side of the liquid-metal heat exchanger from the vane exchanger outlet manifold to the return tank

4. The liquid metal pump section between the return tank and the supply tank

Each section was independently evacuated to a vacuum between 10^{-5} and 10^{-6} mm Hg, and a mass spectrometer helium leak detector was employed. Leak repairs were made by Nichrobrazing the connections. After considerable effort, the final leak check on the assembled system was successfully made with a vacuum of 10^{-6} mm Hg and maintained for 30 minutes.

Prior to starting the hot test, 300°F liquid metal was circulated through the entire system as a final test for leakage. During this test, the operation of the liquid metal pump was checked and the flow characteristics of the liquid metal system were established.

Figures 48 and 49 show the completed system arrangement. In addition to the system components previously described, a stainless steel porous mesh filter was included in the fill line to prevent contaminants, which may have formed during prolonged storage of the liquid metal in the supply tanks or during prior use of the liquid metal,from entering the vane coolant passages.

5.5 INSTRUMENTATION

The liquid-metal coolant, airfoil and gas shelf metal, and combustion gas temperatures were measured by sheathed chromel-alumel thermocouples. The liquid metal thermocouples were tack-welded to the stainless steel tubing at the locations of interest and insulated. Figure 45 shows the location of the liquid-metal thermocouples in the coolant test loop. These thermocouples are identified as T-1 through T-16 in the figure.

The three liquid-metal-cooled vanes were each instrumented with five thermocouples located at the mid-span vane height, at the chordwise locations shown in Figure 35.

A four-element temperature sampling probe was located across the four gas passages formed by the three liquid metal cooled vanes and the two adjacent transpiration-cooled slave vanes. The probe was located at mid-span

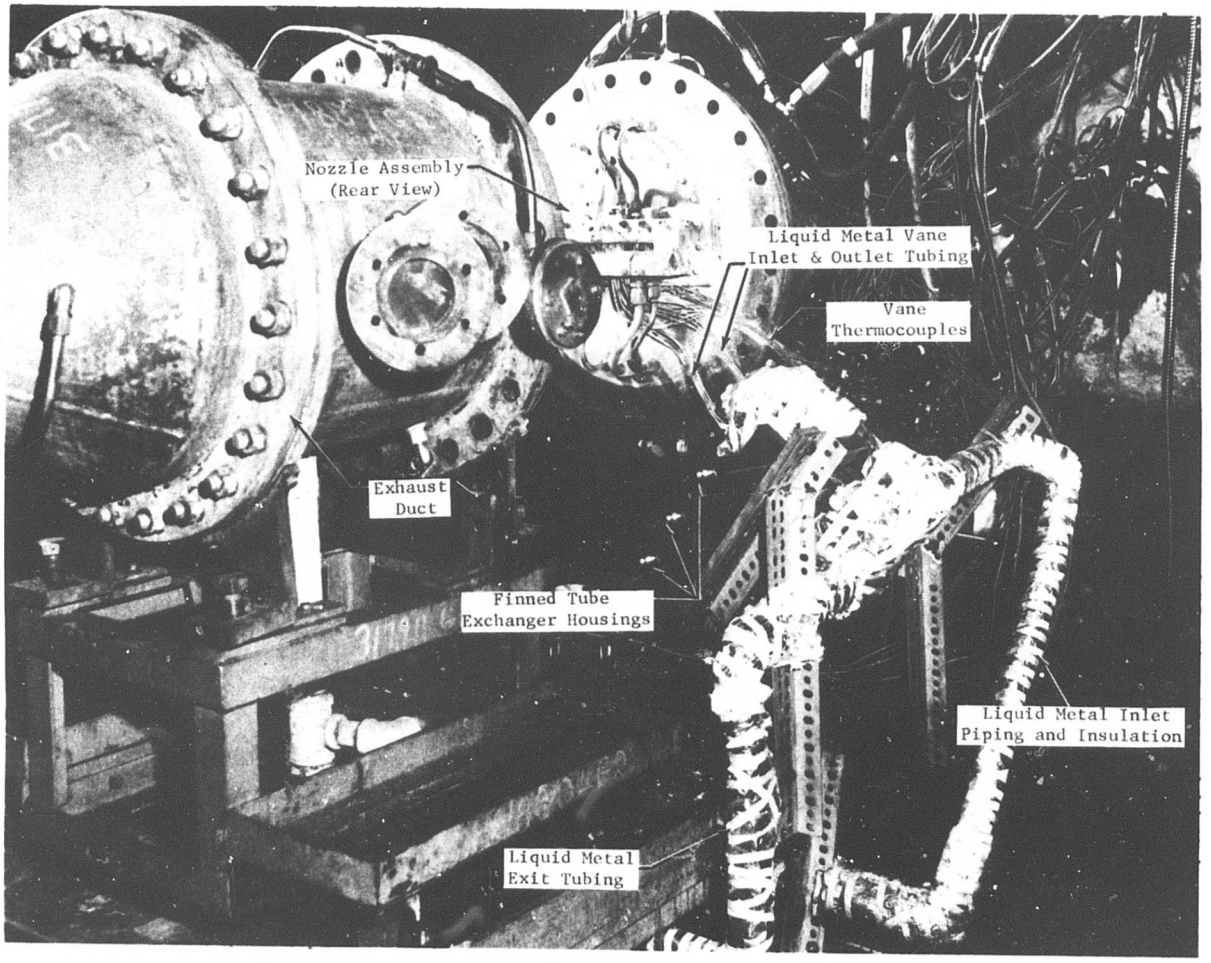

Figure 48. Liquid-Metal-Cooled Turbine Nozzle Test Cell Installation.

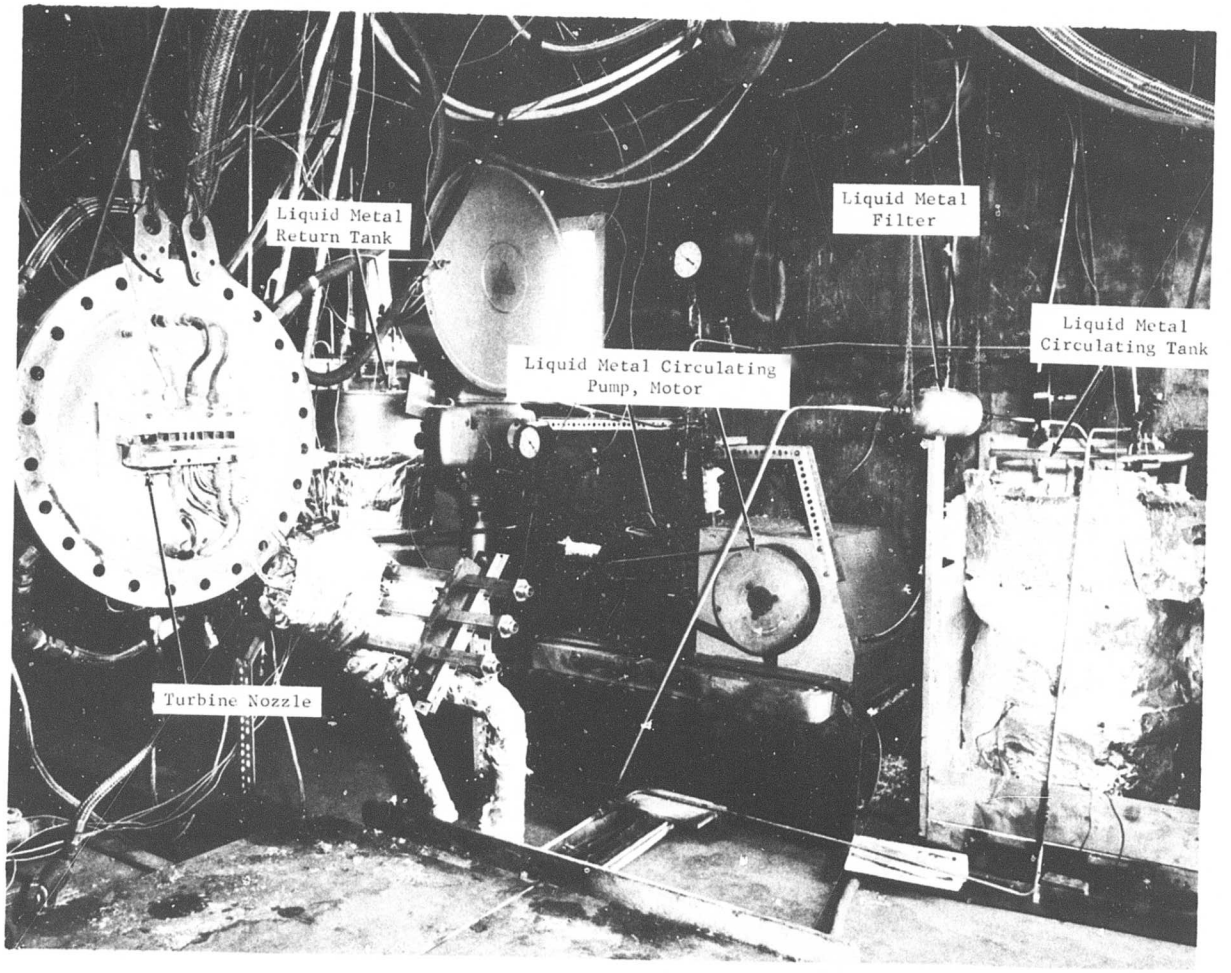

Figure 49. Turbine Cascade's "Breadboard" Liquid Metal Loop.

height, and each element was at the center of a discrete gas passage, 0.250 inch downstream of the vane trailing edges (Figure 50).

The remainder of the instrumentation consisted of temperature and pressure measurements across ASME-type sharp-edge orifices to calculate main and secondary airflow rates. Main fuel flow was measured with a rotometer.

Liquid metal flow rate was determined by differences in collection tank weight for a measured time. Liquid metal pressures were measured directly with stainless steel tube compound Bourdon gages.

A summary of the locations of temperatures, pressures, and mass flows measured for the test is given in Table XXXII.

TABLE XXXII. LIQUID-METAL-COOLED TURBINE NOZZLE RIG INSTRUMENTATION

Identification	Location and Description
Temperature	
T 1-1,1-2,1-3	Upstream Exchanger; Liquid Metal In
T 2-1,2-2,2-3	Upstream Exchanger; Liquid Metal Out
T 3-1,3-2,3-3	Vane; Liquid Metal In
T 4-1,4-2,4-3	Vane; Liquid Metal Out
T 5-1,5-2,5-3	Downstream Vane Exchanger; Liquid Metal In
T 6-1,6-2,6-3	Downstream Vane Exchanger; Liquid Metal Out
T 7	Concentric Tube Liquid Metal Exchanger; Cold Liquid Metal In
T 8	Concentric Tube Liquid Metal Exchanger; Cold Liquid Metal Out
T 9	Concentric Tube Liquid Metal Exchanger; Hot Liquid Metal In
T 10	Concentric Tube Liquid Metal Exchanger; Hot Liquid Metal Out
T 13	Liquid Metal Pump Inlet
T 14	Liquid Metal Pump Outlet
T 101,106,111	Vane Metal Temperature at Leading Edge
T 102,107,112	Vane Metal Temperature at 2/5 Chord, Pressure Side
T 103,108,113	Vane Metal Temperature at 2/5 Chord, Suction Side
T 104,109,114	Vane Metal Temperature at 3/5 Chord
T 105,110,115	Vane Metal Temperature at 4/5 Chord
T 17	Upstream and Downstream Vane Exchangers, Air In
T 18-1,18-2,18-3	Upstream and Downstream Vane Exchangers, Air Out
T 116	Vane Gas Shelf Metal Temperature
T 118	Nozzle Exhaust Gas Temperature, Vane 1 and Slave Vane
T 119	Nozzle Exhaust Gas Temperature, Vanes 1 and 2
T 120	Nozzle Exhaust Gas Temperature, Vanes 2 and 3
T 121	Nozzle Exhaust Gas Temperature, Vane 3 and Slave Vane
T 201	Main Air Temperature at Orifice
T 202	Main Air Temperature at Preheater Exit
T 203	Vane Exchanger Air Temperature at Orifice

TABLE XXXII - Continued

Identification	Location and Description
Pressures	
P 1	Liquid Metal Supply Tank
P 2	Liquid Metal Return Tank
P 3	Liquid Metal Pump Inlet
P 4	Liquid Metal Pump Outlet
P 101	Combustor Inlet Air
P 102	Nozzle Exit Static
P 103	Nozzle Inlet Static
P	Argon Cover Pressure, Supply Tank
P	Argon Cover Pressure, Return Tank
P	Main Combustor Fuel Pressure, Inlet
P	Preheater Fuel Pressure, Inlet
Mass Flows	
ΔP	Main Airflow Orifice
ΔP	Vane Exchanger Airflow Orifice
Scale	Liquid Metal Flow
Rotometer	Main Combustor Fuel Flow

A schematic of the test facility and location of test equipment instrumentation is shown in Figure 51.

5.6 TEST PROGRAM AND RESULTS

The objective of the test program was to evaluate the thermal and structural characteristics of the liquid-metal-cooled vanes over a 5-hour test period.

The test program was formulated into:

1. Shakedown phase
2. Hot test phase

The shakedown phase was conducted for each of the following:

1. Combustor
2. Liquid metal coolant system
3. Turbine cascade

The initial test on the combustor without the turbine cascade installed was conducted to check out ignition, gas outlet temperature profile, and

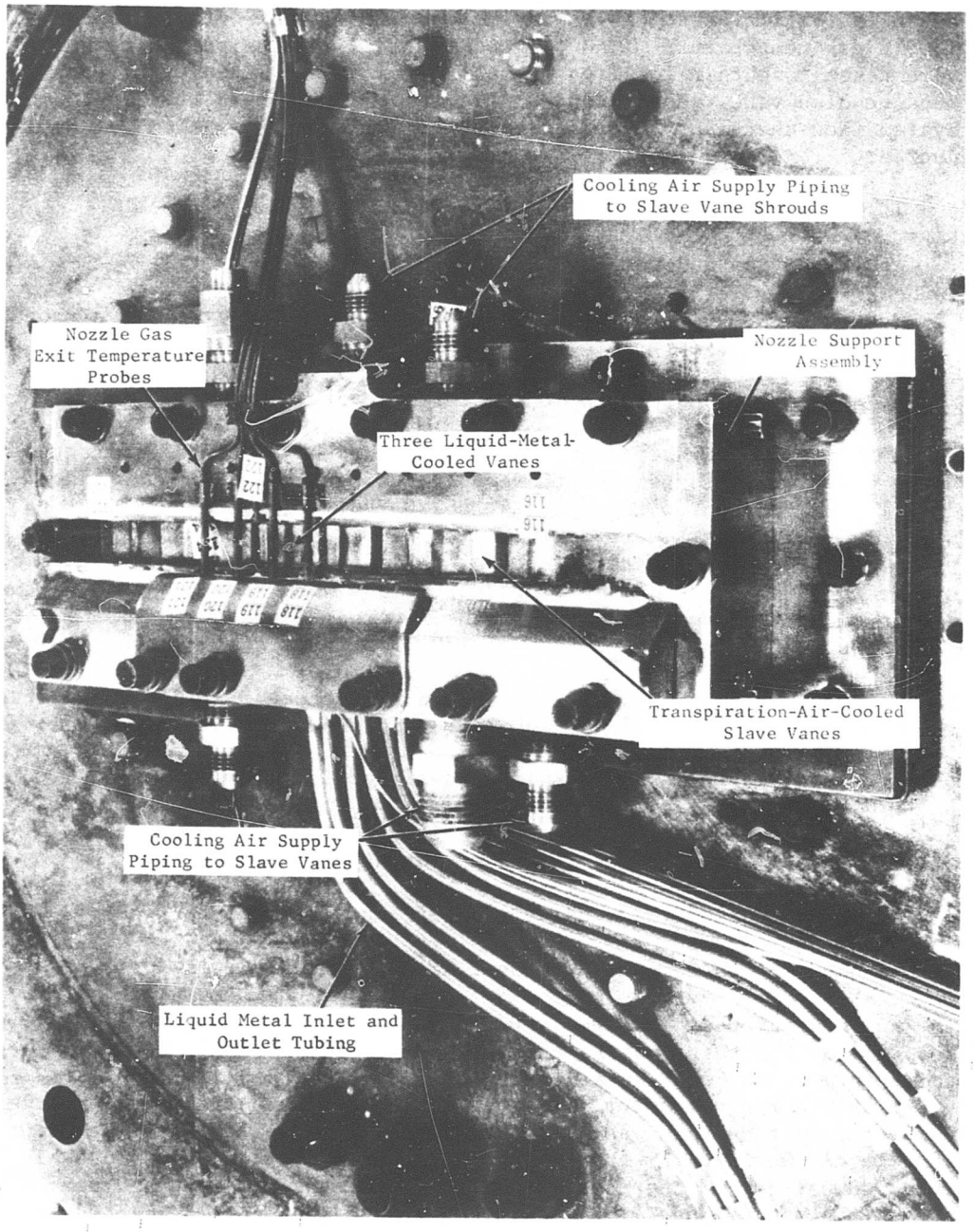

Figure 50. Turbine Cascade Installation and Instrumentation.

durability of the graphite liner sections that had required replacement during an earlier test program. The combustor check-out was conducted at 1800°F gas temperature without incident. Mid-annulus height measurements were taken to obtain local gas temperatures in the vicinity of each liquid-metal-cooled vane. The second shakedown phase involved the liquid metal system flow checks at temperatures up to 600°F. This shakedown was conducted:

1. To establish a leakage-free system

2. To outgas and wet the tube walls

3. To determine the flow characteristic of the system for a range of tank cover pressures up to 16 psi and 120 PPH

4. To establish the flow characteristic of the pump

The system flow characteristic was established by setting differences in argon cover pressure between the supply and return tank in the range of 3 to 15 psi for a flow range of 24 to 120 PPH. The tanks used for the system were the containers in which the liquid metal is supplied from the producer. These tanks are structurally limited to 16 psig. Furthermore, higher than anticipated system pressure drops were incurred through the addition of valves, secondary flow paths, increased length of piping, etc. As a result, the full rated flow of 179 lb/hr vane could not be achieved.

Final shakedown testing was conducted on the cascade at stator inlet gas temperatures between 600° and 1500°F. This shakedown test included:

1. Check-out of the transpiration-air-cooled slave vanes

2. Operating and response characteristics of the liquid metal system with changes in gas operating conditions

3. Check-out of the sensing and read-out instruments.

This shakedown was completed without significant problems.

The hot cascade test followed. During this test period, the airflow was supplied by the test equipment compressor at 90 psig, throttled to 63.2 psig, and preheated to 600°F by a direct-fired test equipment heater prior to entering the rig combustor. The rig combustor was operated to provide combustor exit average gas temperatures of 1550° to 2500°F. The temperature levels were set by the four single-element temperature probes located downstream of the vane trailing edge at the mid-span and spaced across the gas passages formed by the three center test vanes.

Figure 52 presents the average combustor exit gas temperature versus fuel-air ratio based on a mid-span traverse across the original eight-vane cascade (Reference 10). Figure 52 also presents the average of the four readings at the center of each test vane passage. This figure shows that

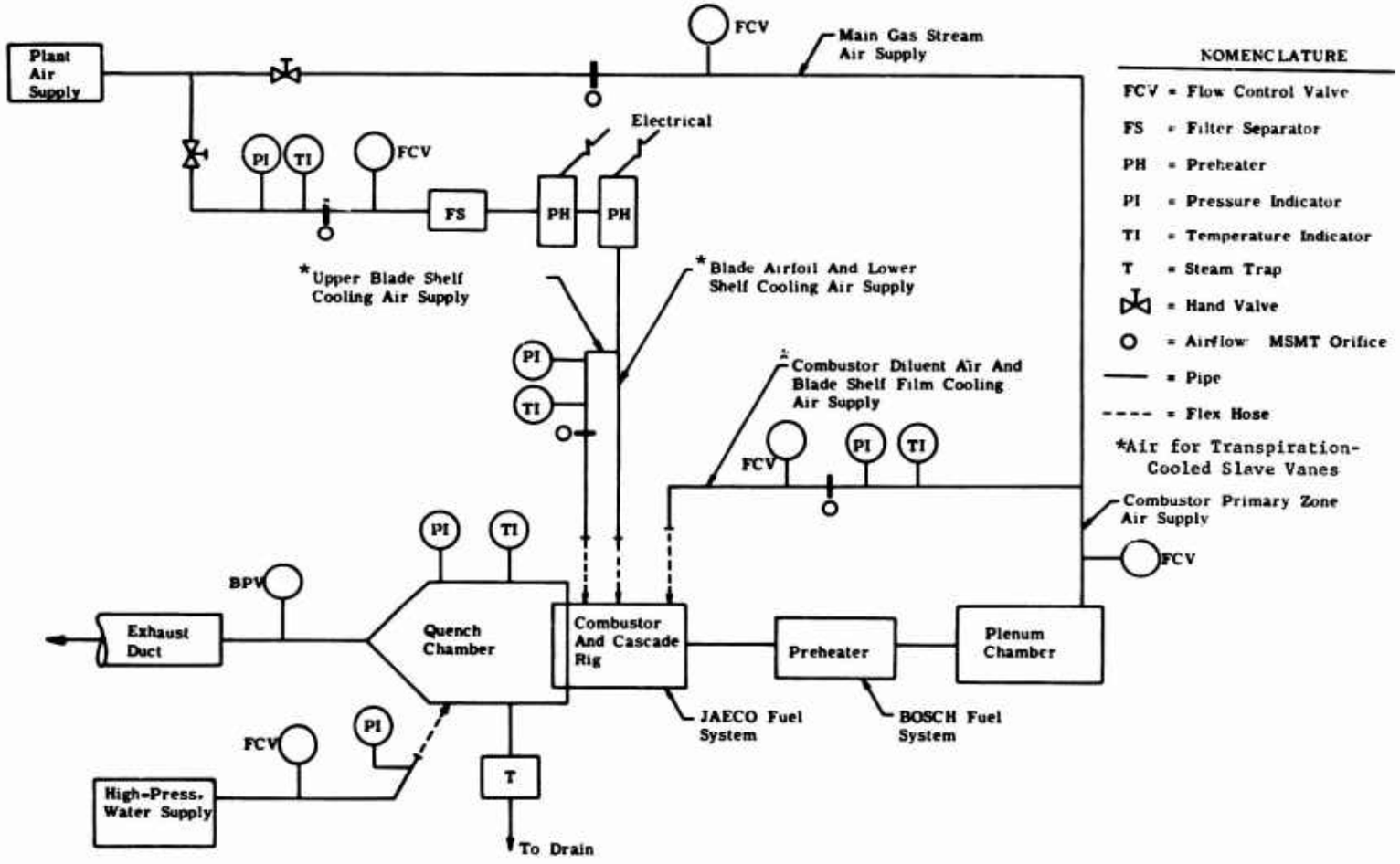

Figure 51. Schematic of Air and Fuel Facility for Turbine Cascade Test.

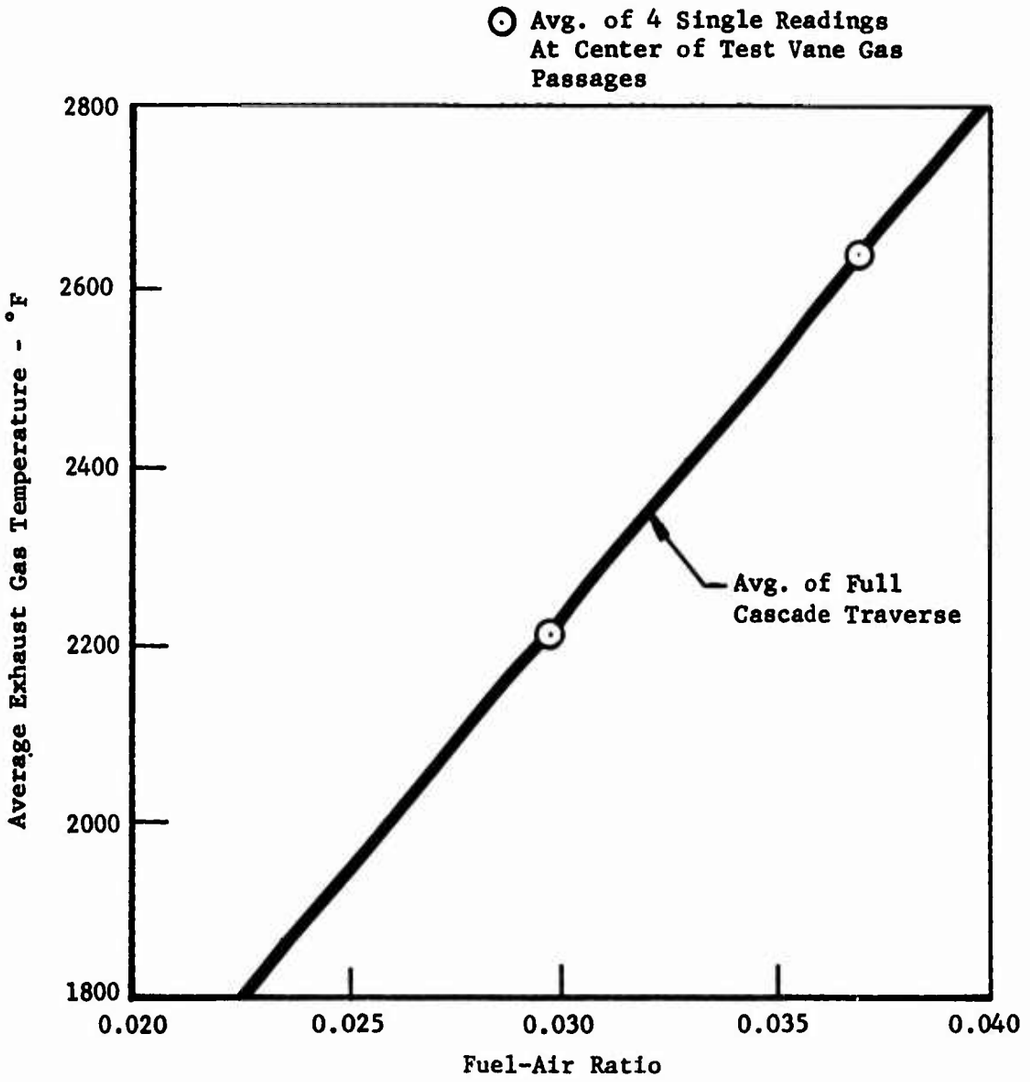

Figure 52. Combustor Exit Average Gas Temperature at Mid-Span Versus Fuel-Air Ratio.

single-element probes obtain representative values of average gas temperature for the cascade rig.

Figure 53 presents the combustor exit gas temperature traverse obtained during the original eight-vane cascade test (Reference 10). This figure shows that the center test vane is exposed to a relatively flat gas temperature profile between the pressure and suction side gas flow passages. Therefore, the vane metal temperatures measured on the center vane were considered appropriate for correlation of design predictions of vane temperature with test data.

At each gas temperature level, the liquid metal flow was adjusted by setting a differential between the gas cover pressure on the supply and the return tanks with a limitation of 16 psig maximum tank pressure. Flow rates of approximately 24 to 120 PPH were set for most test points.

The airflow to the vane exchangers was set at .104 lb/sec and 142°F.

The electrical resistance heater for the liquid-metal pipe supplying the vanes was adjusted to obtain the desired liquid-metal temperature, but the capacity of the heater usually limited the temperature level.

Readings of all instrumentation listed in Table XXXI were obtained for each test point.

During this test period, the combustor exit gas average temperature was initially set at the following increasing levels: 1550°, 1800°, 2100°F. At each of these settings, the liquid-metal flow was adjusted to cover three flow rates. Measurements of five metal temperatures in each of the three test vanes were taken to obtain the effect of varying the coolant flow. The final test point was conducted at a fuel-air ratio of .0385, producing a local peak of 2950°F in the gas passage between the two adjacent liquid-metal vanes on the right side. One liquid-metal flow rate (about two-thirds of the design flow) was set at this point and vane metal temperatures were recorded. However, the predicted metal temperatures were not exceeded since the liquid metal temperature entering the vane was lower than design.

The hot testing was completed in 5:45 hours. Operating times at the selected gas temperature settings were as follows:

Below 1550°F	2:40 hr
1550°F	1:00 hr
1800°F	0:55 hr
2100°F	0:40 hr
2500°F	0:30 hr

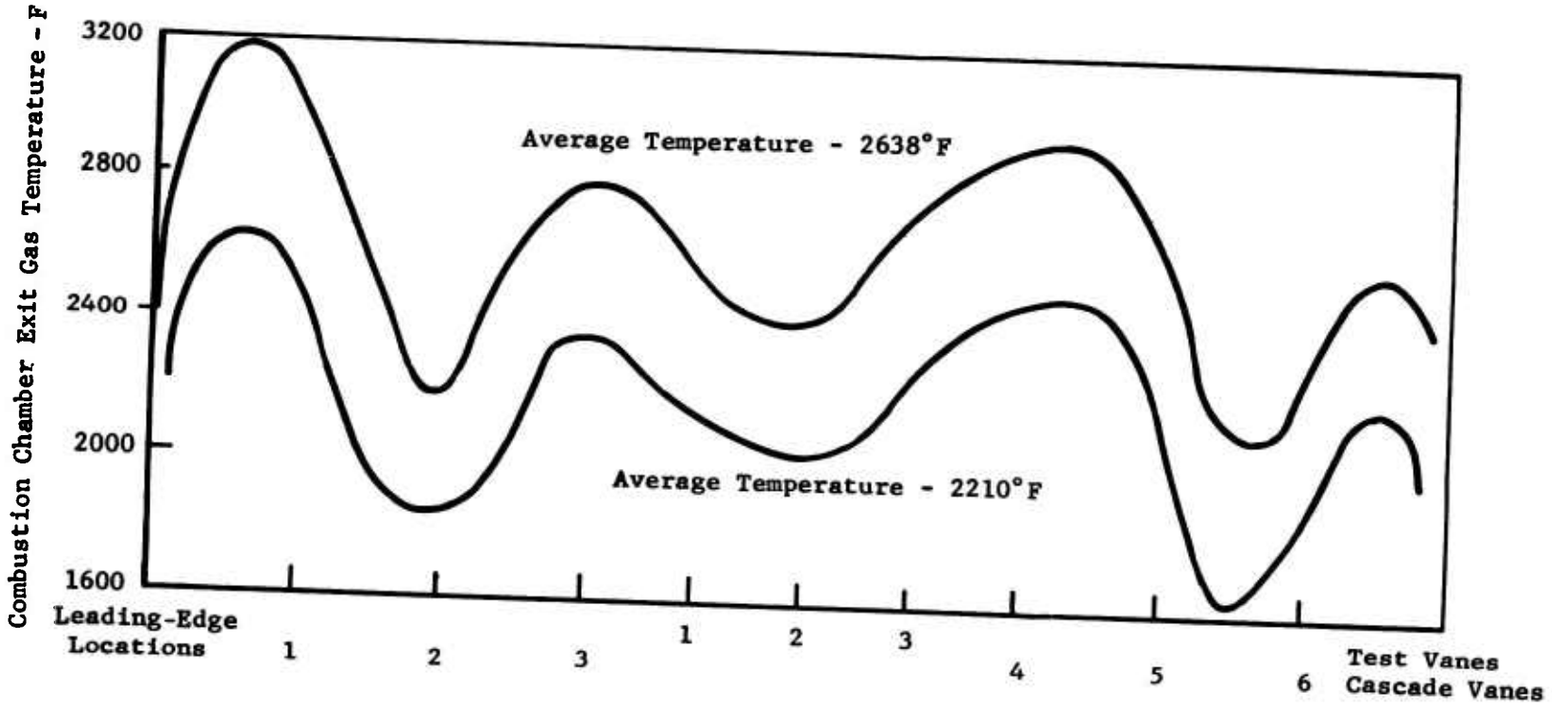

Figure 53. Cascade Temperature Profile.

Post-test inspection of the liquid-metal-cooled vanes revealed their condition to be excellent. Based on this limited number of test hours and about 30 vane temperature cycles, the mechanical design arrangement appears satisfactory. None of the critical areas of the design and fabrication under evaluation displayed vibratory, thermal, or structural problems during this test. The critical areas that were evaluated included the following:

1. 0.010-inch wall thickness near the trailing-edge coolant passage
2. Tube-to-vane-shelf header weld attachment
3. Shelf header to vane weld attachments
4. Finned-tube heat exchanger elements for heat rejection from the vane to compressor discharge air
5. Leading and trailing edges

Photographs of the trailing-edge view of the liquid metal cooled vanes after completion of the 2500°F test are presented in Figures 54, 55, and 56.

The methods used to predict the vane metal temperatures for the test conditions are the same as described in Section 3.1 for the thermal analysis of the vane design. Since the tests were not conducted at the design state conditions of temperatures, pressures and flows, it was necessary to analytically predict the vane metal temperature at the test conditions in order to make a comparison with the observed thermocouple readings.

The analysis to predict the vane temperature at the test conditions utilized a parametric ratio to establish the heat transfer film rate from the gas to the vane. For example, the heat transfer rate near the leading-edge stagnation point is described by the equation

$$h = 1.14 \frac{k_f}{D} \left(\frac{V_\infty \rho_f D}{\mu_f} \right)^{\frac{1}{2}} \left(\frac{\mu C_p}{k} \right)_f \left[1 - \left(\frac{\theta}{90} \right)^3 \right] \qquad (19)$$

Recognizing that $\left(\mu C_p/k\right)_f$ is a constant in the region of interest, $\left[1 - \left(\frac{\theta}{90}\right)^3\right]$ is a geometry function which remains unchanged and $1.14\ k_f/D$ is approximately a constant, then

$$h \quad \text{Constant} \left(\frac{V_\infty \rho_f}{\mu_f} \right)^{\frac{1}{2}} \qquad (20)$$

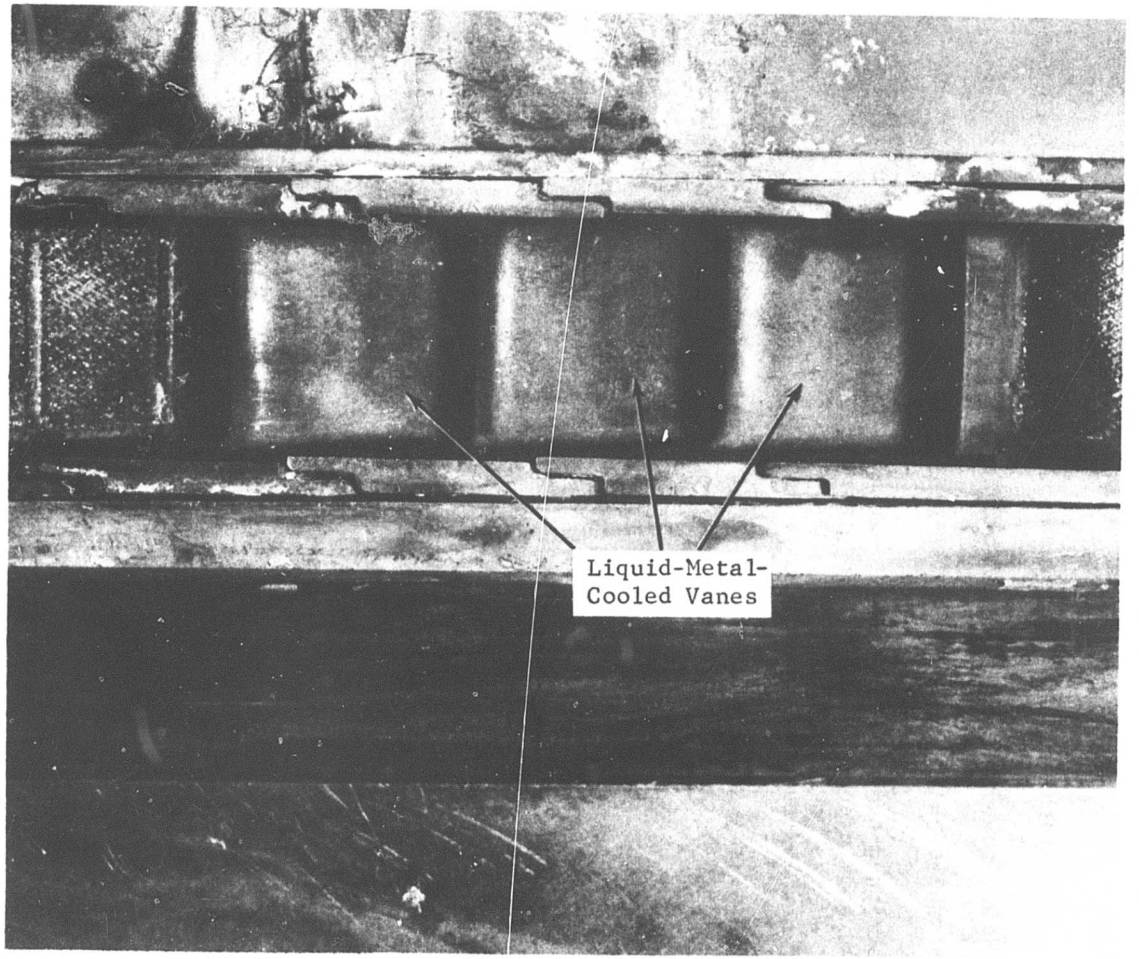

Figure 54. Post-Test Suction-Side View of Nozzle Assembly.

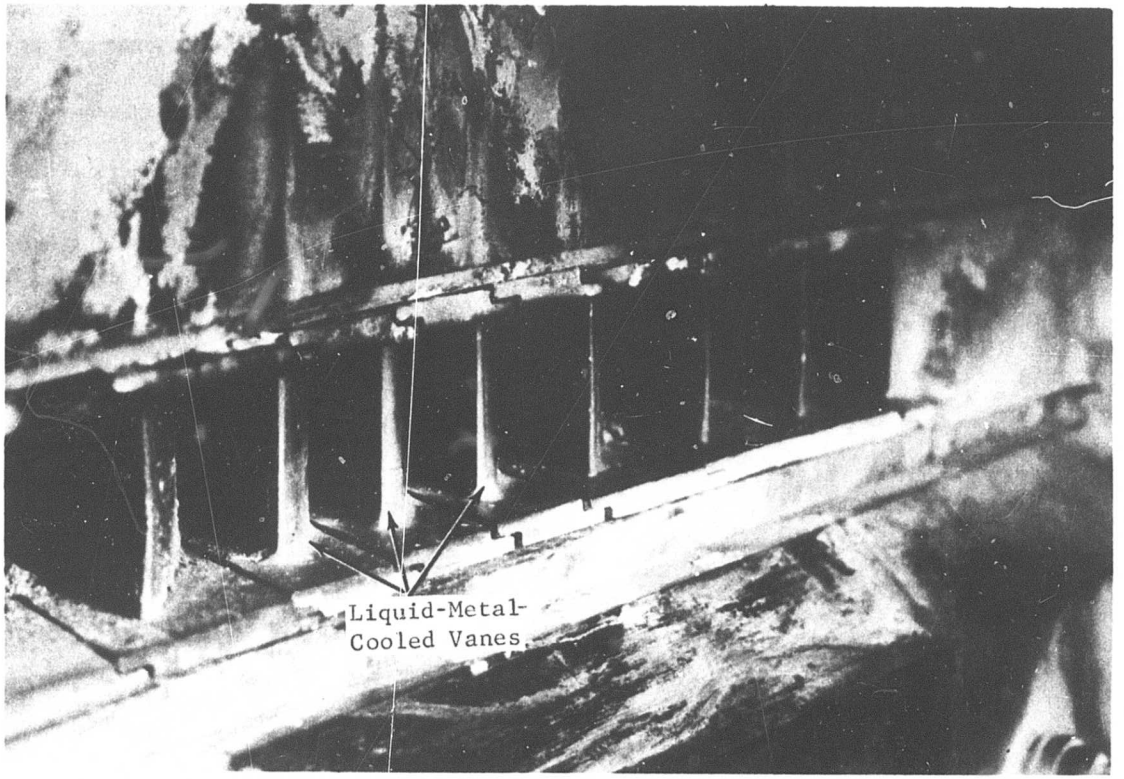

Figure 55. Post-Test Trailing-Edge View of Nozzle Assembly.

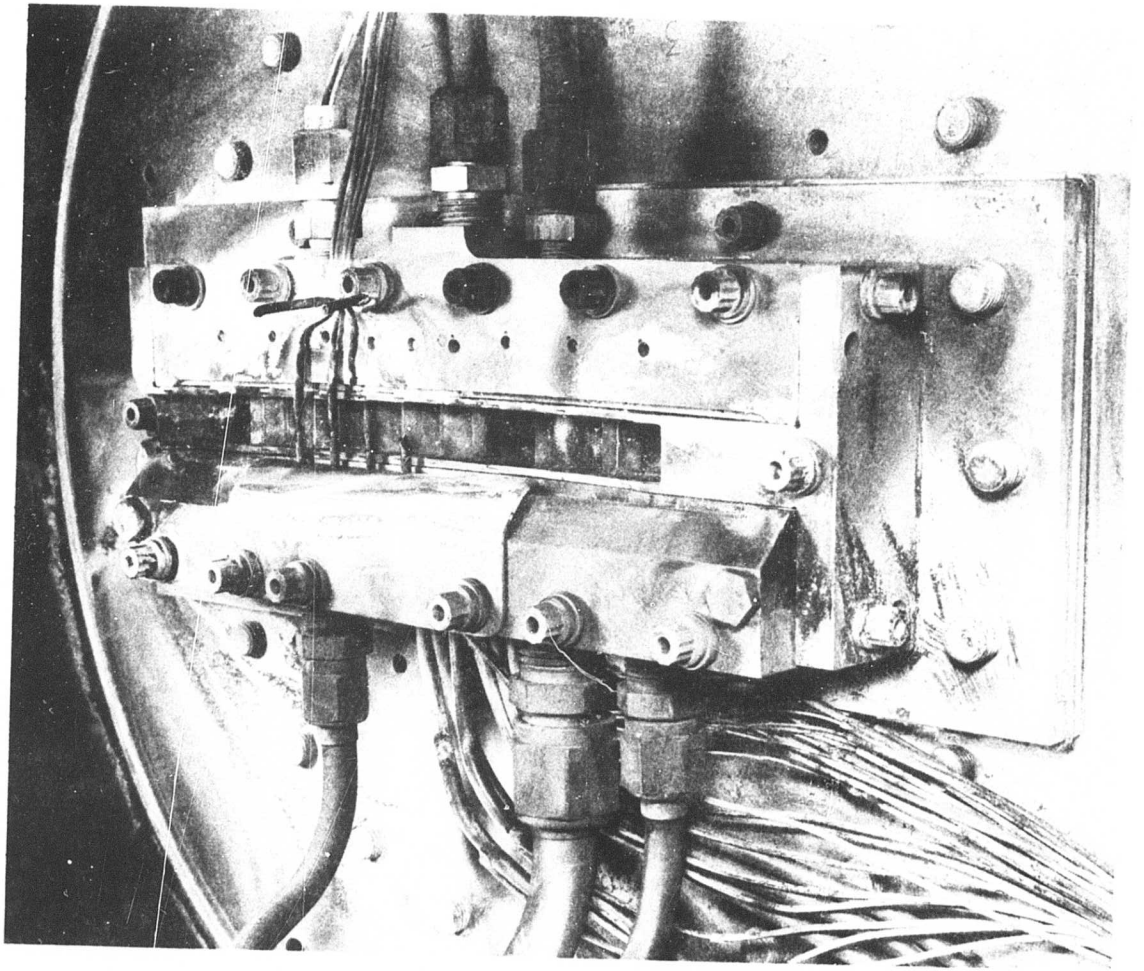

Figure 56. Post-Test Turbine Nozzle, Trailing-Edge View.

Consequently, the value of the heat transfer rate at the test conditions is described by the relationship

$$h_T = h_D \left(\frac{V_{\infty T}}{V_{\infty D}}\right)^{\frac{1}{2}} \left[\frac{(\rho/\mu)_T}{(\rho/\mu)_D}\right]_f^{\frac{1}{2}} \qquad (21)$$

where the subscripts

T = test
D = design

The heat transfer rate from the vane to the coolant is evaluated directly at the test conditions.

The measured gas and coolant temperatures are used directly. Then the analytically predicted temperatures are calculated at the thermocouple locations using the fact that the temperature change across any thermal resistance, in the case of convection and conduction, is proportional to the value of the resistance.

The conditions of the two test points used to predict the vane temperatures are as follows:

Fuel-Air Ratio	.0385	.030
Gas Temperature, °F	2600	2100
Gas Total Pressure, in. Hg	101	101
Gas Flow, lb/sec/vane	.0589	.0589
NaK Temperature, °F	900	875
NaK Flow, lb/hr/vane	124	124

The gas temperature is the average mid-span value in the gas passage adjacent to the center vane based on the profile established in Figure 53. The NaK temperature is the average of the coolant inlet and outlet pipes of the center vane. The NaK flow is one-third of the total flow measured flowing from the supply tank to the three test vanes. The gas flow is ratioed from the cascade flow by the percentage the center vane throat area is of the total cascade throat area.

The metal temperatures predicted for the center of the vane wall thickness (the location of the thermocouple) and the observed temperatures for the 2600°F point are shown in Table XXXIII.

TABLE XXXIII. COMPARISON OF TEST AND PREDICTED VANE TEMPERATURES		
	Test	Predicted
Leading Edge - T101	1186°F	1203°F
Suction Side - T103	970°F	947°F
Pressure Side - T102	950°F	947°F
Near Trailing Edge - T104	1130°F	971°F
Trailing Edge - T105	1155°F	1140°F

Table XXIII shows excellent agreement for all locations except the temperature located upstream of the trailing edge. The trailing-edge section is most susceptible to thermal gradients unless an appropriate selection of coolant passage size and location is provided. Therefore, the difference between the observed and predicted temperatures near the trailing edge may be attributed to a possible machining discrepancy in the size or location of the two small coolant passages. This could not be verified without destructive inspection of the vane assembly.

For the testpoint at 2100°F gas temperature, the vane metal temperature correlation is as follows:

	Test	Predicted
Leading Edge	1096°F	1092°F

Thus, the reduced gas temperature test point showed equally good correlation as the 2600°F condition for the region of highest heat flux. The above comparisons demonstrate that the methods and correlations used in the heat transfer analysis (1) are appropriate for the thermal design of liquid-metal-cooled turbine vanes and (2) offer a high degree of confidence in predicting the off-design vane metal temperatures.

Figures 57 and 58 present the measured metal temperature data over a range of liquid metal flow rates and at 1500°, 1800°, 2100° and 2500°F gas temperature. Vane temperature was measured at the leading and trailing edges and at approximately 40% and 60% of the chordal distance from the leading edge. At the 40% chordal location, a comparison of suction side and pressure side temperatures shows less than 30°F difference in the coolant flow range of interest.

A method of comparing analytically predicted vane heat exchanger performance with the measured performance when the heat exchanger is subjected to the test conditions instead of the design conditions was also established. Since the liquid-metal heat transfer rate is very high, the heat exchanger performance is estimated to be approximately proportional to the air-side heat transfer rate.

The correlation for the air-side heat transfer rate of the finned tubes is

where $$h = j\, G\, Cp\, (Pr)^{-2/3} \qquad (22)$$

$$j = f(Re) = \text{constant} \left(\frac{G}{\mu}\right)^{-.417} \qquad (23)$$

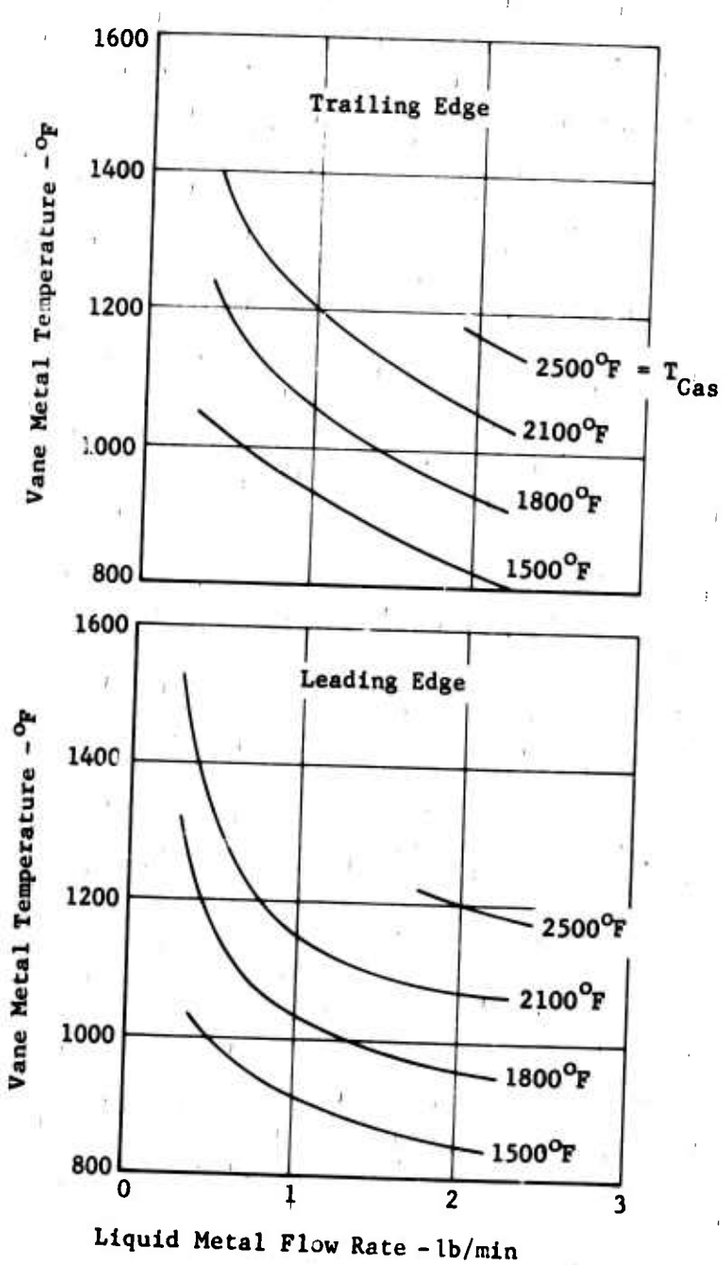

Figure 57. Liquid-Metal-Cooled Vane Leading- and Trailing-Edge Metal Temperature Test Data.

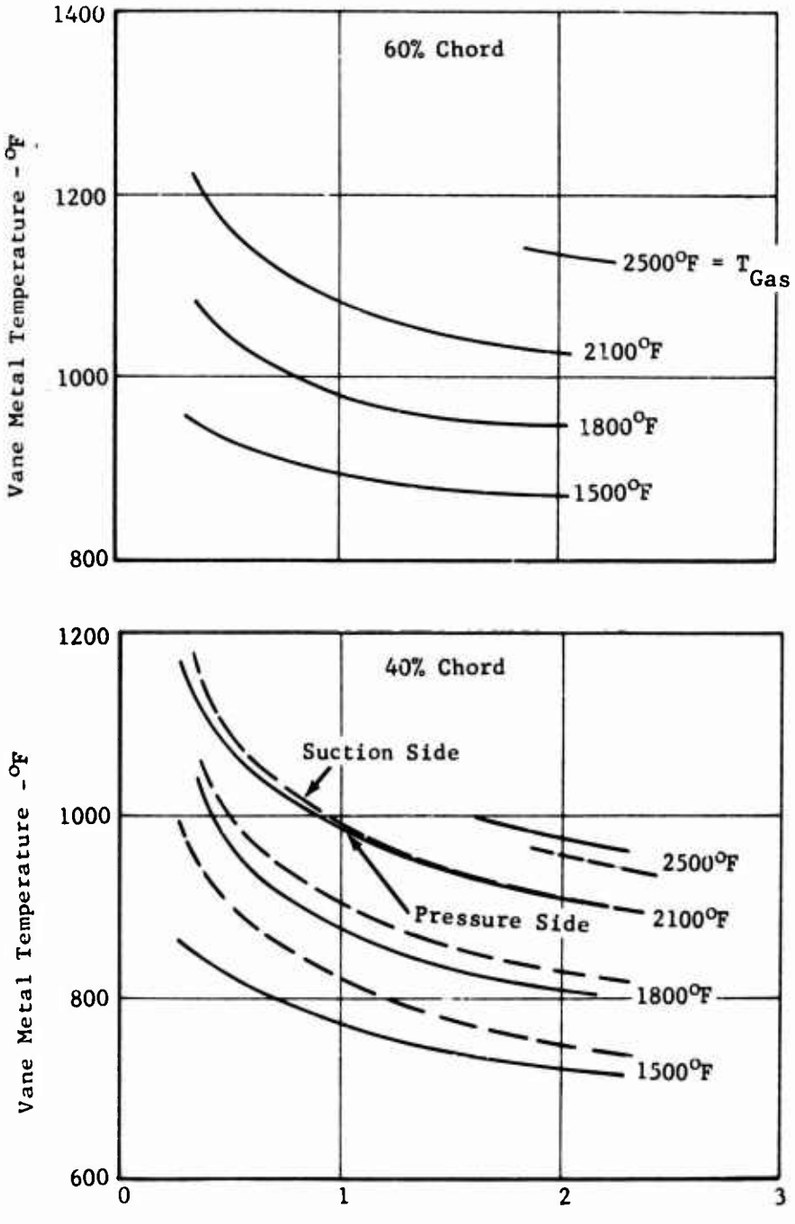

Figure 58. Liquid-Metal-Cooled Vane Mid-Chord Metal Temperature Test Data.

as obtained from experimental data. Substituting for these terms in the heat flow equation ($Q = hA\Delta T$) and recognizing that Pr is a constant, then

$$Q = \text{Constant}\ \ GC_p\left(\frac{G}{\mu}\right)^{-.417}\Delta T \qquad (24)$$

The heat exchanger fabricated for this test used finned tubes having 32 fins per inch which were readily available instead of the 40 fins per inch specified in the design. The heat transfer factor (j) for the 32-fins-per-inch tubes was extrapolated from experimental data.

The exchanger core had spaces between the fins and walls of the core housing which allowed an estimated 25% of the air to bypass the finned heat exchanger surfaces. Thus, the data analysis used an effective flow through the exchanger core rather than the measured flow to the core housing.

Table XXXIV presents the measured test data and the design data for the vane heat exchanger that was used to calculate the heat flow. The heat flow calculated for the test conditions is .884 Btu/sec. This exchanger's performance when subjected to the design conditions provides a heat transfer of 1.27 Btu/sec. This is a 50% increase over the required .833 Btu/sec which is the vane's design heat load. Therefore, the performance of the exchanger configuration indicates that the exchangers are over size for the vane cooling design requirements.

The operating experience obtained during the test on the liquid-metal-cooled vane and the vane heat exchanger demonstrated the feasibility of these components to operate at or better than the predicted performance values. The operating experience of the vanes at 2500°F average gas temperature also demonstrated the feasibility of the design for gas turbines. This conclusion is based on tests of other cooled turbine configurations which indicate the feasibility of the design upon very short time exposure at the high gas temperatures.

Although engine gas conditions were not simulated for the exchanger, the operating experience of liquid-metal heat exchangers (for gas turbine regenerator applications) using the same finned tube design at gas temperatures of 1350° to 1500°F for over 500 hours (Reference 23) indicates the feasibility of the vane exchanger component's meeting engine durability requirements.

TABLE XXXIV. COMPARISON OF HEAT EXCHANGER DESIGN AND TEST PERFORMANCE

	Test		Design
Airflow/Vane Exchanger, lb/sec	0.0345		0.036
Net Flow Area/Vane Exchanger, sq. inch	0.388		0.238
Air Temperature - In, °F	142		871
Out, °F	337		961
Avg., °F	239		915
Heat Exchanger Pass	1st	2nd	
NaK Temperature - In, °F	895	975	1522
Out, °F	837	911	1442
Avg. °F	866	945	1462
NaK Temp. - Average of 2 Passes, °F	905		-
ΔT Avg. Air to NaK, °F	666		547
Calculated Heat Flow/Vane Exchanger, Btu/sec	0.884		1.27

6.0 CONCLUSIONS

The design phase of the program demonstrated that:

1. Internal closed-circuit cooling concepts for turbine vanes and blades, which return the heat removed from the airfoil to the engine cycle, provide a modest improvement of 5.0% in SFC compared to transpiration air cooling.

2. Application of liquids and gases in a closed-circuit turbine cooling concept will effectively cool the airfoils to obtain the turbine operating life design requirement of 1000 hours with metal temperatures in the range of 1500° - 1700°F.

3. Use of the compressor discharge air as a heat sink to return the heat removed from the blades and vanes to the engine cycle is feasible.

4. Power extraction from either spool of the engine shaft for pumping the coolant and heat sink is not excessive, although weight and volume of current-technology pumps are large relative to engine size.

5. When the overall system characteristics are considered, the liquid metal cooling is the most promising of the advanced concepts investigated for blade and vane cooling.

6. Application of the internal cooling concept to the rotor offers a greater improvement in engine performance than internal cooling of the stator.

7. The rotating heat exchanger, required for returning the heat from the rotor blades to the engine cycle, introduces design complexities in locating the turbine bearing support and introduces significant structural design and manufacturing problems for the turbine.

The fabrication and test phase of the program demonstrated that:

1. Fabrication of liquid-metal-cooled vanes with small coolant passages using current machining and welding practices is feasible.

2. The method of heat transfer analysis was confirmed within the test range, based on excellent correlation between the predicted and measured vane metal temperatures.

3. Limited feasibility of a liquid-metal-cooled vane and exchanger mechanical design was demonstrated in a cascade rig at inlet gas temperatures up to 2500°F.

7.0 RECOMMENDATIONS

Evaluate the effect of the modest improvement in SFC shown by the liquid-metal-cooled turbine on advanced missions to determine actual economic or performance justifications for this concept. If justification exists, then:

1. Conduct a feasibility fabrication and test evaluation of the liquid-metal-cooled rotor concept to demonstrate the thermosyphon and the rotating heat exchanger design principles.

2. Conduct a cyclic test on a liquid-metal-cooled turbine stator vane in a high-temperature cascade rig to evaluate its low cycle fatigue characteristics.

8.0 LITERATURE CITED

1. Muller, C., Cox, L., SINGLE STAGE AXIAL COMPRESSOR COMPONENT DEVELOPMENT FOR SMALL GAS TURBINES, USAAVLABS Technical Report 68-90A, B, C.

2. Eckert, E. R. G., and Esgar, J. B., SURVEY OF ADVANTAGES AND PROBLEMS ASSOCIATED WITH TRANSPIRATION COOLING AND FILM COOLING OF GAS TURBINE BLADES, NACA RME50 K15.

3. Gabel, R. M., and Tabbey, A. J., ADVANCEMENT OF HIGH TEMPERATURE TECHNOLOGY FOR SMALL GAS TURBINE ENGINES - FLUID COOLED AXIAL FLOW TURBINE, USAAVLABS Technical Report 68-65.

4. Banmeister, T., MARKS STANDARD HANDBOOK - MECHANICAL ENGINEERS, McGraw Hill, New York, 1967.

5. Rosenow, W. M., Chow, H. Y., HEAT MASS AND MOMENTUM TRANSFER, Prentice Hall, 1961.

6. Watt, J. J., Evans, A., Hibbard, R. R., FOULING CHARACTERISTICS OF ASTM JET A FUEL WHEN HEATED TO 700°F IN A SIMULATED HEAT EXCHANGER TUBE, NASA TND4958.

7. Stepka, F. S., CONSIDERATION OF TURBINE COOLING SYSTEMS FOR MACH 3 FLIGHT, NASA TND4491.

8. Whitlow, J. B., Eisenberg, J. D., Shovlin, M. D., POTENTIALS OF LIQUID METHANE FUEL FOR MACH 3 COMMERCIAL SST, NASA TND 3471.

9. ALKALI METAL COOLANTS, International Atomic Energy Agency, Vienna, 1967.

10. Franklin, W., Heilbron, J., Moskowitz, S., SMALL GAS TURBINE ENGINE COMPONENT TECHNOLOGY, Turbine Volume II, USAAVLABS Technical Reports 68-50A and 68-50B.

11. Moskowitz, S., TRANSPIRATION AIR COOLED TURBINE PROGRAM, Volume I and II, Curtiss-Wright Report WADR422.

12. POST-TEST REPORT OF THE WTF60 DEMONSTRATOR ENGINE NO. 2, R1055.

13. Horvath, J., and Moskowitz, S., DESIGN AND DEVELOPMENT OF A LIQUID METAL REGENERATOR SYSTEM, Curtiss-Wright Report 60-050163F.

14. Silverstein, C. C., STUDY OF HEAT PIPE APPLICATIONS IN NUCLEAR AIRCRAFT PROPULSION SYSTEMS, Contract NAS 3-11841, NASA Lewis Research Center, Cleveland, Ohio, March 4, 1969.

15. Kays, W., and London, A. L., COMPACT HEAT EXCHANGERS, 2nd Edition, McGraw-Hill, New York, 1964.

16. SST PROPULSION SYSTEM COMPONENT RESEARCH AND STUDY PROGRAM, HIGH TEMPERATURE TURBINE, Volume I, Curtiss-Wright Report SST:00-277.

17. Kreith, F., PRINCIPLES OF HEAT TRANSFER, International Textbook Company, Pennsylvania, 1968.

18. McAdams, W. H., HEAT TRANSMISSION, McGraw Hill, New York.

19. Manson, S. S., Halford, G. R., APPLICATION OF A METHOD OF ESTIMATING HIGH TEMPERATURE LOW CYCLE FATIGUE BEHAVIOR OF MATERIAL, ASM Transactions VOL 61, 1968.

20. Moon, D. P., Simon, R. C., Favor, R. J., THE ELEVATED-TEMPERATURE PROPERTIES OF SELECTED SUPERALLOYS, ASTM Data Series D57-S1.

21. Devan, J. H., CORROSION OF IRON AND NICKEL BASE ALLOYS IN HIGH TEMPERATURE SODIUM AND NaK, Oak Ridge National Laboratory.

22. Helmbrecht, J. L., Kirby, R. F., Weber, F., AN INVESTIGATION OF TURBINE BLADE/DISK ATTACHMENT METHODS FOR SMALL, COOLED GAS TURBINES, USAAVLABS Technical Report 69-91, January 1970.

23. Saco, F. W., Horvath, J. A., Cox, L. R., RESEARCH AND DEVELOPMENT OF ADVANCED LIQUID METAL REGENERATOR FOR APPLICATION TO AIRCRAFT TURBINE ENGINES, Curtiss-Wright Report WAD R-721.

APPENDIX I
FORCED CIRCULATION HEAT TRANSFER CRITERIA

From Reference 17,

$$Nu = .023\ Re^{.8}\ Pr^{.33} \tag{25}$$

$$Nu = hD/k \tag{26}$$

Combining these equations gives

$$h = .023 Re^{.8}\ Pr^{.33}\ \frac{k}{D} \tag{27}$$

where

$$Re = \frac{\rho VD}{\mu} \tag{28}$$

and

$$Pr = \frac{\mu C_p}{k} \tag{29}$$

Substituting terms for k and D in equation (27) gives

$$h = .023\ Re^{.8}\ \ Pr^{.33}\ \frac{\mu C_p}{Pr}\ \ \frac{\rho V}{\mu Re} \tag{30}$$

and combining terms gives

$$h = .023 \left(\frac{VC_p}{Re^{.2}}\right)\ \ \left(\frac{\rho}{Pr^{.67}}\right) \tag{31}$$

The second term contains fluid-dependent properties and therefore is used as the criterion in selecting heat transport fluid in the form

$$\left(\frac{C_p \mu}{k}\right)^{.67} \Big/ \rho \tag{32}$$

APPENDIX II
NATURAL CIRCULATION HEAT TRANSFER CRITERIA

From Reference 17,

$$Nu = A\left(Gr\ Pr^2\right)^{.25} \tag{33}$$

$$Nu = hD/k \tag{34}$$

where

$$Gr = \frac{\gamma \omega^2\ \beta \Delta T\ \rho^2 D^3}{\mu^2} \tag{35}$$

and

$$Pr = \frac{C_p \mu}{k} \tag{36}$$

Combining equations (33) and (34) gives

$$h = \frac{k}{D}\quad A\left(Gr\ Pr^2\right)^{.25} \tag{37}$$

Substituting terms gives

$$h = \left[A^4\ \frac{\gamma \omega^2 \beta \Delta T\ \rho^2\ D^3\ C_p^2}{k^2}\qquad \left(\frac{k}{D}\right)^4\right]^{2.5} \tag{38}$$

and combining terms gives

$$h = \left(\frac{A^4 \gamma \omega^2 \Delta T}{D}\right)^{.25} \left(\rho^2 C_p^{\ 2}\ \ k^2 \beta\right)^{.25} \tag{39}$$

The second term contains fluid-dependent properties and therefore is used as the criterion in selecting the heat transport fluid in the form

$$\rho^2 C_p^{\ 2}\ \ k^2 \beta \tag{40}$$